

**Editor-in-Chief B.E.Paton**

**Editorial board:**

Yu.S.Borisov	V.F.Khorunov
A.Ya.Ishchenko	I.V.Krivtsun
B.V.Khitrovskaya	L.M.Lobanov
V.I.Kirian	A.A.Mazur
S.I.Kuchuk-Yatsenko	
Yu.N.Lankin	I.K.Pokhodnya
V.N.Lipodaev	V.D.Poznyakov
V.I.Makhnenko	K.A.Yushchenko
O.K.Nazarenko	A.T.Zelnichenko
I.A.Ryabtsev	

**International editorial council:**

N.P.Alyoshin	(Russia)
U.Diltey	(Germany)
Guan Qiao	(China)
D. von Hofe	(Germany)
V.I.Lysak	(Russia)
N.I.Nikiforov	(Russia)
B.E.Paton	(Ukraine)
Ya.Pilarczyk	(Poland)
P.Seyffarth	(Germany)
G.A.Turichin	(Russia)
Zhang Yanmin	(China)
A.S.Zubchenko	(Russia)

**Promotion group:**

V.N.Lipodaev, V.I.Lokteva  
A.T.Zelnichenko (exec. director)

**Translators:**

A.A.Fomin, O.S.Kurochko,  
I.N.Kutianova, T.K.Vasilenko  
PE «Melnik A.M.»

**Editor**

N.A.Dmitrieva  
**Electron galley:**  
D.I.Sereda, T.Yu.Snegiryova

**Address:**

E.O. Paton Electric Welding Institute,  
International Association «Welding»,  
11, Bozhenko str., 03680, Kyiv, Ukraine  
Tel.: (38044) 287 67 57  
Fax: (38044) 528 04 86  
E-mail: journal@paton.kiev.ua  
http://www.nas.gov.ua/pwj

State Registration Certificate  
KV 4790 of 09.01.2001

**Subscriptions:**

**\$324**, 12 issues per year,  
postage and packaging included.  
Back issues available.

All rights reserved.

This publication and each of the articles  
contained herein are protected by copyright.  
Permission to reproduce material contained in  
this journal must be obtained in writing from  
the Publisher.

Copies of individual articles may be obtained  
from the Publisher.

## CONTENTS

Contribution of Welders into Great Victory ..... 2

### SCIENTIFIC AND TECHNICAL

*Yushchenko K.A., Savchenko V.S., Chervyakov N.O. and Zvyagintseva A.V.* Probable mechanism of cracking of stable-austenitic welds caused by oxygen segregation ..... 5

*Makhnenko V.I., Velikoivanenko E.A., Rozynka G.F. and Pivtorak N.I.* Improvement of method for estimation of the risk of fracture within the thinning zone on walls of main pipelines ..... 10

*Gajvoronsky A.A., Poznyakov V.D., Sarzhevsky V.A., Vasiliev V.G. and Orlovsky V.Yu.* Influence of thermodeformational cycle of hardfacing on the structure and properties of railway wheels at their reconditioning ..... 15

*Maksymova S.V., Khorunov V.F. and Zelinskaya G.M.* Structural state of rapidly quenched Cu-Ti system brazing filler metal ..... 19

*Nazarenko O.K. and Zagornikov V.I.* Influence of working distance of welding electron gun on weld geometry ..... 23

### INDUSTRIAL

*Paton B.E., Lobanov L.M., Nedoseka A.Ya., Fedchun A.Yu., Yolkin A.A. and Obodovsky B.M.* Reliability of welded structure operation. Assessment and control ..... 27

*Akhonin S.V., Belous V.Yu., Romanyuk V.S., Stesin V.V., Veliky S.I., Semenenko A.V. and Polishchuk A.K.* Narrow-gap welding of up to 110 mm thick high-strength titanium alloys ..... 34

*Mashin V.S., Pashulya M.P., Shonin V.A. and Klochkov I.N.* Consumable electrode pulsed argon-arc welding of sheet aluminium alloys ..... 38

*Kononenko V.Ya.* Application of method of dry underwater welding in repair of underwater passages of gas and oil pipelines in Russia ..... 42

### BRIEF INFORMATION

*Kuchuk-Yatsenko S.I., Kharchenko G.K., Smiyani O.D., Falchenko Yu.V., Zagadarchuk V.F. and Butkova E.I.* Hydrogen distribution in flash-butt welded joints on steel 10G2FB ..... 47

News ..... 49

OJSC «Mezhgosmetiz-Mtsensk» — on a way of mastering production of all welding consumables relevant in the market ..... 51

### NEWS

10th International Specialized Exhibition «Welding and Cutting» ..... 52

---

## CONTRIBUTION OF WELDERS INTO GREAT VICTORY

*The remarkable date, the 65 years of Great Victory over fascist Germany and its satellites, is also celebrated by many-million group of welders: scientists, engineers, technicians and workers.*

*The stimulus for development of welding was given after the First World War having put forward a number of technical problems before welders. By the end of the 1930s welding became leading technology in the production of armaments of many countries, having almost completely replaced riveting.*

*During the World War II the necessity in acceleration of armament production gave a powerful impetus for widening the application and modernization of welding processes. The main emphasis was made on search of reserves, hidden capabilities of technologies. Perfidious attack of fascist Germany on the Soviet Union, loss of considerable part of the territory of Ukraine with metallurgical and machine-building plants, dismantling of plant equipment and its transportation to eastern regions dragged rates of weapon production at the end of 1941. The application of welding engineering allowed quick disassembling of equipment of evacuated plants in the very shortest terms, accelerating the assembly at the new site and starting the production. The designers, production managers understood that only simplification of manufacturing process, including also welding, will allow production of necessary amount of weapon for the front in the shortest period.*

*In the pre-war years the Soviet designers constructed the most advanced tanks: heavy KV-1, medium T-34, floating T-40 and SAU, based on them. Armored bodies, assemblies and structure elements were welded manually using special electrodes. To fulfill this work, thousands of high-skilled welders were required. The solution was found in application of automatic welding.*

*At the end of the 1930s the technology of automatic submerged arc welding of structural steels was developed under supervision of Evgeny O. Paton at the Electric Welding Institute. At the beginning of Great Patriotic War the Institute was evacuated from Kiev to Nizhny Tagil and arranged at the Ural Railway-Carriage Works where high-speed welding began to*

*be implemented in production of aviation bombs. Soon, the specialists and equipment of Kharkov plant No. 183 were transported there, where tank T-34 was constructed. The plants were united into one enterprise, called the Ural tank plant. E.O. Paton forwarded efforts of personnel to the development of technology of automatic submerged arc welding of special, armored steels and application of the new technology to manufacture intricate three-dimensional structures of armored bodies of tanks. It should be noted that such task was solved for the first time in the world. In the shortest terms it was succeeded to find out the causes of cracks initiation in welds. The technology of defectless welding was developed (V.I. Dyatlov, A.I. Ivanov); the nature of processes was studied and presence of arc charge under the flux layer proved experimentally (B.E. Paton, A.M. Makara); the fluxes of blast-furnace slags were developed (A.I. Korennoj); the phenomenon of self-control of arc processes with consumable electrode was revealed (V.I. Dyatlov), on the basis of which the simplified automatic welding heads with constant speed of electrode wire feed were developed (P.I. Sevbo, B.E. Paton). In 1942–1943, 20 designs of installations for welding of tank bodies and 8 designs for welding of aviation bombs and ammunition were developed and realized. One more remarkable achievement was the construction of the first assembly-welding production line, proposed by Yu.E. Maksaryev, the director of plant, and Evgeny O. Paton.*

*The works on application of new welding process were carried out in cooperation with the Institute, tank design bureaus and plants. A.A. Morozov, the leading designer of tank T-34, Zh.Ya. Kotin, the leading designer of heavy tanks IS and KV, participated actively in the solution of these questions. The colleagues of the Electric Welding Institute trained workers and set up the equipment at the plants of the country. Automatic welding found its large-scale application in Chelyabinsk where the S.M. Kirov Leningrad Tractor Plant (tanks KV, T-34 and SAU) was evacuated; at Gorky Automobile Plant (artillery installations, shells and other); at S. Ordzhonikidze Ural Heavy Machine-*

---

*Building Plant (Sverdlovsk) (bodies of tanks). By the end of 1943 the submerged arc welding was mastered at 52 plants. In the years of war 4 million meters of weld were welded, 5 million of kilowatt-hours of electricity saved, labor-consumption for tank body manufacture was five times decreased. The welding could be performed by teenagers; only at Ural Tank Plant 250 welders were released. By the end of the war the plants produced up to 30 thousands of heavy and medium tanks and self-propelled guns per year.*

*Already at the beginning of the 1930s the aircrafts of corrosion-resistant steels and aluminium alloys with welded frames of fuselage, wings and tail unit were designed in the number of countries. In the USSR, these were planes of A.I. Putilov «Stal-2», the resistance welding of which was carried out by P.N. Lvov. Contribution into development of resistance welding of assemblies of planes and welding-in of lining of chromium-nickel steels was made by A.S. Gelman, E.V. Sokolov and other specialists of TsNIIT-Mash (Moscow). The successful application of brazing of aluminium alloys was due to works on technology and development of brazing alloys, carried out in prewar years in MAI, NII GVF (P.N. Lvov, N.V. Geveling, S.N. Lotsmanov). Increase of «life» of aircrafts was possible due to application of welded and brazed tubular longerons, corrugated linings, underframes.*

*Since the first days of war the work of Moscow Mechanical Engineering Institute (nowadays N.E. Bauman MGTU)) was directed to the manufacture of armament. K.K. Khrenov, G.A. Nikolaev, S.T. Nazarov and other colleagues solved a series of problems on manufacture and repair of military machinery. With their participation the designs of artillery and shooting weapon were worked out in the shortest time using widely the resistance welding in the technological process. Thus, S. Shpagin developed a stamped-welded design of a pistol-gun which considerably simplified the production of this automatic weapon. The welders of Leningrad switched over to the production of military products and did all possible for the city defense. N.O. Okerblom, V.P. Vologdin, A.A. Alekseev, D.N. Sagalovich, F.F. Benua and other organized repair of tanks and other combat machinery, developed new technologies of manufacturing pontoons and other floating means. Thus, in November 1941 the structures for crossing Neva*

*were manufactured at Baltic Ship-Building Yard in several days. The construction of torpedo-boats, guard-boats, trawlers kept on. Manual arc (including underwater) and gas welding were applied for construction of auxiliary ships, pontoons, cutters, repair of ships. Only in the second half of a year of 1941, 84 ships were completed. In the period of blockade in Leningrad and Kronstadt about 850 ships were repaired applying welding, cruiser «Petropavlovsk», sunken after bombardment, was lifted and repaired. For communication with Bolshaya Zemlya during navigation in 1942, 14 barges of loading capacity of 900 t were welded in unprecedented rates. In spring 1942 the Welding-assembly trust of Narkomstroi (A.S. Falkevich) constructed a welded underwater fuel pipeline of high pressure of 30 km extension, including 21.5 km under water at the depth from 1 up to 12.5 m across the Ladozhskoye lake. Non-certified pipes were joined using manual electric arc and gas welding. During war other pipelines were also constructed (Astrahan–Stalingrad is largest). Oil tanks, cisterns of large capacity began to be all-welded.*

*In liberated regions and regions of combat actions it was urgently necessary to restore railroads. The colleagues of TsNIITMash and National Commissariat of Communications offered new technological processes of arc and resistance welding of rail butts. The installation for resistance welding of rails with the movable platform was designed and manufactured at the plant «Revtrud». Over 30,000 butts were performed in a year by the first rail-welding train in the USSR. In 1943, 10 such trains were already operated. For welding wires under field conditions the magnesium thermite was developed in TsNIIzheldortrans (M.I. Vakhnin, et al.).*

*In the years of war the urgent demand for underwater welding and cutting of metal appeared. Even earlier, K.K. Khrenov proved the possibility of application of arc welding and cutting using consumable electrode under water in laboratory conditions. In the special laboratory, organized in March 1942 at Moscow Electromechanical Institute of Engineers of Railway Transport, the training of divers-welders began. The special trains were formed, the personnel of which released waterways of rivers from exploded bridges, participated in restoration of bridges, rising of sunken ships and their repair. Several stations of underwater ship repair were*

---

built. Following the example of Soviet Union welding and cutting under water began to be applied to other combat countries as well.

In 1941 the plant in village Novaya Utkha (Sverdlovsk region) began production of electric welding equipment, where part of workers and engineers and technicians of plant «Elektrik» was evacuated from Leningrad. During years of war 6000 movable welding machines, 15,000 welding transformers, about 500 heads of AGE-5-2 for arc welding were produced.

The deficit of metal including steel rolled metal forced manufacturing of metal structures of ill-conditioned steels. The electrodes of series UONI-13 designed by K.V. Petran turned to be universal, providing high quality of a weld. New electrode coatings of non-deficit materials were developed in N.E. Bauman MVTU (K.K. Khrenov and others). In TsNIITMash timber and granite were added to the composition of electrode coating, the electrodes TsS-1 and TsS-2 were designed for surfacing of hard alloys of Sormite type, electrodes for welding of carbon steels (A.A. Alov, V.I. Yarkho, G.I. Glushkov and others).

In the years of war the need in gas welding and cutting arose. Gas cutting was the main technology at dismantling the destroyed metallic structures and preparation of components at the plants, gas welding and brazing was widely applied during repair in field conditions. To produce cutters and torches the plants in Barnaul and Sverdlovsk were built; machines for cutting, installations for pyrolytic gas were produced at the Uralmash. In 1944 All-Union Research Institute of Autogenous Industry (VNIIavtogenmash, director A.N. Shashkov) was founded where research works on development of technologies and modernization of equipment for gas-plasma treatment were started.

In 1941–1945 the field movable repair bases began to be manufactured, where the set of equipment included the installations for arc welding and cutting.

Under difficult period of military times the scientists of the country continued investiga-

tions, the majority of which was directed to the solution of problems arose in production of weapon and restoration of metallic structures. In the years of war colleagues of the Electric Welding Institute wrote and published more than dozen of works. Among them — third edition of fundamental monograph of E.O. Paton «High-speed automatic submerged arc welding», «Automatic welding in shipbuilding» and «Manual on welding of armored structures». In January 1943 on the initiative of Director of the Institute, the scientific conference on submerged arc welding was held in Nizhny Tagil. G.A. Nikolaev published monograph «Application of welding in artillery systems and shooting guns». In 1941 the section on scientific development of problems of electric welding and electrothermics of Academy of Sciences of USSR was organized. Under management of V.P. Nikitin the method of automatic welding with separation of processes of thermal preparation of base and filler metal was developed. N.N. Rykalin conducted research works in the field of electrodes melting and penetration of base metal. A.A. Alov worked on study of slag inclusions and pores in weld metal. The successful investigations of resistance spot welding of large thicknesses were carried out by A.S. Gelman. V.P. Vologdin and N.O. Okerblom worked on the discovery of mechanism of formation of stresses and strains in welding process. G.A. Nikolaev, K.K. Khrenov solved problems of welding special steels and quality control of welding. K.V. Lyubavsky and F.I. Pashukanis developed a number of fluxes (including those of non-deficit materials) for automatic welding of low-carbon and alloyed steels. At the same place the modernization of welding equipment continued (I.L. Brinberg).

Owing to the efforts of many scientists, inventors, workers the welding became leading technology in building enterprises, production and repair of armaments and made a great contribution into Great Victory.

A.N. Kornienko,  
Dr. of Historical Sci., PWI



# PROBABLE MECHANISM OF CRACKING OF STABLE-AUSTENITIC WELDS CAUSED BY OXYGEN SEGREGATION

K.A. YUSHCHENKO, V.S. SAVCHENKO, N.O. CHERVYAKOV and A.V. ZVYAGINTSEVA  
E.O. Paton Electric Welding Institute, NASU, Kiev, Ukraine

Current concepts of the nature of formation of cracks classified as ductility-dip cracks in multilayer welds or HAZ of steels and alloys with single-phase structure have been reviewed. It is noted that the mechanism of formation of such cracks is a subject of discussion. A hypothesis of the probable influence of oxygen on the processes of intergranular fracture is set forth, as oxygen decreases cohesion strength of grain boundaries in the established temperature range and leads to intergranular fracture.

**Keywords:** arc welding, high-alloy steels, nickel alloys, welded joints, grain boundaries, ductility-dip cracks, cohesion energy, Auger-spectroscopy

Welded joints on high-alloy steels with stable-austenitic structure and nickel superalloys are known to be highly sensitive to hot cracking during fusion welding. As to their nature, hot cracks are of two types: solidification and underbead (ductility-dip) cracks formed under thermal-force loading of the zones of metal of the multilayer welds (Figure 1). The temperature range of formation of solidification cracks (brittle temperature range – BTR) depends upon the range of the solid-liquid state of metal in solidification of the weld. The lower limit of this range is determined by the value of solidus temperature  $T_s$  at the end of solidification. The ductility-dip crack (DDC) temperature range is determined by an approximate ratio of  $(0.6-0.8)T_s$  (Figure 1). The cracks in this range initiate and propagate along the boundaries of high-angle austenitic grains (Figure 2).

Some researchers relate the mechanism of ductility-dip cracking to embrittlement of grain boundaries, resulting from formation of a chain of precipitated carbides  $Me_{23}C_6$  [2–4]. Investigations were conducted on nickel alloy Inconel 52. According to the suggested

mechanism, metal carbides (of the  $Me_{23}C_6$  type) precipitating along the grain boundaries (Figure 3) act as stress raisers that cause microstrains, thus promoting initiation of discontinuities and, as a consequence, grain boundary fracture. By accepting this mechanism of formation of cracks, it can be assumed that the intergranular fracture surface should have a pit-like (cup-shaped) character of fracture, at which the majority of pits comprise a carbide particle. This mechanism is characteristic of a tough intergranular fracture of high-alloy steel with a stable-austenitic structure at room temperature (Figure 4).

At the same time, examinations of the fracture surface in the zones of formation of DDCs [5] do not confirm occurrence of this mechanism. The authors of study [5] note formation of a wavy fracture surface in plane of grains, which are sometimes decorated with carbides. The sites of carbides are free from local plastic strains that form characteristic zones with the pit-like fracture mechanism (Figure 5). Analysis of the majority of results of fractographic examinations of the fracture surfaces shows [5] that carbides could not participate in formation of cracks within the ductility-dip range. Hence, the probability exists of occur-

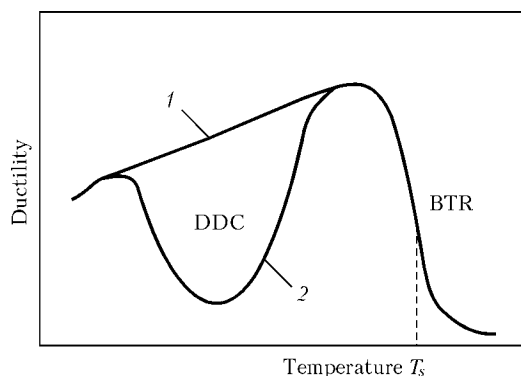


**Figure 1.** Diagram of formation of hot cracks in welded joints on high-alloy steels and alloys [1]: 1 – material without ductility dip; 2 – with ductility dip

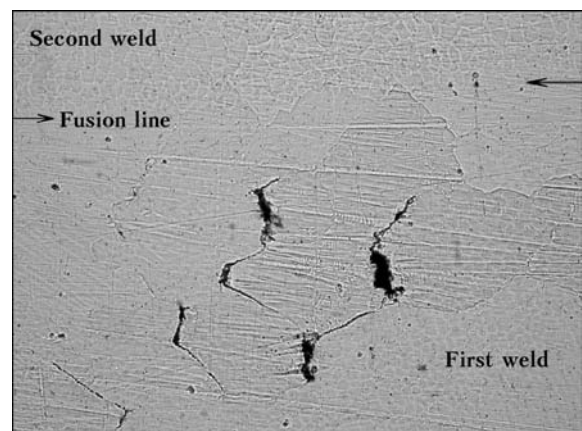


**Figure 2.** Microstructure ( $\times 200$ ) of metal of the beads deposited with wire In52 with DDCs in multilayer welds

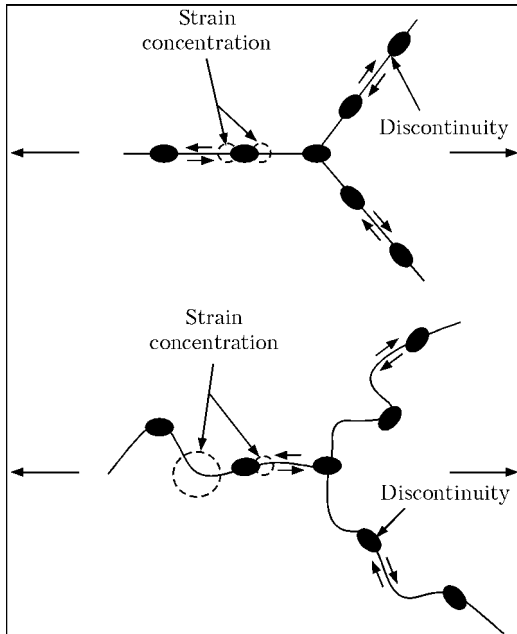


Figure 3. Effect of intergranular precipitates in formation of DDCs for straight and wavy grain boundaries [4]

rence of the fracture mechanism other than that put forth by the authors of the hypothesis described in studies [2–4]. Another confirmation of invalidity of the carbide theory are the results of evaluation of sensitivity to ductility-dip cracking using a high-alloy steel of the AISI 310 type (Table) with a different content of impurities [6].

Analysis of the published results of study [6] shows that steel SUS 310EHP, which is super pure in terms of the content of impurities, is insensitive to solidification cracks (Figure 6). Nevertheless, the authors note the presence of DDCs (DDC zone) in the weld metal, despite the super low content of impurities, including carbon, this excluding formation of carbides along the grain boundaries. Therefore, it can be concluded that formation of DDCs in TIG welding is not controlled by precipitation of carbides along the high-angle austenite grain boundaries.

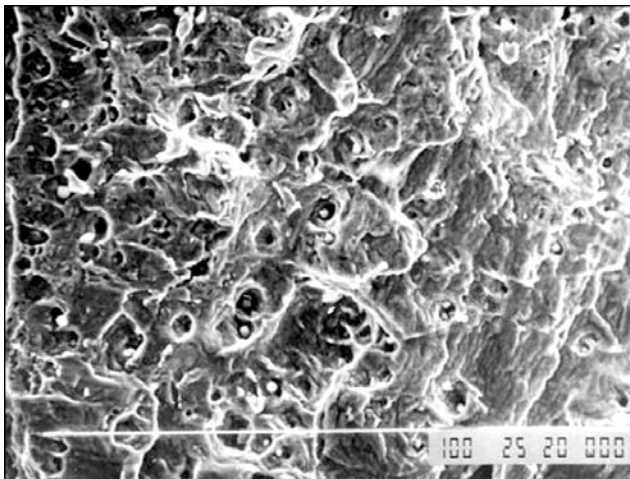


Figure 4. Fractogram of fracture surface on stable-austenitic weld metal with pit-like fracture character

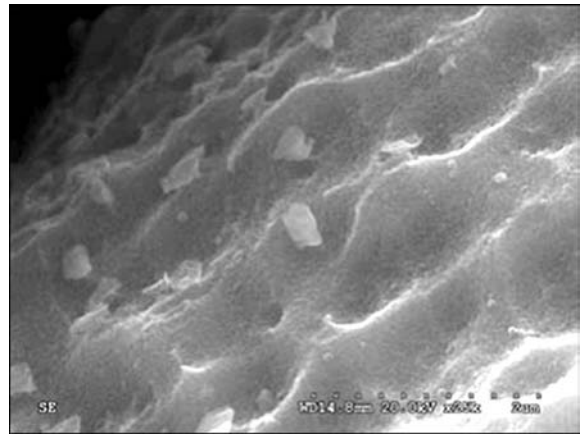


Figure 5. Fractogram of surface of DDCs with characteristic structure identified as wavy and decorated with carbide precipitates [5]

Analysis of chemical composition of super pure steel SUS 310EHP (see the Table) indicates that, along with such impurity elements as carbon, silicon, manganese, phosphorus and sulphur, the super pure metal also contains oxygen, its content being an order of magnitude higher than the content of carbon.

Consider the possible effect of oxygen on the processes of DDC formation. As shown earlier, the probable mechanism of DDC formation is enrichment of grain boundaries with impurity elements, which segregate to the boundaries in a temperature range of about  $(0.6-0.8)T_s$ , owing to the diffusion processes accelerated by plastic strains during welding [7].

Based on these conclusions, oxygen may affect the processes of intergranular embrittlement only in the case where this very active element exists in metal in a dissolved state and has a comparatively high diffusion coefficient in the fcc lattice. These data can be obtained by using the method of electromotive forces of metals in solid electrolytes with oxygen conductivity. The method is employed to determine parameters of diffusion of oxygen in solid solution of metallic

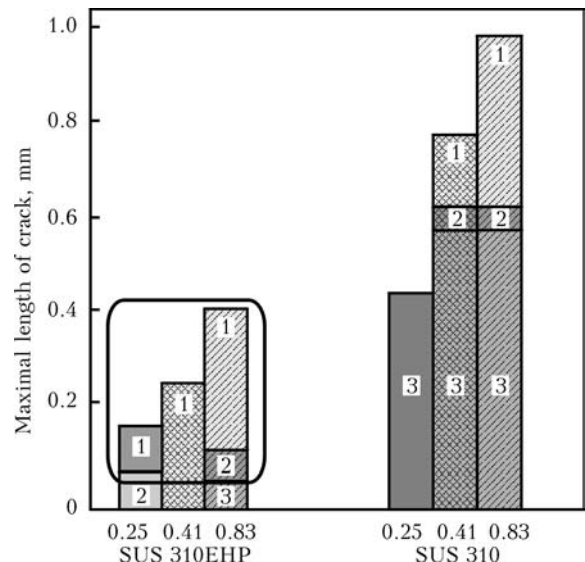


Figure 6. Maximal length of DDCs (1), transition zone (2) and solidification cracks (3) in stainless steels of the 310 type at strains of 0.25, 0.41 and 0.83 % [6]



Chemical composition of high-alloy steel SUS 310 [7] compared with super pure steel SUS 310EHP, wt.%

Steel grade (AISI 310 type)	C	Si	Mn	P	S	Ni	Cr	O	N	Ti	Fe
SUS 310EHP	0.0002	0.0025	0.0001	0.0011	0.0008	21.58	21.13	0.0029	0.0022	0.18	Base
SUS 310	0.12	1.00	1.48	0.020	0.011	20.59	25.12	-	-	-	Same

materials, including with the fcc lattice [8, 9]. In this case, a solid electrolyte consisting of zirconia (85 %) with additions of Y<sub>2</sub>O<sub>3</sub> (15 %) is used as an ion conductor.

The above electrochemical method allows using ZrO<sub>2</sub> as a practically pure ion conductor to investigate diffusion of oxygen in solid metals at high temperatures. In this case, the diffusion flow of oxygen transforms into the electric current, the value of which can be measured.

Qualitative investigations conducted by the authors using the solid electrolyte on high-alloy steel EI417 (Kh23N18) (GOST 5632-72) showed the presence of current in an electric circuit, this being indicative of the diffusion of oxygen in the crystalline lattice.

The published data on the quantitative proportion of oxygen show that in a structural steel that is not deoxidised by aluminium the total content of oxygen is 105 ppm, and that of diffusible oxygen is 40 ppm [10]. In deoxidation, the total and diffusible oxygen contents decrease accordingly.

The rate of diffusion of oxygen in iron with  $\gamma$ -structure at high temperatures is shown in Figure 7.

Analysis of the presented data allows compiling a series of diffusion mobility of hydrogen, oxygen, carbon, nitrogen and sulphur depending upon the temperature, the diffusion coefficient of oxygen being more than two orders of magnitude higher than that of sulphur.

Therefore, there are preconditions for diffusion redistribution of oxygen between the grain body and boundary, which is likely to be accelerated by dislo-

cation transfer of impurity elements at plastic strains under the effect of a welding thermal cycle.

It can be assumed on the basis of these data that in the SUS 310EHP metal, which is super pure in terms of sulphur, carbon and phosphorus, the element that leads to the DDC formation [7] is oxygen. It should be taken into account in this case that the source of ingress of oxygen into the weld pool and weld (by an example of TIG welding) is not only oxygen contained in the base and filler metal, but also the always existing probability of saturation of the weld pool with oxygen in argon welding.

The model of intergranular fracture in formation of DDCs can be represented by a diagram shown in Figure 8. According to this diagram, strength of interatomic bonds is determined by attractive and repulsive forces between the elementary particles that are in the equilibrium state and determine the energy of cohesion of atoms at the grain boundaries.

The process of segregation of some elements, including oxygen, in the field of stresses at the boundary crack apex (Figure 9) leads to a change in the cohesion strength, thus favouring redistribution of the atomic interaction forces and sensitivity to intergranular embrittlement as a whole (Figure 10).

The latter follows both from general considerations of the effect of segregations on the cohesion strength of interfaces, and from estimations of the strength by the formula in studies [14, 15], derived from an upgraded model of allowance for the role of segregations:

$$\sigma_m^s = \frac{\sigma_m^0}{1 + 1/2X_i(a_1/a_0 - 1)},$$

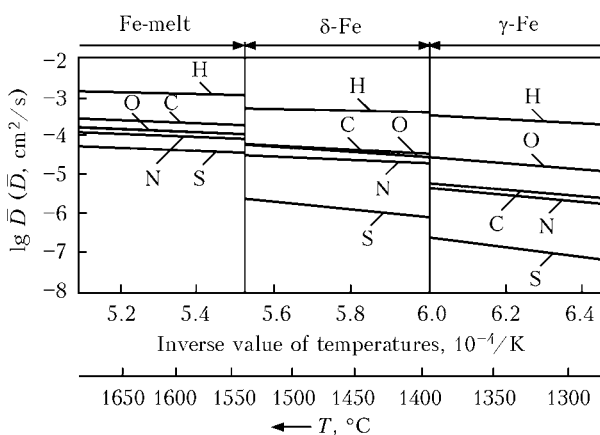


Figure 7. Temperature dependence of mean value of diffusion coefficient for elements in iron [11]

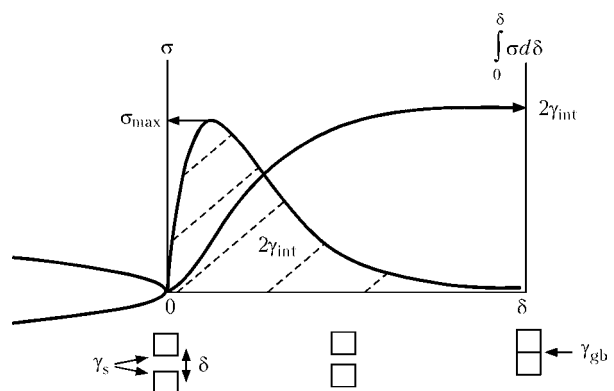


Figure 8. Model of variations in cohesion strength  $\sigma$  and cohesion energy  $2\gamma$  of grain boundaries in crack mouth at intergranular fracture [12]:  $\gamma_s$  – surface energy;  $\gamma_{gb}$  – grain boundary energy;  $\gamma_{int}$  – calculated values of cohesion energy;  $\delta$  – crack opening displacement



S, C, O, rel. un.

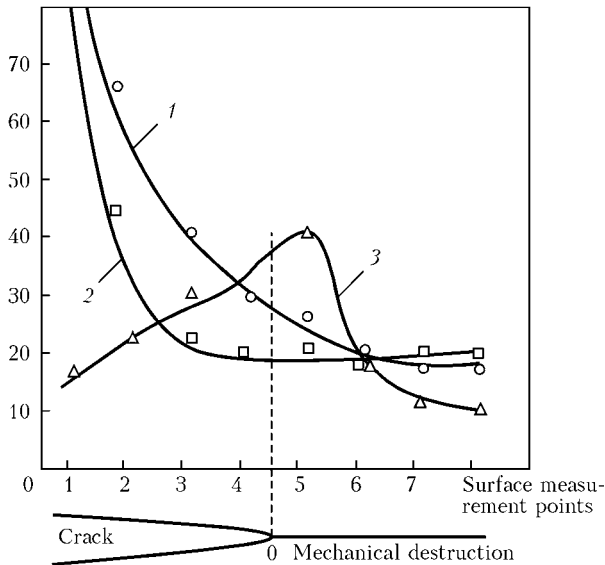


Figure 9. Character of distribution of impurity elements ahead of the crack apex at high-temperature fracture [13]: 1 – oxygen; 2 – carbon; 3 – sulphur

where  $\sigma_m^0$  is the strength of cohesion of a clean interface;  $X_i$  is the concentration of a segregating element at the interface;  $a_1$  and  $a_2$  are the atomic sizes of the segregating atoms and matrix atoms, respectively.

Consider the probable effect of carbon and oxygen on the processes of variations in cohesion strength of interfaces, proceeding from sizes of the atomic radii of iron and nickel as a base of the majority of high-alloy steels and alloys with a stable-austenitic structure (values of the atomic radii of some elements [16] are as follows, nm: 0.1411 Fe, 0.1377 Ni, 0.1606 O, 0.1281 C) for oxygen –  $(a_1/a_0 - 1) > 0 [-\sigma]$  and for carbon –  $(a_1/a_0 - 1) < 0 [+ \sigma] 2\gamma \rightarrow [-\sigma]$ .

Considering the positive value of the  $(a_1/a_0 - 1)$  ratio for oxygen, one may expect decrease in the values of interfacial cohesion strength in iron- and nickel-base materials and resistance to DDC formation as a whole caused by this element.

As shown by similar calculations, in contrast to oxygen, carbon gives a negative value of the above ratio. It does not decrease the interfacial cohesion strength of iron- and nickel-base materials. Thus, it

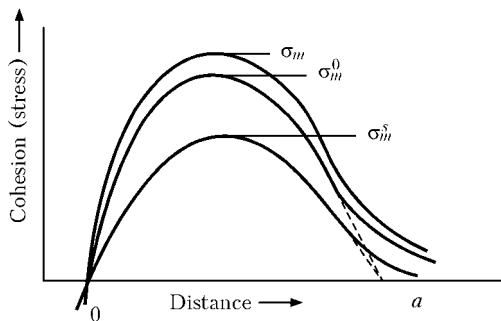


Figure 10. Variation in cohesion intergranular stress as a function of distance from the crack apex [14]:  $\sigma_m$  – cohesion energy of grain body;  $\sigma_m^0$  – cohesion energy of clean boundary;  $\sigma_m^s$  – cohesion energy of boundary with an impurity;  $a$  – distance from the crack front in stress field

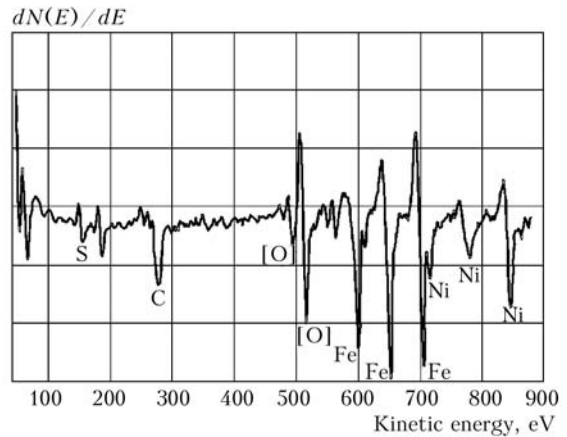


Figure 11. Energy spectrum of relative distribution of main alloying and impurity elements on the crack surface in weld metal of the 34NKD type metal

does not lead to formation of DDCs in the investigated grades of materials in accordance with the accepted model.

Along with the parameters of atoms and in accordance with the given formula, a decisive effect on the cohesion strength processes is exerted by the concentration of impurity elements along the grain boundaries as a result of their segregation.

The concentration of oxygen and carbon on the surface of brittle intergranular fracture was evaluated by Auger-spectroscopy on uniaxial tension specimens of iron-nickel alloy 34NKD stretched in a  $10^{-5}$  mm Hg vacuum at a ductility dip temperature of 850 °C and strain rate of  $2.85 \cdot 10^{-4} s^{-1}$ . The choice of the above material was based on the absence of chromium in it (in contrast to the majority of high-alloy steels and alloys with a stable-austenitic structure), whose peak in the Auger-spectroscopy energy spectrum almost coincides with the oxygen peak, which does not allow separating contents of these elements.

Chemical composition of alloy 34NKD (according to TU 14-1-3798-84) used for the experiments is as follows, wt.%:  $\leq 0.03$  C,  $\leq 0.10$  Mn,  $\leq 0.10$  Si,  $\leq 0.10$  Ti,  $< 0.008$  P,  $< 0.01$  S, 34-35 Ni, 1.5-2.0 Co, 9.2-0.4 Cu.

The contents of carbon, oxygen and sulphur were estimated from the Auger-analysis data using the «Riber» instrument LAS-2000 at a depth of about 5 nm from the crack surface after its ion beam cleaning

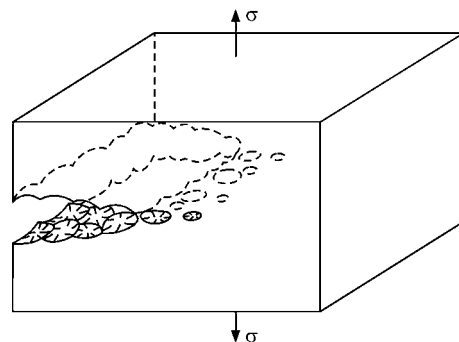


Figure 12. Model of formation of meniscus instability of material in formation of a wavy character of surface fracture [15]



from sorbates. The energy spectrum of a relative distribution of elements is shown in Figure 11.

The content of some elements on the intergranular fracture surfaces of the 34NKD alloy specimens was as follows, at.-%: 29.3 C, 34.0 O and 1.2 S.

Analysis of the results indicates to enrichment of the surfaces of grain boundaries with oxygen, carbon and sulphur. Based on the values of the  $(a_1/a_0 - 1)$  ratio, oxygen and sulphur may decrease the cohesion strength of grain boundaries. Carbon does not lead to decrease in the cohesion strength, as its  $(a_1/a_0 - 1)$  ratio has a negative value, and the value of cohesion strength  $\sigma_m$  does not decrease (see the formula). Compared to sulphur, oxygen leads to a higher loss of the cohesion strength, proceeding from its increased content at the boundary. The increased oxygen content, compared with the sulphur content, can be attributed to high parameters of the diffusion coefficient of oxygen (see Figure 7).

Preliminary results make it possible to set forth the hypothesis of a probable mechanism of formation of cracks in the base and weld metals of welded joints on high-alloy steels within the ductility-dip temperature range. It is likely that formation of the embryo discontinuities of microscopic sizes (Figure 12) leads not only to the formation and localisation of micropores in plane of the grain boundary, but also to the super equilibrium and super critical concentration of an impurity element in them, this practically causing a micro brittle fracture along the grain boundaries with a minimal formation of the plastic strain zones.

## CONCLUSIONS

1. Actively diffusing impurities, such as carbon, oxygen, hydrogen and phosphorus, which are dissolved in metal, are redistributed in cooling of metal under the stress and temperature gradient conditions between a solid solution and different defects of structure of dislocation clusters, twins, grain boundaries and inclusions. The activated process of formation and movement of dislocations in the DDC range leads to a super equilibrium enrichment of grain boundaries with impurities. The higher the diffusion coefficient and concentration of an element, other conditions being equal, the higher is the effect of decrease in strength, and the higher is the degree of localisation of tensile stresses and strains at the boundary.

2. It is not improbable that the centres of the eutectic origin liquid phase of molecular sizes may also be formed in this case, as there is a close relationship between the rate of diffusion of impurity elements, activation of the process under certain condi-

tions of the thermal-deformation effect, quantity and location of micro- and macrocracks in austenitic metal along the grain boundaries, characteristics of fracture and concentration of impurity elements on the fractured planes with propagation of cracks, and high percentage of the impurities (carbon, oxygen, hydrogen, sulphur, phosphorus, etc.) fixed on the crack surface. It can be concluded at a high probability degree that fracture in the ductility-dip temperature range occurs by the cohesion mechanism, and it is reasonable to choose methods for elimination of these cracks on the basis of this mechanism.

- Collins, M.G., Lippold, J.C. (2008) An investigation of ductility dip cracking in nickel-based filler materials. Pt 1. *Welding J.*, 82(10), 288–295.
- Young, G.A., Capobianco, T.E., Penik, M.A. et al. (2008) The mechanism of ductility dip cracking in nickel-chromium alloy. *Ibid.*, 87(2), 31–43.
- Capobianco, T.E., Hausou, M.E. (2005) Auger spectroscopy results from ductility dip cracks opened under ultra-high vacuum. In: *Proc. of Int. Conf. on Trends in Welding Research* (16–18 May, 2005, Callaway Gardens Resort, Pine Mountain, Georgia, USA), 767–772.
- Lippold, J.C., Nissley, N.E. (2007) Further investigations of ductility dip cracking in high chromium, Ni-base filler metals. *Welding in the World*, 9/10, 24–30.
- Noecker, F.F., DuPont, J.N. (2009) Metallurgical investigation into ductility dip cracking in Ni-based alloys. Pt 2. *Welding J.*, 3, 62–77.
- Nishimoto, K., Saida, K., Kiuchi, K. et al. (2008) Hot cracking behaviour of high-purity type 310 stainless steels. *Material joining process. IIW Doc. IX-H-G98-08*.
- Yushchenko, K., Savchenko, V. (2008) Classification and mechanisms of cracking in welding high-alloy steels and nickel alloys in brittle temperature ranges. In: *Hot cracking phenomena in welds II*. Berlin, Heidelberg: Springer, 95–114.
- Pang, Y.-W., Altstetter, G.I. (1987) The diffusion and solubility of oxygen in solid nickel. *Metal. Transact. A*, (7), 43–50.
- Rickert, H., Steiuer, R. (1966) Elektrochemische Messung der Sauerstoffdiffusion in Metallen bei hoeheren Temperaturen. *Zeitschrift fuer Physikalische Chemie*, 49(3–5), 127–137.
- Pietschmann, G., Noky, D. (1988) Anwendung des Sauerstoffpotentials-messtechnik in der Stahlwerk Praxis. *Neue Huette*, 6, 210–214.
- Bester, H., Lange, K.W. (1972) Abschaeztung mittlerer Werte fuer die Diffusion von Kohlenstoff, Sauerstoff, Wasserstoff, Stickstoff und Schwefel in festem und fluessigem Eisen. *Archiv fuer das Eisenhuettenwesen*, 3, 207–213.
- Yamaguchi, W. (2008) First-principles calculations of the grain-boundary cohesive energy – embrittling or strengthening effect of solute segregation in a bcc FeE3(111) grain boundary. *J. Japan Inst. of Metals*, 72(9), 658.
- Hippisley, S.A., Rauh, H., Bullough, R. (1984) Stress-driver solute enrichment of crack-tips during low-ductility intergranular fracture of low-alloy steel. *Acta Metallurgica*, 32(9), 1381–1394.
- Hondros, E.D., Seah, M.P. (1977) Segregation to interfaces. *Int. Metals Rev.*, 12, 288–292.
- Zhebynev, D.A., Ukolova, O.G., Gelman, A.A. et al. (1985) Study of chemical composition of diffusion zone in solid phase Ti-6 % Al-4 % V alloy joint. Method of scanning Auger spectroscopy. *Fizika i Khimiya Obrab. Materialov*, 6, 108–114.
- King, H.W. (1982) Atomic size parameters for the elements. *J. Phase Equilibria*, 2(4), 527.
- Dico, P., Ocelik, V., Hajko, V. et al. (1987) Porusovanie pasok kovovych skiel pri monotonnom Tahovom zatavovaní. *Kovove Materialy*, 25(5), 523–536.



# IMPROVEMENT OF METHOD FOR ESTIMATION OF THE RISK OF FRACTURE WITHIN THE THINNING ZONE ON WALLS OF MAIN PIPELINES

V.I. MAKHNENKO, E.A. VELIKOIVANENKO, G.F. ROZYNKA and N.I. PIVTORAK

E.O. Paton Electric Welding Institute, NASU, Kiev, Ukraine

It is shown that application of the mathematical models, which are based on elimination of such assumptions as direct normals and a plane stress state, in deformation of the thinning zone in pipeline walls and presence of one local critical point with extreme (determinate) fracture conditions allows revealing the effect of peculiarities of an internal or external defect on a limiting pressure, as well as behaviour of a material within the deformation range from the beginning of plastic flow to fracture.

**Keywords:** welded pipelines, wall thinning, risk of fracture, improvement of estimation method, probability of fracture, Weibull law parameters, limiting pressure, external (internal) thinning defects

Numerous experimental tests and treatment of emergency fractures of modern gas pipelines show that fracture of metal within the zone of different thinnings of the pipe walls under conditions of intensive biaxial loading occurs at relatively low plastic strains acting in this region (up to 2.5–3.0 %). At such strains the main mechanism of fracture is cleavage, taking place under the effect of corresponding effective normal stresses at the fracture centre. This concept of fracture is also used in recommendations [1], where a criterion of the limiting state is permissible minimal thickness  $\delta_{\min}$  of the pipe wall within the thinning zone with initial dimensions  $s_0$  along the pipe generating line and  $c_0$  along the circumference, which is determined as follows:

$$\delta_{\min} \leq [\delta] R_j(s_0, c_0, D, [\delta]), \quad (j = s, c), \quad (1)$$

where  $[\delta]$  is the calculated permissible thickness of the pipe wall at a given point at the absence of thin-

ning; and  $R_j$  is the value depending upon  $[\delta]$ ,  $s_0$ ,  $c_0$  and pipe diameter  $D$  [1] ( $0.2 \leq R_j < 1.0$ ).

These recommendations [1] have been well verified experimentally and are accepted as an approximate, rather conservative approach to estimation of acceptability of thinning defects. In this case, ignored are such factors as external or internal thinning defect, defect geometry within dimensions  $s_0$ ,  $c_0$ ,  $(\delta - \delta_{\min}) = a$ , properties of a material in the form of deformation resistance in a region above the yield stress and before fracture due to cleavage at critical strains of about 2.5–3.0 %, which are approximately an order of magnitude higher than those outside thinning, at which the value of  $[\delta]$  is determined at a stage of pipeline design.

The question of stochasticity of a number of geometric data with regard to thinnings, as well as of mechanical properties of a material within the thinning zone after a long-time operation often arises in practical estimations of the risk of fracture.

The task of this study was to develop the calculation algorithms to be used to answer the above questions at reasonable costs while investigating behaviour of different local thinnings on pipelines under loading conditions.

For this, it was necessary to choose a model of deformation of the pipe wall, not relating it to the main hypotheses of thin-walled shells (direct normal and plane stress state), as well as a model of fracture of a material at relatively low strains, where stochasticity of initiation of fracture has not yet been forgotten due to a developed plastic flow

The deformation model is based on the 3D mathematical description in the cylindrical system of coordinates  $r$ ,  $z$ ,  $\beta$  of the deformed region of the pipeline wall (Figure 1) delineated by coordinate planes  $z = \text{const}$ ,  $\beta = \text{const}$  with an internal or external defect, the surface of which is set by the following equation:

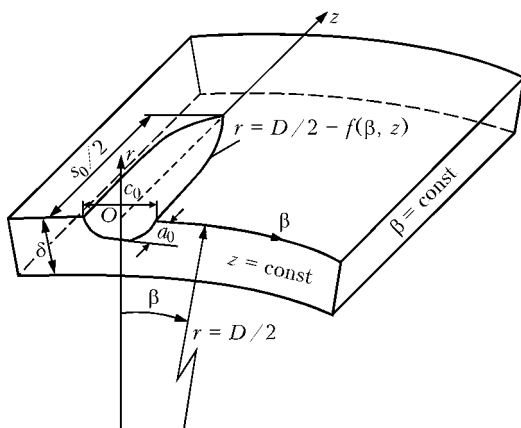


**Figure 1.** Schematic of the region of pipeline wall (region  $V$ ) cut out by coordinate planes  $z = \text{const}$  and  $\beta = \text{const}$ , and thinning defect with dimensions  $a$ ,  $s_0$  and  $c_0$



$$r = \frac{D}{2} - f(\beta, z). \tag{2}$$

$$d\varepsilon_{ij}^p = d\lambda(\sigma_{ij} - \sigma). \tag{7}$$

The boundary conditions set at the boundary planes (Figure 1) and surface of the defect correspond to those set for the entire pipe with no allowance for thinning, which is quite acceptable at sufficiently local thinning dimensions  $s_0$  and  $c_0$ .

Classical relationships between components of strain tensor  $\varepsilon_{ij}$  and displacement vector  $U_i$  in the context of the theory of low elasto-plastic strains [2] hold inside region  $V$  limited by the above boundary planes and surface of the defect, i.e.

$$\begin{aligned} \varepsilon_{rr} &= \frac{\partial U_r}{\partial r}, \quad \varepsilon_{\beta\beta} = \frac{U_r}{r} + \frac{\partial U_\beta}{r\partial\beta}, \quad \varepsilon_{zz} = \frac{\partial U_z}{\partial z}, \\ 2\varepsilon_{r\beta} &= \frac{1}{r} \frac{\partial U_r}{\partial\beta} + r \frac{\partial}{\partial r} \left( \frac{U_\beta}{r} \right), \quad 2\varepsilon_{z\beta} = \frac{\partial U_\beta}{\partial z} + \frac{\partial U_z}{r\partial\beta}, \\ 2\varepsilon_{rz} &= \frac{\partial U_r}{\partial z} + \frac{\partial U_z}{\partial r}. \end{aligned} \tag{3}$$

Relationships (3) are also valid for components of strain increment tensor  $\Delta\varepsilon_{ij}$  and displacement increment vector  $\Delta U_i$  used at plastic deformation in the context of the theory of elasto-plastic flow.

Components of stress tensor  $\sigma_{ij}$  inside region  $V$  meet equilibrium equations, i.e.

$$\begin{aligned} \frac{\partial}{\partial r} (r\sigma_{rr}) + \frac{1}{r} \frac{\partial \sigma_{r\beta}}{\partial\beta} + \frac{\partial \sigma_{rz}}{\partial z} &= \sigma_{\beta\beta}, \\ \frac{\partial}{\partial r} (r\sigma_{r\beta}) + \frac{1}{r} \frac{\partial \sigma_{\beta\beta}}{\partial\beta} + \frac{\partial \sigma_{\beta z}}{\partial z} &= 0, \\ \frac{\partial}{\partial r} (r\sigma_{rz}) + \frac{1}{r} \frac{\partial \sigma_{z\beta}}{\partial\beta} + \frac{\partial \sigma_{zz}}{\partial z} &= 0. \end{aligned} \tag{4}$$

Relation between the stress tensor and displacement increment within the framework of the theory of elasto-plastic flow can be written down as follows:

$$d\varepsilon_{ij} = d \left[ \left( \frac{\sigma_{ij} - \sigma}{2G} \right) + K\sigma \right] + d\lambda(\sigma_{ij} - \sigma), \tag{5}$$

$(i, j = r, z, \beta),$

where  $d\lambda$  is the scalar coordinate function, which is determined by the Mises yield condition with isotropic hardening, i.e.

$$\begin{aligned} d\lambda &= 0, \text{ if } f = \sigma_{\text{eq}}^2 - \sigma_s^2(\omega) < 0, \\ &\text{or } f = 0, \text{ but } df < 0, \\ d\lambda &> 0, \text{ if } f = 0 \text{ and } df > 0. \end{aligned} \tag{6}$$

Condition  $f > 0$  is inadmissible.

Here  $\sigma = 1/3(\sigma_{rr} + \sigma_{\beta\beta} + \sigma_{zz})$ ;  $\sigma_{\text{eq}}$  is the equivalent stress for tensor  $\sigma_{ij}$ ;  $\sigma_s(\omega)$  are the deformation stresses for a given material depending upon strain hardening parameter  $\omega$ ;  $\omega = \int d\varepsilon_{\text{eq}}^p$  is the Odquist parameter;  $d\varepsilon_{\text{eq}}^p$  is the increment of equivalent plastic strain for tensor  $\varepsilon_{ij}^p$ ; and

To implement model (2) through (4), this study used the method of step-by-step tracing of loading of volume  $V$  by a growing external load (e.g. internal pressure  $\bar{P}$ ). Yield condition (6) was allowed for at each tracing step by the iteration method [3].

The fracture model is based on an idea of probable fracture due to cleavage within the thinning zone (volume  $V$ ), where maximal main stresses  $\sigma_1$  in this volume meet condition

$$p = 1 - \exp \left[ - \int_V \left( \frac{\sigma_1 - A}{B} \right)^\eta \frac{dV}{V_0} \right], \quad \sigma_1 > A. \tag{8}$$

Integration was carried out only with respect to elementary volumes  $\Delta V$ , for which  $\sigma_1 > A$ ;  $A$ ,  $B$  and  $\eta$  are the parameters of the Weibull three-parameter distribution law; and  $V_0$  is the structural parameter of a given steel at brittle fracture  $V_0^{\text{br}} \sim (0.05 \text{ mm})^3$  at the crack apex and at tough fracture  $\sim h^3$ , where  $h$  is the characteristic size of finite elements providing a sufficiently accurate numerical solution for  $\sigma_1$  by deformation models (2) through (7) within the thinning zone. In other words, the value of  $V_0$  can be assumed to be equal to  $\Delta V$  in breaking down of volume  $V$  (Figure 1) into finite elements. The rest of the parameters in model (8) are determined by comparing the calculation by models (2) through (7) with the corresponding experimental data. Our investigations show that the recommendations of study [1], based on numerous experiments, i.e. expression (1), can be used as a first approximation, assuming that fracture probability  $p$  is not in excess of 0.05.

Certain simplifications can also be made in fracture model (8), allowing for the presence of extreme planes  $\beta = \text{const}$  and  $z = \text{const}$ , where normal stresses  $\sigma_{\beta\beta}$  or  $\sigma_{zz}$  are close to  $\sigma_1$ , and a layer corresponding to  $\beta = \text{const}$  with thickness  $\Delta\beta R$ , or  $z = \text{const}$  with thickness  $\Delta z$  can be assumed to be an integration volume in (8). Allowing for this consideration based on the corresponding experimental data, e.g. [1], and following the principle of the maximum likelihood (minimising the discrepancy by probability  $p$ ) in variation of thinning sizes ( $s_0, \delta_{\text{min}}$ ) parameters  $A, B$  and  $\eta$  can be determined at given geometric dimensions and mechanical properties of the pipeline material. The outcome of this approach shows that the sufficiently good results can be obtained at  $\eta = 4.0$  and  $A = \frac{\sigma_t + \sigma_y}{2}$  ( $\sigma_t$  and  $\sigma_y$  are the tensile strength and yield stress of the material, respectively, in the thinning zone).

The value of  $B$  at the above recommendations with respect to  $V_0$  can readily be checked on the basis of model (8). As a result, the data on  $A, B$  and  $\eta$  for a specific steel, as well as sizes of different shapes of thinning being known, the probability of fracture can be calculated for different geometric parameters of a

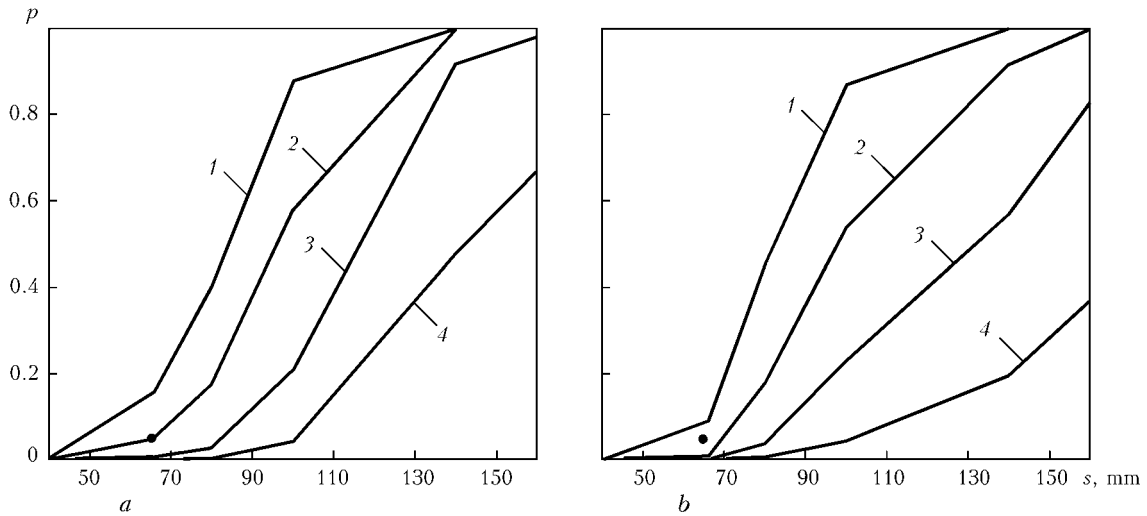


**Figure 2.** Probability of fracture in the defect (wall thinning) zone with  $a = 14$  mm and  $c = 40$  mm, depending on  $s$  and  $\bar{P}$  for external (a) and internal (b) defect in the  $1420 \times 20$  mm pipe at  $\sigma_y = 440$  MPa,  $A = 500$  MPa and  $B = 420$  MPa (● – experimental data): 1 –  $\bar{P} = 10$ ; 2 – 9; 3 – 8; 4 – 7 MPa

pipeline and internal pressure  $\bar{P}$  on the basis of models (2) through (8).

Figures 2 and 3 show the results for the 17G1S steel pipeline with  $D \times \delta = 1420 \times 20$  mm at the presence of a surface wall thinning defect, the shape of which can be described depending upon coordinates  $z, r, \beta$  by the following second-order equation:

$$\left(\frac{R_q - r}{a}\right)^2 + \left(\frac{2z}{s_0}\right)^2 + \left(\frac{D\beta}{c_0}\right)^2 = 1, \quad (9)$$

where  $R_q = D/2$  for the external defect and  $R_q = (D - 2\delta)/2$  for the internal defect; and  $a, s_0$  and  $c_0$  are the dimensions of the defect with symmetry axes  $z = 0$  and  $\beta = 0$ .

Noteworthy among the data in Figures 2 and 3 is a differing load-carrying capacity of the external and internal defects, i.e. resistance to the internal pressure, as well as a substantial effect of the defect depth (value  $a$ ).

As seen from Figures 2 and 3, the external defect is characterised by a lower resistance to the internal

pressure than the internal one. However, this difference is high in the zone of high fracture probabilities ( $p > 0.1$ ), which is of low interest to practice. Therefore, the absence of differentiation of thinning defects between the internal or external ones in study [1] is reasonably justified, based on the data on the external thinning defect in pipeline walls. Nevertheless, this fact should be kept in mind.

The data in Figure 3 for shallower defects ( $a = 10$  mm), compared with the data in Figure 2 for deep defects ( $a = 14$  mm), are characterised by a lower restriction of deformation, lower stresses and, accordingly, lower failure probabilities, this being determined not only by lower stresses, but also by a value of  $B$  at constant  $A = 500$  MPa and  $\eta = 4.0$ . So, based on the above choice according to the given recommendations [1],  $B = 420$  MPa for  $a = 14$  mm in Figure 2, and  $B = 830$  MPa for  $a = 10$  mm.

Of certain interest are the data shown in Figures 4 and 5, which illustrate the effect of dimension  $c$  for a deep thinning with  $a = 14$  mm at constant  $s = 66$  mm on the probability of fracture, according to the model

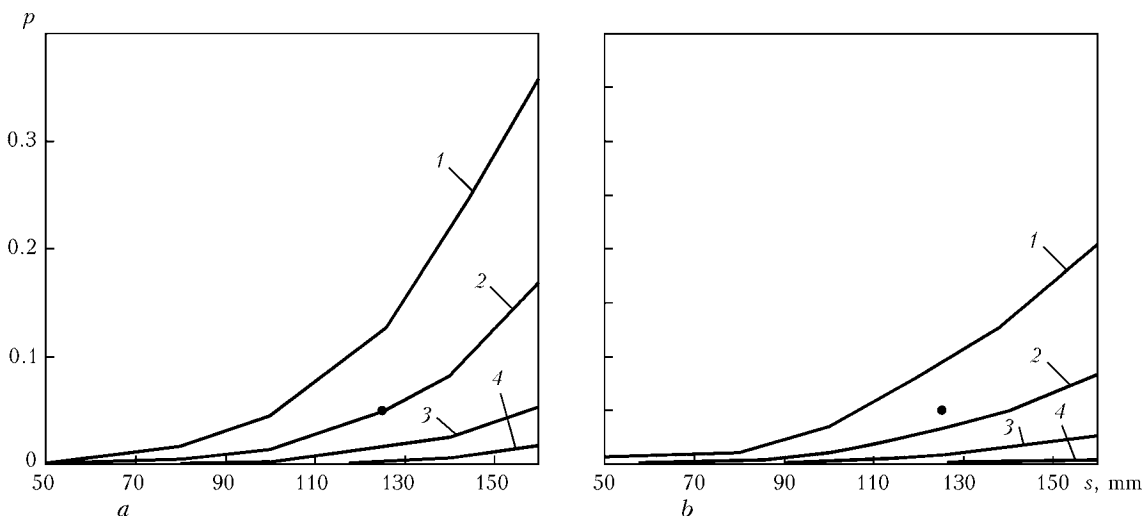


**Figure 3.** Probability of fracture in the defect (wall thinning) zone with  $a = 10$  mm and  $B = 830$  MPa depending on  $s$  and  $\bar{P}$  for external (a) and internal (b) location of the defect (the rest of designations are the same as in Figure 2)

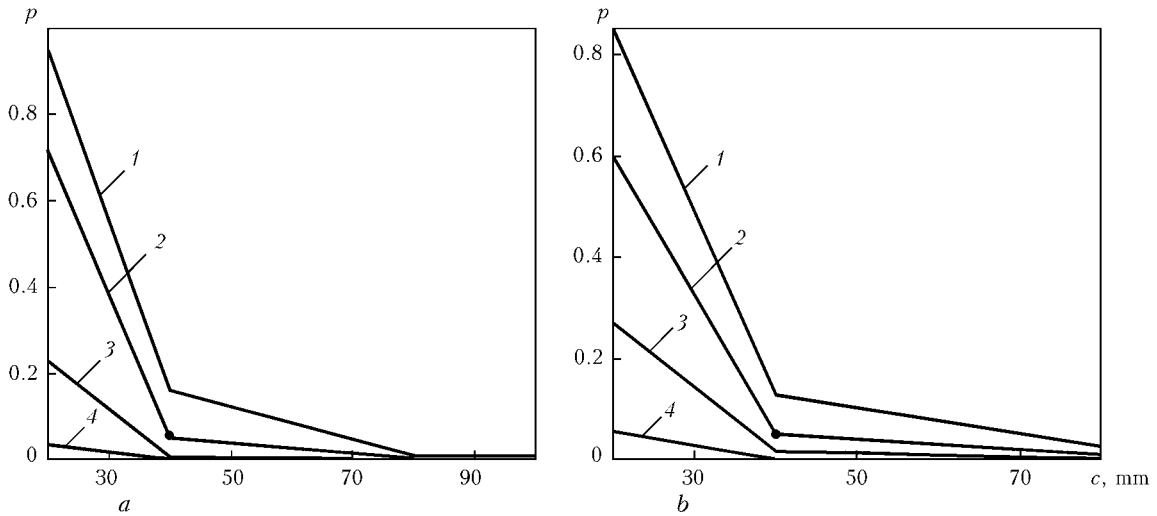


**Figure 4.** Effect of defect width  $c$  on fracture probability  $p$  in a pipe measuring  $1420 \times 20$  mm with  $\sigma_y = 440$  MPa for different  $\bar{P}$  and constant  $s = 66$  mm at the defect depth:  $a - a = 14$  mm,  $B = 420$  MPa;  $b - a = 10$  mm,  $B = 830$  MPa;  $1 - \bar{P} = 10$ ;  $2 - 9$ ;  $3 - 8$ ;  $4 - 7$  MPa

employed. These data on a relatively low effect of the  $c$  value of the thinning defect at sufficiently high  $s$  and  $c$  on the fracture resistance are in good agreement with the experimental data given in [1] and other studies. The new data, compared with this situation, are those of the type shown in Figure 4 at  $c < 20$  mm (comparable with thickness of the pipe wall). In this case, the groove-like thinning defect is close to a crack, and the concentration of stresses grows accordingly, this affecting the value of the failure probability.

When estimating the load-carrying capacity of thinning defects, it is important to know the distribution of load in metal in plastic deformation that leads to a decrease in the concentration of stresses.

Figure 6,  $a$  shows the data on the effect of ratio  $\sigma_t/\sigma_y$  at constant  $1/2(\sigma_t + \sigma_y) = A = 500$  MPa on limiting pressure  $\bar{P}_{limit}$  in a pipe under consideration, measuring  $D \times \delta = 1420 \times 20$  mm, at fracture probability  $p = 0.05$  and presence of a thinning defect with depth  $a = 10$  mm, extended along axis  $s = 140$  mm and along circumference  $c = 40$  mm.

Depending upon Odquist hardening parameter  $\omega$  (6), the use was made of the power law of hardening of a material in deformation:

$$\sigma_s^{(\omega)} = \sigma_y \left( 1 + \frac{\omega}{\varepsilon_0} \right)^m, \text{ where } \varepsilon_0 = \frac{\sigma_y}{E}, \quad m = 0.14.$$

Ratio  $\sigma_t/\sigma_y$  was varied in a range with  $\sigma_t = 350 - 440$  MPa at  $A = 500$  MPa. For pipe steels, such a wide range of variations in  $\sigma_t/\sigma_y$  is unlikely. However, it allows the effect of material deformation conditions beyond the bounds of elasticity on the limiting state within the thinning defect zone to be demonstrated more clearly.

It can be seen that limiting pressure  $\bar{P}_{limit}$  grows with increase in  $\sigma_t/\sigma_y$  at constant  $A = 1/2(\sigma_t + \sigma_y)$ . This effect is attributable to the character of redistribution of load within the defect zone depending upon the level of material yield stress  $\sigma_y$ . The lower the value of  $\sigma_y$ , the more uniform is the distribution of normal stresses within the defect zone under loading, this eventually leading to decrease in probability  $p$ .

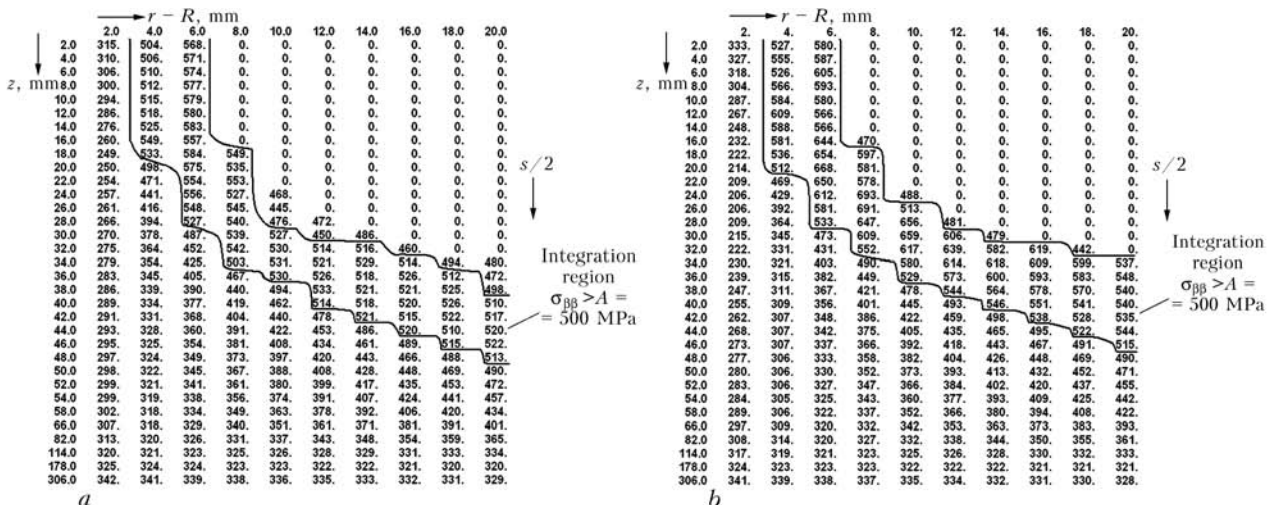


**Figure 5.** Distribution of circumferential stresses  $\sigma_{\beta\beta}$  in symmetry plane  $\beta = \beta_{cr}$  at  $\bar{P}_{limit} = 10$  MPa,  $\sigma_y = 440$  MPa,  $a = 14$  mm,  $s = 66$  mm,  $c = 40$  (a) and 20 (b) mm





# INFLUENCE OF THERMODEFORMATIONAL CYCLE OF HARDFACING ON THE STRUCTURE AND PROPERTIES OF RAILWAY WHEELS AT THEIR RECONDITIONING

A.A. GAJVORONSKY, V.D. POZNYAKOV, V.A. SARZHEVSKY, V.G. VASILIEV and V.Yu. ORLOVSKY  
E.O. Paton Electric Welding Institute, NASU, Kiev, Ukraine

Influence of preheating temperature on delayed fracture of HAZ metal has been assessed. It is established that in order to ensure a high resistance to delayed fracture, preventing cold cracking in the joint HAZ metal, the cooling rate  $w_{6/5}$  should not be higher than 5 °C/s. In this case it is necessary to apply preheating at the temperature above 200 °C.

**Keywords:** arc hardfacing, solid-rolled carriage wheels, HAZ, structure, mechanical properties

Solid-rolled wheels for railway transportation are made of carbon steels subjected to special heat treatment to achieve the required strength and wear resistance. Comparative composition and mechanical properties of wheel steels are given in Tables 1 and 2. Carbon content in steels is equal to 0.44–0.67 wt.%, and strength level is higher than 900 MPa. Wheels wear along the rolling profile in service. In view of the features of rolling-friction wheel–rail pair, mostly the wheel flange working surface is exposed to wear. The railway transportation enterprises apply the technologies of flange hardfacing to restore the wheel rolling profile, which is cost-effective. Repairing flange wear by hardfacing allows reducing the waste of rim metal at its mechanical turning along the rolling profile, as well as improving the wheel wear resistance through deposition of metal with preset properties

To restore solid-rolled wheels of freight transportation, made from steel 2, the technologies of single- and twin-submerged-arc welding with solid wires are used [1, 2]. These technologies are based on the results of investigation of weldability of high-strength carbon

steels [2–4]. To recondition the flanges of solid-rolled wheels technological recommendations, as well as special hardfacing and auxiliary equipment have been developed. Submerged-arc hardfacing of wheel flanges is performed in the modes, providing heat input on the level of 10–14 kJ/cm. The technology envisages compulsory application of preheating of wheel rims up to the temperature of 150–200 °C (depending on the used hardfacing process) and postweld delayed cooling of wheels in heat chambers at not more than 50 °C/h rate. In case of fulfillment of a set of requirements made to the hardfacing technology, in particular, process equipment, welding consumables, technique and modes of hardfacing, maintaining the thermal cycle during reconditioning, a high quality of the deposited metal and wheel reliability in operation are guaranteed.

Before 2006, the rolling stock of railway freight transportation in Ukraine and CIS countries was fitted with solid-rolled wheels, made from steel of type 2 with carbon content closer to the lower limit (C ≤ 0.60 wt.%). Starting from 2006, in order to reduce the wear and improve the performance, solid-rolled carriage wheels began to be made from new wheel

**Table 1.** Composition of wheel steels, wt.%

Wheel steel type	C	Mn	Si	V	S, not more than	P, not more than	C <sub>eq</sub> , wt.%
1 (GOST 10791–89)	0.44–0.52	0.80–1.20	0.40–0.60	0.08–0.15	0.030	0.035	0.68
2 (GOST 10791–89)	0.55–0.65	0.50–0.90	0.22–0.45	≤ 0.10	0.030	0.035	0.73
T (TU U 35.2-23365425-600:2006)	0.58–0.67	0.70–0.90	≤ 0.40	0.08–0.15	0.020	0.025	0.79

**Table 2.** Mechanical properties of wheel steels

Wheel steel type	HB	σ <sub>t</sub> , MPa	δ <sub>5</sub> , %, not less than	ψ, %, not less than	KCU <sub>+20</sub> , J/cm <sup>2</sup>
1 (GOST 10791–89)	≥ 248	900–1100	12	21	30
2 (GOST 10791–89)	≥ 255	930–1130	8	14	20
T (TU U 35.2-23365425-600:2006)	≥ 320	≥ 1100	8	14	18



steel of T type, the ultimate strength of which is  $\sigma_t \geq 1100$  MPa, and hardness is more than *HB* 320. Unlike wheel steel of type 2 the new steel has a higher content of carbon (up to 0.67 wt.%) and vanadium (up to 0.15 wt.%). Carbon equivalent  $C_{eq}$  of wheel steel of type T is equal to 0.79 wt.%. Therefore, welded joints of the above wheel steel have a higher cold cracking susceptibility, compared to wheel steel of type 2 ( $C_{eq} \geq 0.73$  wt.%) [5].

This leads to the suggestion that the hardfacing technologies which are used with success at reconditioning of flanges of wheels from type 2 steel cannot be used for repair of higher strength wheels. Hence the need for development of a new technology of hardfacing repair of flanges of railway wheels from wheel steel of type T, which made it necessary to study its weldability.

This work gives the results of experimental studies on assessment of the influence of thermodeformational cycle of welding on the structure, mechanical properties and delayed fracture resistance of HAZ metal of joints of new wheel steel. These studies were performed on wheel steel of type T of the following composition, wt.%: 0.625 C; 0.73 Mn; 0.31 Si; 0.11 V.

Structure of HAZ metal of welded joints made by arc welding processes is heterogeneous, and dimensions of its individual sections are small. Therefore, structural changes, occurring under the impact of thermodeformational cycle of welding and their influence on mechanical properties in the HAZ overheated zone were studied on model samples. For this purpose, Gleeble 3800 system fitted with a thermostat and high-speed dilatometer was used [6]. Studied cylindrical samples had the diameter of 6 mm and length of 80 mm. In keeping with the testing procedure, they were heated up to the temperature of 1200 °C at the rate of 150 °C/s, and then cooled by different thermal cycles, which were selected so that in the temperature range of 600–500 °C the sample cooling rate  $w_{6/5}$  changed in the range from 2.85 to 33 °C/s. Temperature of the start and end of overcooled austenite transformation was determined by the tangent moving away from the dilatometric curve, and the ratio of phases formed as a result of austenite transformation, was established by the line-segment approach [7]. Figure 1 gives the generalized investigation results.

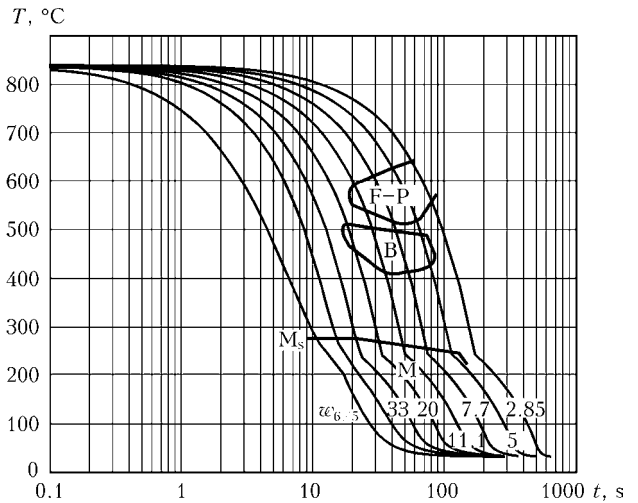


**Figure 1.** Thermokinetic diagram of overcooled austenite transformation in HAZ metal of wheel steel of type T ( $C = 0.625$  wt.%): M – martensite;  $M_s$  – start of martensite transformation; B – bainite; F – ferrite; P – pearlite

As shown by the conducted studies, in wheel steel of type T under the impact of the thermodeformational cycle of welding at cooling rate  $w_{6/5} \geq 33$  °C/s overcooled austenite transformation occurs solely in the martensite region. Temperature of the start of martensite transformation is equal to 280 °C, and quenched metal microhardness is *HV*0.5 594. With lowering of the cooling rate the metal structure forms intermediate phases of ferrite-pearlite mixture and bainite, with lowering of martensite content. At  $w_{6/5} = 20$  °C/s (Figure 2, a) an intermediate bainite transformation of overcooled austenite occurs in the temperature range of 510–450 °C, and martensite transformation starts at 270 °C. The proportion of phases in the structure is equal to 96 vol.% of martensite and 4 vol.% of bainite. Quenched metal microhardness decreases to *HV*0.5 500.

At  $w_{6/5} = 11.1$  °C/s (Figure 2, b) overcooled austenite transformation starts in the ferrite-pearlite region at 500–410 °C with bainite formation, martensite transformation starts at the temperature of 260 °C. Proportion of phases in the structure is as follows, vol.%: 83 martensite, 14 bainite and 3 ferrite-pearlite mixture. Quenched metal microhardness is *HV*0.5 420. At  $w_{6/5} = 7.7$  °C/s (Figure 2, c) volume fraction of martensite component in the structure decreases to 60 %, with 13 % bainite, and ferrite-pearlite



**Figure 2.** Microstructures ( $\times 500$ ) of HAZ metal of wheel steel of type T at  $w_{6/5} = 20.0$  (a), 11.1 (b) and 7.7 (c) °C/s



**Table 3.** Influence of cooling rate on mechanical properties of HAZ metal of wheel steel of type T (C = 0.625 wt.%)

$w_{6/5},$ °C/s	$\sigma_t,$ MPa	$\sigma_y,$ MPa	$\delta_5,$ %	$\psi,$ %	KCU, J/cm <sup>2</sup>	
					+20 °C	-40 °C
5	1140	850	6.3	16.3	7.3	8.5
10	1280	940	3.4	9.6	5.7	4.2
20	1320	980	3.1	9.6	6.0	4.2

**Table 4.** Influence of cooling rate on mechanical properties of HAZ metal of wheel steel of type 2 (C = 0.55 wt.%) [2]

$w_{8/7},$ °C/s	$\sigma_t,$ MPa	$\sigma_y,$ MPa	$\delta_5,$ %	$\psi,$ %	KCU <sub>-40</sub> , J/cm <sup>2</sup>
1.15	940	600	13.3	33.3	6
5.90	970	605	12.9	33.3	6
32.0	1060	715	9.3	24.9	5

volume fraction is equal to 27 %. Quenched metal microhardness decreases to HV0.5 406. At  $w_{6/5} = 5$  °C/s transformation of overcooled austenite occurs in the ferrite-pearlite region already by 77 % at 620–520 °C. At such a cooling rate, martensite content decreases abruptly, and is equal to just 10 vol.%, that of bainite is 13 vol.%, metal microhardness being equal to HV0.5 360. At  $w_{6/5} = 2.85$  °C/s overcooled austenite transformation occurs with formation of just the ferrite-pearlite mixture (HV0.5 358).

With lowering of the cooling rate martensite content in the HAZ metal structure decreases, volume fraction of ferritic-pearlitic component increases, and bainite content is stabilized on the level of 13–14 % with microhardness decreasing more than 1.5 times.

Assessment of the influence of cooling rate on the mechanical properties and impact toughness of wheel steel of type T was performed using model samples treated by the thermodeformational cycle of welding in MSR-75 unit [8]. For this purpose base metal samples of 120 × 12 × 12 mm size were heated by passing current up to 1200 °C at the rate of 150 °C/s. Sample cooling rate was 5, 10 and 20 °C/s. Then the heat-treated blanks were used to cut out standard samples for static tension testing of type II to GOST 1497–84 and impact bending of type I to GOST 9454–78. Table 3 gives mechanical properties of simulated HAZ metal of higher-strength wheel steel. For comparison Table 4 gives the data on the influence of cooling rate on the properties of wheel steel of type 2 with carbon content of 0.55 wt.% [2].

As a result of investigations it was found that at  $w_{6/5} \geq 10$  °C/s, when martensite is the main structural component, HAZ metal of joints of wheel steel of T type features increased strength and low ductility. Compared to steel of type 2 strength of quenched metal is 25–30 % higher, and ductility is almost 3 times lower. In addition, lowering of the ductility level at increase of cooling rate and formation of martensite structure of the metal also runs more intensively. While the values of relative elongation  $\delta_5$  and reduction  $\psi$  of HAZ metal of wheel steel of type 2 decrease by 30 % at increase of cooling rate, in steel of type T quenched metal ductility decreases by 45 %. Here even at relatively small (5 °C/s) cooling rate ductility values of HAZ metal of wheel steel of type T are 1.5 times lower than those of wheel steel of type 2 at high (32 °C/s) cooling rate.

Influence of thermodeformational cycle of welding on the change of impact toughness of new wheel steel is manifested in a similar fashion. It is established that at increase of cooling rate up to 5–20 °C/s impact toughness of HAZ metal at negative temperature decreases almost 2 times. It should be noted that for wheel steel of type 2 at increase of cooling rate to 32 °C/s impact toughness values are lowered by 17 %.

At hardfacing of flanges of solid-rolled wheels tensile residual stresses are formed in the HAZ metal, their maximum level in the longitudinal direction reaching 650 MPa [2]. Therefore, in order to ensure the high cold cracking resistance, it is first of all necessary for wheel steel HAZ metal to have a sufficient ductility margin. This promotes a more complete running of the processes of relaxation of local stresses due to development of microplastic deformations, thus essentially increasing the HAZ metal resistance to delayed cracking [9, 10]. Conducted studies showed that the ductile properties of HAZ metal of wheel steel of type T decrease considerably under the impact of thermodeformational cycle of welding. In this connection it is anticipated that the HAZ metal of welded joints of the new wheel steel will feature a lower resistance to delayed cracking.

This value of the HAZ metal of higher strength wheel steel was evaluated by applying the universally known Implant method [5]. Unlike the traditional method the implants of 6 mm diameter from the studied steel were made without a notch [11]. Blanks from high-strength low-alloyed steel were used as the technological plates. The sample was inserted into a hole of the technological plate with a gap. Welding and loading of the samples were performed in a specialized unit, produced at PWI. During comparative testing, mechanized CO<sub>2</sub> welding with Sv-08G2S wire of 1.2 mm diameter was used in the modes ensuring the heat input on the level of 11.5 kJ/cm. Sample preheating temperature was varied from 20 up to 200 °C, this allowing adjustment of the HAZ metal cooling rate in the range of 25–5 °C/s.

Figure 3 gives the results of investigation of preheating temperature influence on critical fracture stresses of HAZ metal of new higher strength wheel steel. As is seen from the Figure, in welding without preheating ( $T_0 = 20$  °C), when a predominantly martensitic component forms in the structure under the impact of the thermodeformational cycle ( $w_{6/5} \sim$

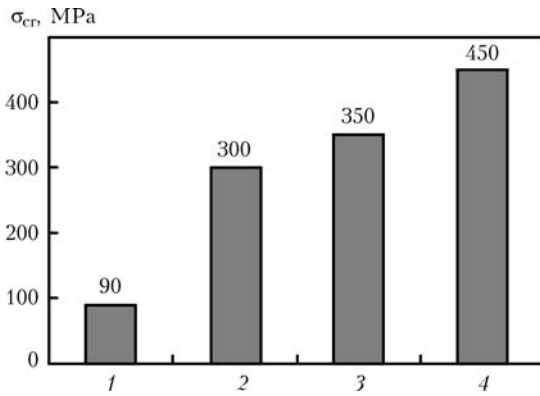


**Figure 3.** Influence of preheating temperature on delayed fracture resistance of HAZ metal of wheel steel of type T: 1 – 20; 2 – 70; 3 – 100; 4 – 150 °C

~ 25 °C/s) HAZ metal of wheel steel of type T has a low level of delayed fracture resistance. Critical fracture stresses  $\sigma_{cr}$  are equal to just about 90 MPa. Application of preheating promotes an essential increase of delayed fracture resistance. At preheating at  $T_0 = 70$  °C, when the cooling rate is  $w_{6/5} \approx 15-18$  °C/s and in the HAZ metal structure the overcooled austenite transformation occurs with formation of intermediate phases, values of critical fracture stresses increase up to 300 MPa. At  $T_0 = 100$  °C ( $w_{6/5} \approx 10-15$  °C/s)  $\sigma_{cr} = 350$  MPa. At  $T_0 = 150$  °C ( $w_{6/5} \approx 7-10$  °C/s), when the HAZ metal forms structures with minimum content of the martensitic component,  $\sigma_{cr}$  values increase up to 450 MPa. In this case, critical fracture stresses are equal to approximately  $0.45\sigma_y$  of HAZ metal or  $0.40\sigma_t$  of wheel steel base metal. At increase of preheating temperature up to  $T_0 = 200$  °C and higher ( $w_{6/5} < 5$  °C/s), when the overcooled austenite transformation in the HAZ metal runs solely with formation of ferrite-pearlite mixture, no delayed fracture of implants takes place.

Thus, analysis of thermokinetic diagram of overcooled austenite transformation of new higher strength wheel steel shows that under the impact of thermodeformational cycle of welding at cooling rate  $w_{6/5} \geq 7.7$  °C/s a quenching structure forms in the HAZ metal of the new wheel steel, in which the martensite component fraction is higher than 60 vol.%. HAZ metal has high strength values ( $\sigma_t \geq 1280$  MPa) and low ductility, which determines its increased susceptibility to delayed fracture at static loading. Under

such cooling conditions the critical breaking stresses are not higher than  $0.45\sigma_y$  of HAZ metal ( $0.40\sigma_t$  of wheel steel).

In order to increase the delayed fracture resistance and prevent cold cracking in the joints (deposits) of higher strength wheel steel, it is necessary for cooling rate  $w_{6/5}$  in the HAZ metal not to exceed 5 °C/s. Lowering of the cooling rate to the specified level is possible in the case of application of preheating to 200 °C and higher.

The given investigation results are the basic ones in development of technological recommendations on hardfacing the flanges of higher strength wheels. In order to achieve a high quality of the deposited metal and reliability of wheels in operation, it is necessary to conduct additional investigations on assessment of the technological factors on the strength of joints at static and cyclic loads. Such investigations are currently being conducted at PWI.

- Pavlov, N.V., Kozubenko, I.D., Byzova, N.E. et al. (1993) Hardfacing of flanges of car wheel pairs. *Zheleznodorozhn. Transport*, **7**, 37–40.
- Sarzhevsky, V.A., Gajvoronsky, A.A., Gordonny, V.G. et al. (1996) Effect of technological factors on structure and properties of HAZ metal in repair-and-renewal hardfacing of flanges of solid-rolled car wheels. *Avtomatch. Svarka*, **3**, 22–27, 33.
- Kuzmina, G.D., Kiselev, S.N., Voronin, N.N. et al. (1997) Dilatometric characteristics and diagrams of anisothermal decomposition of austenite in wheel steel of grade 2. *Svarochn. Proizvodstvo*, **12**, 3–5.
- Kiselev, S.N., Voronin, N.N., Kuzmina, G.D. et al. (2000) Investigation of thermal processes and structure formation in twin-arc hardfacing of car wheels based on computer simulation. *Ibid.*, **3**, 3–8.
- Makarov, E.L. (1981) *Cold cracks in welding of alloy steels*. Moscow: Mashinostroenie.
- Grigorenko, G.M., Kostin, V.A., Orlovsky, V.Yu. (2008) Current capabilities of simulation of austenite transformation in low-alloyed steel welds. *The Paton Welding J.*, **3**, 22–24.
- Cherepin, V.T. (1968) *Experimental technique in physical metals science*. Kiev: Tekhnika.
- Sarzhevsky, V.A., Sazonov, V.Ya. (1981) Unit for simulation of thermal cycles of welding based on MSR-75 machine. *Avtomatch. Svarka*, **5**, 69–70.
- Alekseeva, L.E., Sarrak, V.I., Suvorova, S.O. et al. (1975) About two ways of residual microstress relaxation in martensite of steel. *Metallofizika*, Issue 61, 79–84.
- Sarrak, V.I., Filippov, G.A. (1976) Delayed fracture of steel after tempering. *Fiz.-Khimich. Mekhanika Materialov*, **12**, 44–54.
- Sterenbogen, Yu.A. (1986) Some factors determining the resistance of HAZ metal of martensitic steels to cold cracking. *Avtomatch. Svarka*, **6**, 5–8.



# STRUCTURAL STATE OF RAPIDLY QUENCHED Cu–Ti SYSTEM BRAZING FILLER METAL

S.V. MAKSYMOVA<sup>1</sup>, V.F. KHORUNOV<sup>1</sup> and G.M. ZELINSKAYA<sup>2</sup>

<sup>1</sup>E.O. Paton Electric Welding Institute, NASU, Kiev, Ukraine

<sup>2</sup>G.V. Kurdyumov Institute for Metal Physics, NASU, Kiev, Ukraine

It has been established that the strip of a rapidly quenched brazing filler metal is in the amorphous state with a uniform distribution of alloying elements in its width. Temperature ranges of transition of the brazing alloy from the amorphous to crystalline state have been determined. X-ray examination of phase composition of the rapidly quenched strip in the initial state and after isothermal annealing has been conducted, the  $\delta$ -CuTi and  $\gamma$ -CuTi crystalline structures being identified in the latter case.

**Keywords:** *brazing, brazing filler metal, Ti–Cu system, structure, phase composition, amorphous and crystalline state, super rapid quenching, isothermal annealing, X-ray diffraction analysis*

Amorphous metal alloys attract attention of many researchers owing to their unique properties, such as high mechanical characteristics, corrosion resistance, electromagnetic indicators, etc. [1].

Application of brazing filler metals in the amorphous state opens up new opportunities in the field of brazing. One of the key advantages of amorphous brazing filler metals is their chemical homogeneity. These brazing filler metals provide good wetting of the base metal surface, feature high capillary activity, diffusion activity of their components, and uniform distribution of the latter within the brazing zone, thus reducing the probability of formation of brittle phases and providing the optimal strength of brazed joints. The brazing filler metals are characterised by high viscosity, this making it possible to manufacture imbedded elements of the required size and dispense the brazing filler metal in fabrication of unique critical structures applied in different industrial sectors [2].

The purpose of this study was to conduct comparative investigations of structural peculiarities of rapidly quenched brazing filler metal Ti<sub>57</sub>Cu<sub>47</sub> in the initial and annealed states, as well as evaluate thermal stability of its amorphous state in heating.

Alloys produced by rapid cooling of the melt (quenching) are classed with rapidly quenched alloys. Structure and properties of the rapidly quenched alloys are substantially different from those of the cast alloys produced by traditional melting methods. Depending upon the cooling rate, they may have a highly dispersed dendritic, microcrystalline, nanocrystalline or amorphous structure [3].

The method of rapid ( $1 \cdot 10^4$ – $1 \cdot 10^6$  °C/s) solidification of the melt on the external fast-rotating cooling disk is most widely applied to produce brazing filler metals in the amorphous state [4, 5]. Under the pressure of inert gas, the molten metal passes through the

nozzle and gets to the external surface of the rotating disk, where it solidifies in the form of a thin strip, which is removed under the effect of centrifugal forces. Ductile thin amorphous foils (strips) can be produced even from brittle alloys (eutectic, intermetallic) by super rapid quenching. When cooled at a high rate, such systems tend to suppress formation of centres of the above phases and reach the amorphous state even in the absence of amorphising agents, such as boron, silicon, phosphorus, etc.

The rapidly quenched Ti<sub>57</sub>Cu<sub>43</sub> strips, 30–50  $\mu$ m thick and about 20 mm wide, were used for investigations. As shown by metallography, the typical structure of a free surface of the Ti<sub>57</sub>Cu<sub>43</sub> amorphous strip in contact with air is smooth and mirrored (glassy), and features the absence of any depression or roughness (Figure 1, a).

The underside of the strip in contact with the disk surface has irregularities (Figure 1, b) caused by surface geometry of the disk material, its rotation velocity, etc. Important factors for production of rapidly quenched strips are temperature of overheating above the liquidus line of the melt, alloy viscosity, surface tension and wetting of the disk material with the melt.

It should be noted that rapid quenching of the melt is accompanied by formation of a temperature gradient in a direction normal to the strip plane, which leads to concentration heterogeneity in distribution of elements through thickness of the strip. As a result, surface layers adjoining the free side of the strip are enriched with lighter elements, whereas heavier elements prevail in surface layers on its contact side [6]. The rapidly quenched strip of the brazing filler metal under investigation was produced using no chemical amorphising elements. Investigation of chemical heterogeneity in a cross section of the strip showed that the brazing filler metal components are uniformly distributed along the scanning line (Figure 2).

Investigations of structural state of the rapidly quenched brazing filler metal in the initial and annealed states were performed by the radiography method using diffractometer DRON-3 in MoK $\alpha$ -radia-

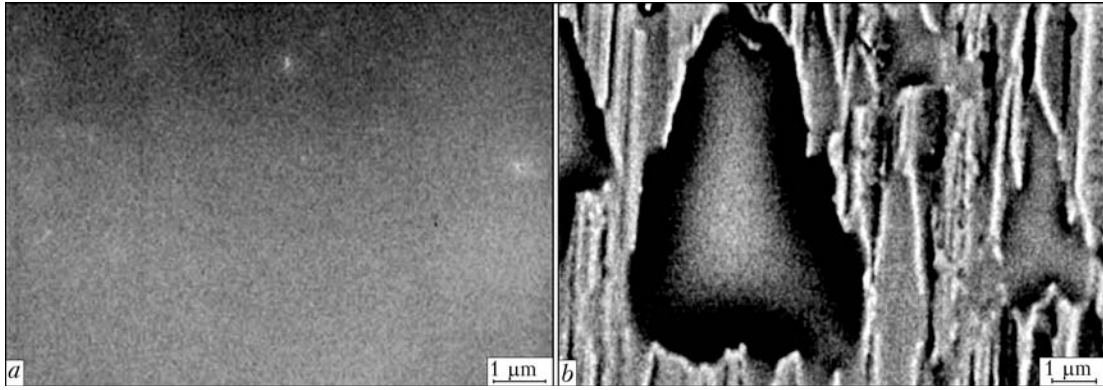


Figure 1. Surface of rapidly quenched strip in contact with air (a) and with disk surface (b)

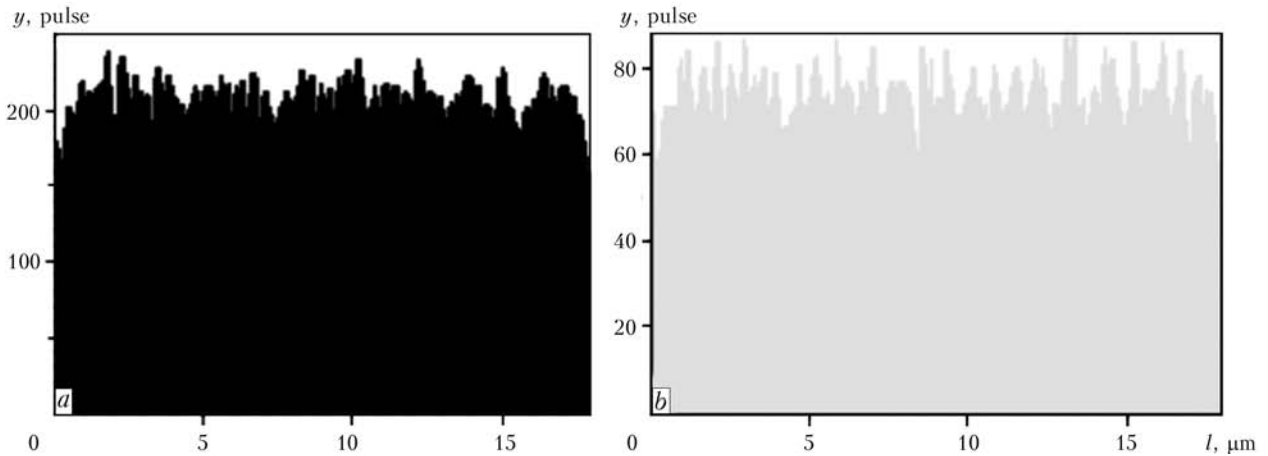


Figure 2. Distribution of titanium (a) and copper (b) in width of rapidly quenched strip ( $y$  – quantity of pulses)

tion in the scanning mode at a step of  $0.1^\circ$  in a range of the main maximum and  $0.5^\circ$  at other distances. Graphite monochromator was placed at the primary beam. Modes of the recording equipment were selected so that they eliminated noise, fluorescent scattering from a specimen, as well as radiation from the continuous spectrum with the  $\lambda/2$  wavelength transmitted by the monochromator crystal.

The method of correction for incoherent scattering, polarisation, absorption and fluorescent scattering by a specimen, as well as normalisation of diffraction curves were standard [7, 8].

It is a known fact that metal glasses give a diffraction pattern similar to that of metal liquids. There-

fore, the experimental design and mathematical tool of Fourier transformation, which is used to investigate liquids, were employed to study their structure [7].

Structural factor  $i(s)$  and radial atom distribution function (RADF) were calculated for brazing filler metal  $Ti_{57}Cu_{43}$ . Main structural characteristics, i.e. position  $s_1$ , height  $i(s_1)$ , width at half-height (half-width)  $\Delta s_{1/2}$  of the first maximum of the structural factor, position  $r_1$  and area  $A$  of the first maximum of RADF were determined from  $i(s)$  and RADF.

Results of X-ray diffraction analysis showed that the diffraction pattern of composition of the brazing filler metal was typical [9] of the amorphous state,

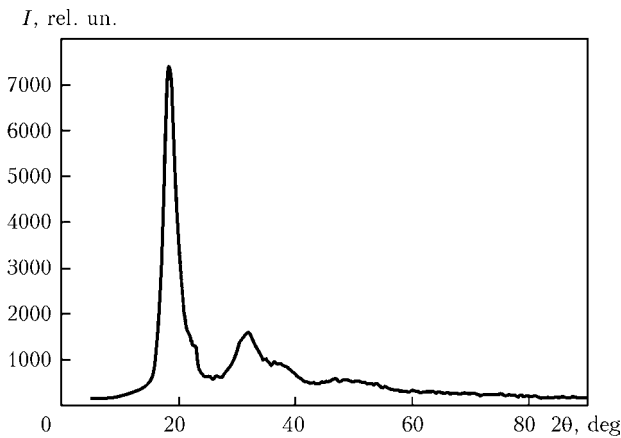


Figure 3. Diffraction curve of amorphous strip

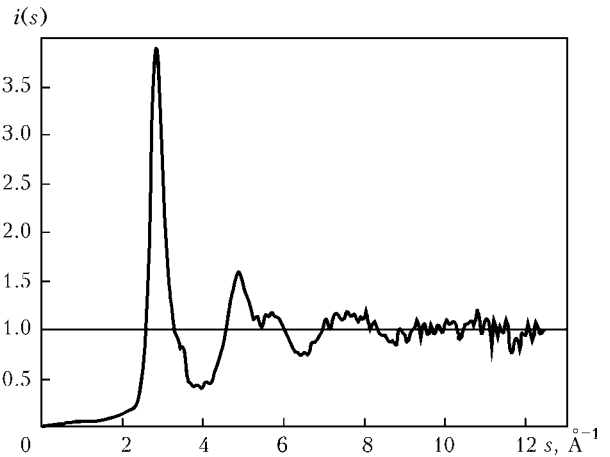


Figure 4. Structural factor of amorphous strip

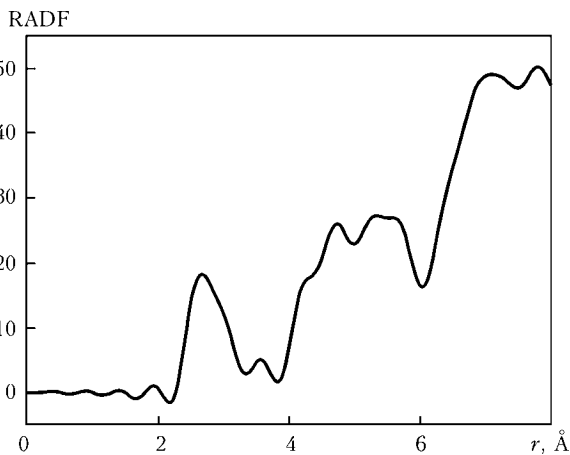


Figure 5. RADF curve

comprising diffusion maxima (Figure 3) with a clearly defined effect of bifurcation of the second maximum of  $i(s)$  (Figure 4). A bulge can be seen on the right branch of the first maximum of structural factor  $i(s)$  at  $s \approx 3.5 \text{ \AA}^{-1}$ . The RADF curve has asymmetry of the first maximum and additional maximum in a region of  $r \approx 3.6 \text{ \AA}$  (Figure 5). This is indicative of the fact that the first diffraction maximum and the first maximum of RADF, like in the case of atomic structure of the melts consisting of two or more components, can be considered a superposition of several maxima, which are caused by existence of several types of atomic groups differing in type of topological and compositional ordering of atoms [7].

Two exothermic thermal effects and one endothermic effect were fixed (Figure 6) in investigation of a melting temperature range by high-temperature differential thermal analysis (in helium atmosphere at a heating and cooling rate of  $80 \text{ }^\circ\text{C}/\text{min}$ ).

The presence of the first insignificant exothermic effect in a temperature range of  $460\text{--}480 \text{ }^\circ\text{C}$  proves the fact of occurrence of structural relaxation, which decreases the level of quenching stresses in different microvolumes and precedes solidification. As the temperature is increased, maximal heat release takes place at  $500 \text{ }^\circ\text{C}$ , this leading to volume solidification of the alloy and indicating to a relatively low thermal stability of the amorphous (metal-stable) state of the rapidly quenched strip. The exothermic effect is absent

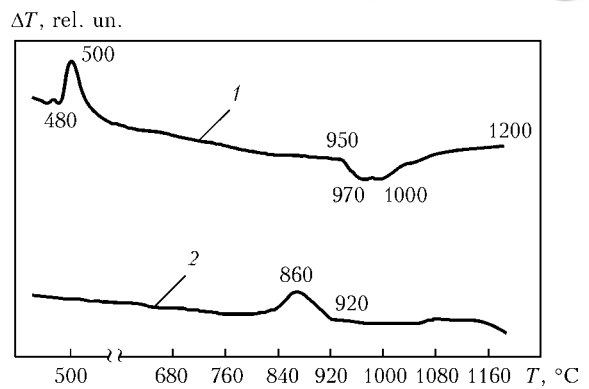


Figure 6. Thermogram of rapidly quenched strip of brazing filler metal  $\text{Ti}_{57}\text{Cu}_{43}$  in heating (1) and cooling (2)

in a case of complete structural relaxation [6]. The endothermic effect takes place with further increase in temperature, this being indicative of complete melting of the brazing filler metal. The melt solidifies in cooling, and only one thermal effect is fixed in the thermogram. This character of distribution of thermal effects evidences the presence of the amorphous state in the rapidly quenched strip.

According to the data of high-temperature differential thermal analysis, low-temperature isothermal annealing was carried out in vacuum at a temperature of  $510 \text{ }^\circ\text{C}$  (and at  $400 \text{ }^\circ\text{C}$ , for comparison) for 1 h.

After annealing, the free surface of the strip had a wavy geometry (Figure 7, a), rather than a mirrored (glassy) one, which is characteristic of the initial state. The underside of the strip in contact with the disk surface remained almost unchanged (Figure 7).

Low-temperature annealing of amorphous alloys causes structural relaxation of residual stresses and leads to reorganisation of their local structure (change in arrangement of atoms, their ordering) [6]. For example, annealing at a low temperature ( $400 \text{ }^\circ\text{C}$ ) hardly affects structure of the rapidly quenched strip (Figure 8, a, b). However, one should note formation of structural microregions with a blurred interface appearing between them.

At an annealing temperature increased to  $510 \text{ }^\circ\text{C}$ , the contrast of microstructure aggravated, and structural changes became more clearly defined (Figure 8, c, d). The surface acquired a slightly pronounced cellular structure with broadened boundaries (Figure 8,

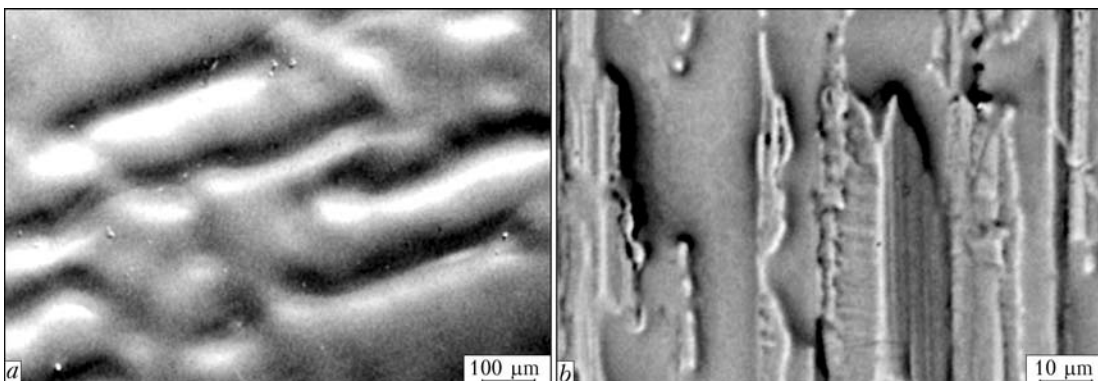


Figure 7. Strip surface in contact with air (a) and disk surface (b) after isothermal annealing at  $510 \text{ }^\circ\text{C}$

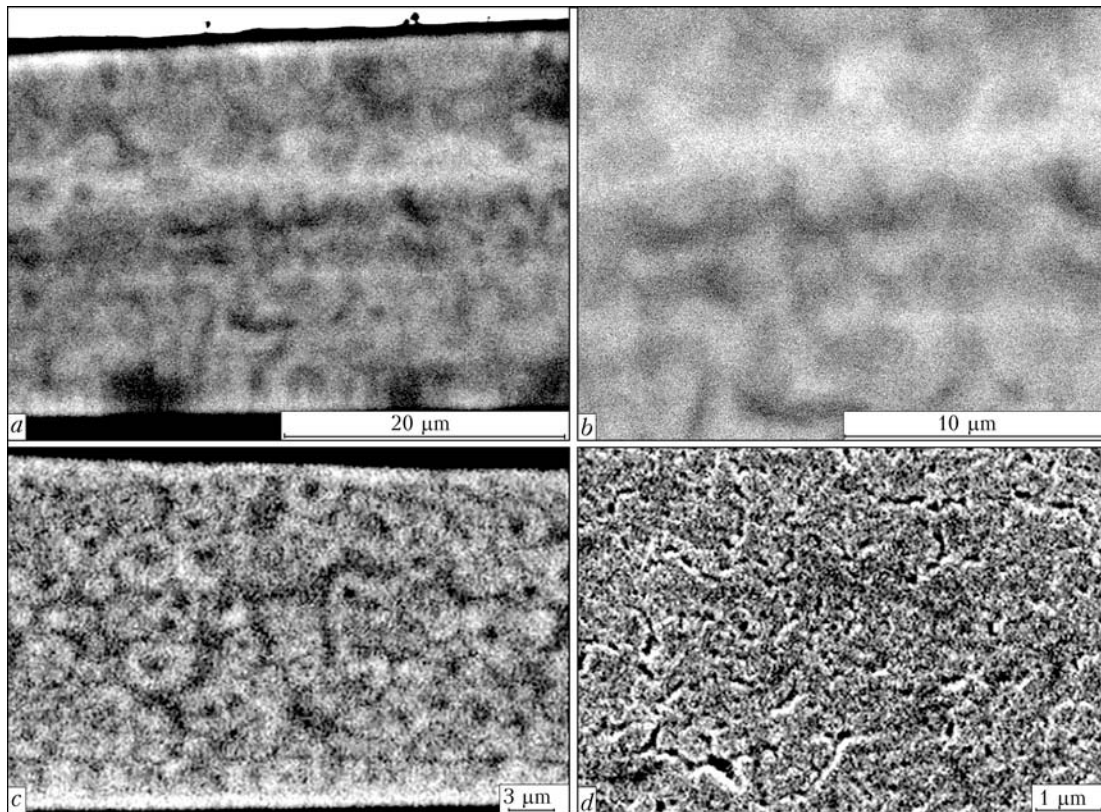


Figure 8. Strip microstructures after isothermal annealing at 400 (a, b) and 510 (c, d) °C

c), which is characteristic of the initial stage of decomposition of the amorphous state. Chemical etching of the annealed specimen revealed appearance of interfaces between individual microvolumes (Figure 8, d).

A typical diffraction pattern of the amorphous state was observed after annealing of the Ti<sub>57</sub>Cu<sub>43</sub> strip at 400 °C.

On the one hand, this system is characterised by a complete absence of amorphising non-metals, such as boron, silicon, etc. But, on the other hand, it belongs to the eutectic type with the presence of intermetallic compounds.

It is a known fact that the presence of intermetallic compounds with a complex type of the crystalline lattice in a system is a key factor of the glass-forming

ability of alloys, which allows achieving the amorphous state.

For instance, the glass-forming ability in the Cu–Ti system is caused by the eutectic character of interaction of glass-forming intermetallic phases, such as CuTi and CuTi<sub>2</sub> [1]. An important feature evidencing that a given chemical compound of a particular type has a glass-forming ability is its formation in solidification from the amorphous state during heating.

These data are in good agreement with the results of X-ray diffraction analysis of alloy Ti<sub>57</sub>Cu<sub>43</sub>, obtained in isothermal annealing in vacuum. For example, the δ-CuTi and γ-CuTi<sub>2</sub> crystalline structures were identified in alloy Ti<sub>57</sub>Cu<sub>43</sub> after its transition from the amorphous state to the crystalline one (Figure 9).

Therefore, when using amorphous brazing filler metals to produce permanent joints by brazing with a long heating, its initial stages are characterised by structural relaxation of the amorphous state with further transition into the crystalline one. Brazing is performed with a brazing filler metal in the microcrystalline state. Finer investigation methods, including high-temperature metallography, are required to study this process in more detail.

Amorphous state of the used brazing filler metal has a positive effect, first of all, on its practicability. Owing to high viscosity, small thickness and chemical homogeneity, the brazing filler metal provides the high quality of brazing, absence of defects (in the form of lacks of penetration) and high strength of the brazed joints. Application of the investigated brazing

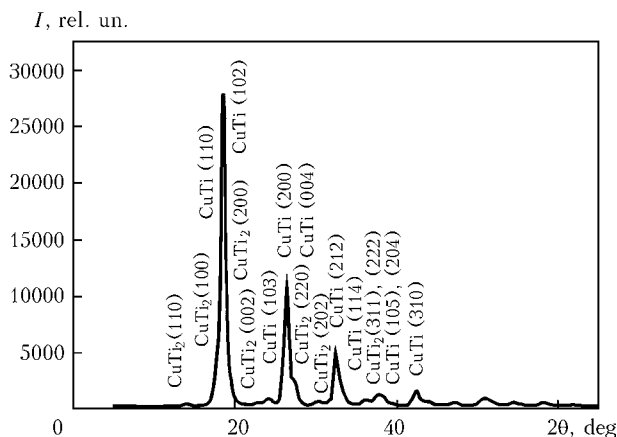


Figure 9. X-ray pattern obtained after isothermal annealing of the brazing filler metal



filler metal in the amorphous state for brazing of precipitation-hardened copper alloy of the Glidcop Al-25 grade provided the brazed joints with a tensile strength of 80–90 % of that of the base metal [10].

It can be concluded from the above-said that rapidly quenched brazing filler metal  $Ti_{57}Cu_{43}$  in the form of a strip is X-ray amorphous. Isothermal annealing at 510 °C leads to transformation of the alloy from the amorphous state to the crystalline one, in which the  $\delta$ -CuTi and  $\gamma$ -CuTi<sub>2</sub> crystalline structures are identified.

1. Kovneristy, Yu.K. (1999) *Volume-amorphising metal alloys*. Moscow: Nauka.
2. Khorunov, V.F., Maksymova, S.V. (2005) Amorphous filler alloys – promising material for advanced brazing processes (Review). *The Paton Welding J.*, **10**, 33–38.
3. Fatkhullin, O.Kh. (2005) State-of-the-art in metal science of rapidly quenched heat-resistant alloys. *Tekhnologiya Lyog. Splavov*, **1–4**, 24–31.
4. Kalin, B.A., Fedotov, V.T., Sevryukov, O.N. et al. (1996) Amorphous brazing filler metal strips. Experience of development of the manufacturing technology and application. *Svarochn. Proizvodstvo*, **1**, 15–19.
5. Kalin, B.A., Plyushchev, A.N., Fedotov, V.T. et al. (2001) Effect of structural state of brazing filler metal on physical-mechanical properties of brazed joints. *Ibid.*, **8**, 38–41.
6. Shpak, A.P., Kunitsky, Yu.A., Lysov, V.I. (2002) *Cluster and nanostructural materials*. Kiev: Akadempriodika.
7. Nemoshkalenko, V.V., Romanova, A.V., Iliinsky, F.G. (1987) *Amorphous metal alloys*. Kiev: Naukova Dumka.
8. Romanova, A.V. (1995) Some historical facts and memories about development of notions of atomic structure of liquid and metal glasses. *Metallofizika, Novejshie Tekhnologii*, **8**, 3–29.
9. Golder, Yu.G. (1978) Metal glasses. *Tekhnologiya Lyog. Splavov*, **6**, 74–93.
10. Maksimova, S.V., Khorunov, V.F., Shonin, V. A. et al. (2002) Vacuum brazing of dispersion-strengthened copper alloy Glidcop Al-25. *The Paton Welding J.*, **10**, 13–17.

## INFLUENCE OF WORKING DISTANCE OF WELDING ELECTRON GUN ON WELD GEOMETRY

O.K. NAZARENKO and V.I. ZAGORNIKOV

E.O. Paton Electric Welding Institute, NASU, Kiev, Ukraine

Geometry of electron beam penetrations in a wide range of gun to workpiece distances was experimentally studied. A weak correlation was established between the gun to workpiece distance and penetration depth in thick metals. The possibility of substantially increasing of working distance without a marked change in the penetration parameters is attributable to a corresponding decrease of the convergence angle of the beam within the workpiece region.

**Keywords:** *electron beam gun, welding gun, working distance, weld depth, focal point, angle of beam convergence*

No international standard on spatial characteristics of welding electron beam has been introduced so far, despite a high interest to the issue of interaction of beam parameters and weld geometry [1, 2]. Focal spot dimensions, i.e. beam minimum section in the welded workpiece plane, are quite often specified in the requirements to welding electron gun. It is believed that a small spot is the main condition for formation of deep welds with minimum transverse dimensions of the cast zone and with simultaneous improvement of secondary electron image of the welding zone. As the focal spot dimensions are directly proportional to the welding gun working distance, many operators are trying to place it as close as possible to the workpiece, despite a concurrent increase of the probability of electric breakdowns in the accelerating gap of the gun, because of metal vapour and gas penetration from the weld pool.

At electron beam welding of thin metal (up to several millimetres), when surface supply of thermal energy is performed and there is practically no crater in the weld pool, dimensions of minimum beam section on the workpiece surface indeed determine the dimensions of the cast zone at other conditions being equal.

However, when the weld forms in the metal of the thickness of tens and even hundreds of millimetres, focal spot dimensions proper no longer determine the cast zone dimensions, and spatial characteristics of the so-called focal depth of the beam, or, in other words, its isthmus, along the length of which the averaged specific energy density in the beam is practically constant, have a much greater role. The longer the isthmus, the easier it is to form a weld of maximum depth with practically parallel side walls. Therefore, it is correct to state that the angle of inclination of side walls of the cast zone is largely determined by the overall configuration of the beam in the isthmus region.

Experimental study of the geometry of electron beam penetrations in a broad range of welding gun working distances, the results of which are discussed below, has been performed as a stage of preparation of normative materials on equipment and technology of electron beam welding.

**Experimental procedure and obtained results.** Experiments were performed using ELA-60 power unit with 60 kV accelerating voltage. Schematic of electron-optic system is given in Figure 1. The gun is fitted with tablet LaB<sub>6</sub>-cathode with radius  $r_{\text{cath}} = 1.5$  mm, working temperature  $T_{\text{cath}} = 2000$  K. Middle of non-magnetic gap of the focusing electromagnetic lens is located at distance  $a = 120$  mm from beam

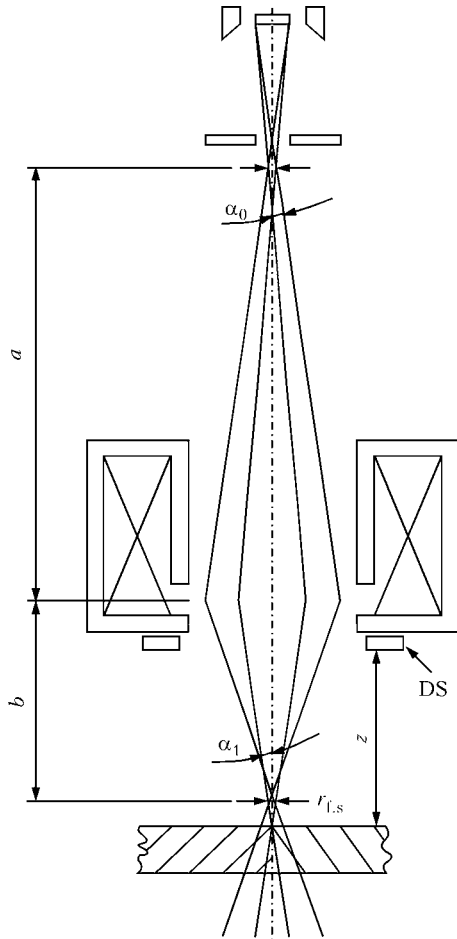


**Figure 1.** Schematic of electron optical system of ELA-60 gun: *a*, *b* – distances from the middle of lens non-magnetic gap to the crossover and focusing plane, respectively;  $\alpha_0$ ,  $\alpha_1$  – half-angles of beam divergence after the cross-over and beam convergence above the isthmus, respectively; DS – deflecting system; *z* – working distance;  $r_{f,s}$  – focal spot radius

cross-over – minimum beam section at emission system outlet. Lens inner diameter  $D = 40$  mm, non-magnetic gap width  $S = 18$  mm.

As transverse beam dimensions considerably depend on the coefficient of spherical aberration of the lens, let us assess it using the following relationships, where lens magnification  $M = b/a$  [3]:

$$\frac{C_{sph}}{S} = \left[ \frac{a}{S} \right]^3 \left[ 1 + \frac{1}{M} \right] p(x) \left[ \frac{1 + 1/M}{a/S} q(x) + 1 \right], \quad (1)$$

$$x = D/S, \quad (2)$$

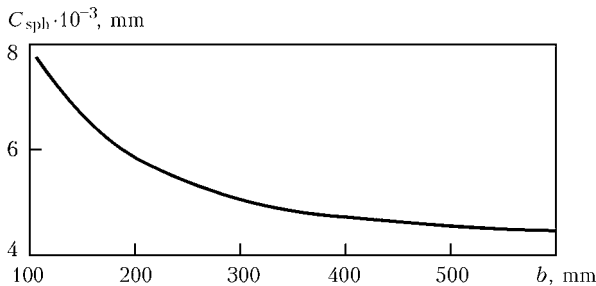


**Figure 2.** Calculated dependence of the coefficient of spherical aberration of magnetic lens of ELA-60 gun on non-magnetic gap-focusing plane distance

$$q(x) = 0.26x - 0.25, \quad (3)$$

$$p(x) = \frac{2.46}{x + 0.47} - 0.28. \quad (4)$$

For  $b = 100-600$  mm calculated values of the coefficient of spherical aberration of the applied focusing lens  $C_{sph}$  are given in Figure 2.

Experiments were performed on plates of low-carbon steel 09G2S 65 mm thick and stainless steel 12Kh18N10T 8 mm thick. Beam focusing plane was located below plate surface at the depth of 32 and 4 mm, respectively, penetration being incomplete, and the plates proper being mounted at an angle of about  $10^\circ$  to the horizon with the purpose of finding the maximum depth as accurately as possible. Location of maximum penetration depth was determined by location of minimum width of the cast zone on plate surface, where sections were cut out for macrosection preparation. Thick plates were located at the following distances from gun edge: 20, 100, 220 and 470 mm, and thins ones – at distances of 45, 125, 245 and 495 mm, respectively. Values  $b = 120$  mm (lens magnification  $M = 1$ ), 220 mm ( $M = 1.7$ ), 320 mm ( $M = 2.7$ ) and 570 mm ( $M = 4.75$ ) correspond to working distances in each case. Welding speed of 5 mm/s and beam power of 24 kW for 65 mm thick metal, welding speed of 25 mm/s and beam power of 4.8 kW for 8 mm metal were unchanged,  $U_{acc}$  being 60 kV in both the cases.

Figure 3 gives the obtained results for different distances to the workpiece.

**Discussion of results.** Obtained experimental data unambiguously point to a weak correlation of penetration depth and distance to the workpiece. At beam power of 4.8 kW just a comparatively small reduction of penetration depth is observed with increase of gun to workpiece distance from 45 up to 495 mm.

In case of application of 24 kW beam in the range of gun to workpiece distances of 200 to 600 mm the penetration depth is practically constant. At minimum distance to the workpiece of 20 mm when focal spot diameter is minimum, penetration depth turned out to be by 25 % smaller than at large working distances.

To clarify the obtained experimental results, let us perform estimation of spatial characteristics of the beam depending on its length. When making the calculations, let us proceed from the fact that beam transverse dimensions are determined by thermal velocities of electrons, spherical aberration and magnification of focusing lens. Owing to a high stability and small pulsations of power unit parameters, we will neglect the influence of chromatic aberration of the magnetic lens on beam transverse dimensions. Influence of beam volume charge is also neglectable, as it is compensated by positively charged ions near the anode opening [4].

Assuming beam radius to be the distance from beam axis to circumference line, where current density de-

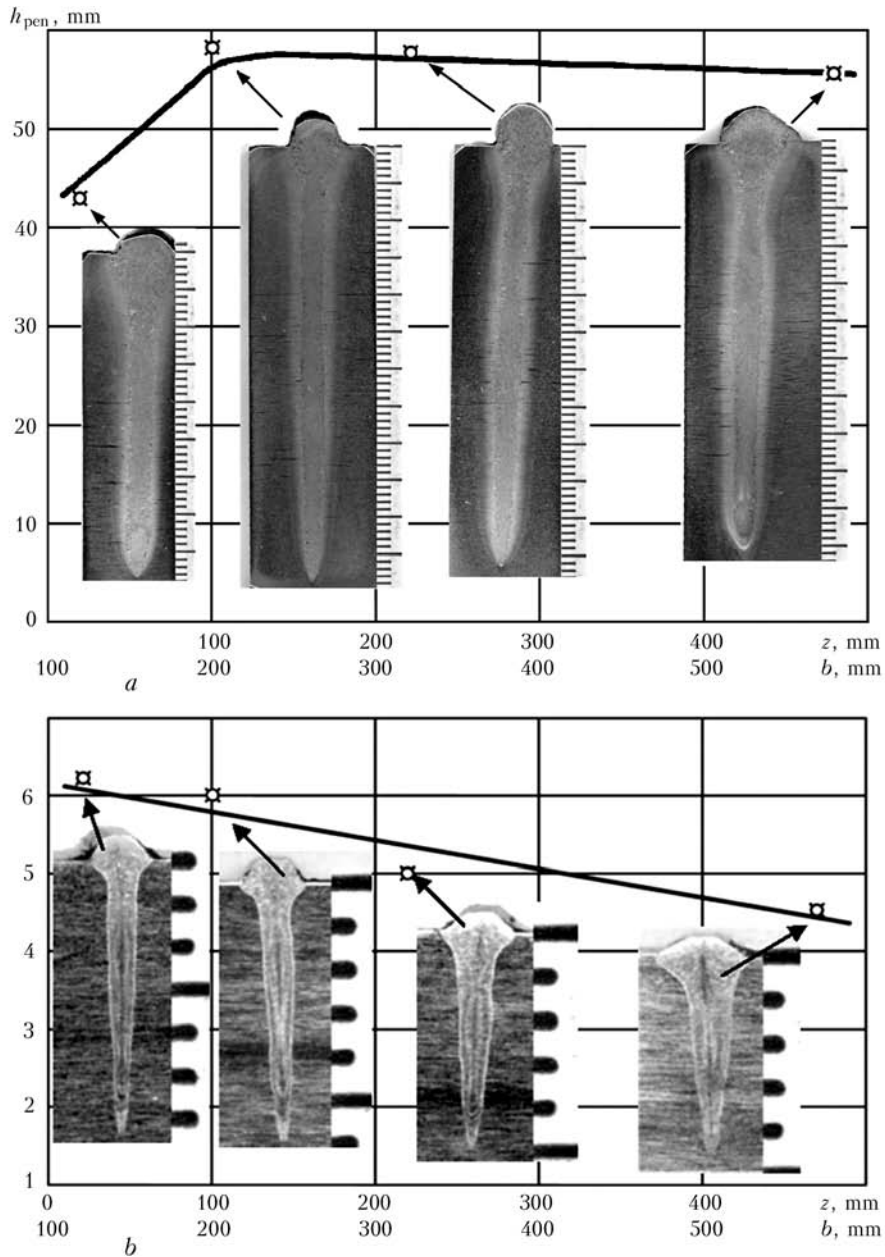


**Figure 3.** Change of penetration depth and transverse macrosections at different distances to the workpiece for steel 09G2S ( $w_b = 24$  kW) (a) and 12Kh18N10T (48 kW) (b)

creases  $e = 2.718$  times relative to current density on beam axis, according to Langmuir, we have

$$r_{cr} = r_{cath} \left\{ \frac{T}{11600 U_{acc}} \right\}^{0.5} \frac{1}{\alpha_0} \quad (5)$$

If beam crossover is projected on the welded work-piece plane by a magnetic lens, free of spherical aberration, beam radius on the workpiece is equal to

$$r_1 = M r_{cr} = r_{cath} \left\{ \frac{T}{11600 U_{acc}} \right\}^{0.5} \frac{1}{\alpha_1} \quad (6)$$

If the electrons have no thermal velocities, but the lens is characterized by spherical aberration, beam radius on the workpiece is equal to

$$r_2 = (M + 1)^4 C_{sph} \alpha_1^3 \quad (7)$$

In the real case, the focal spot radius can be presented as follows:

$$r_{f.s.} = (r_1^2 + r_2^2)^{0.5} \quad (8)$$

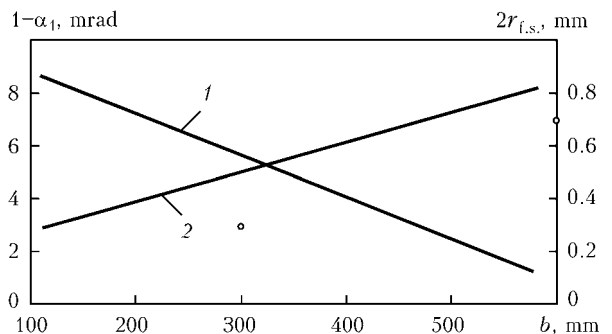


**Figure 4.** Calculated dependencies of half-angle of convergence (1) and focal spot radius (2) for different distances  $b$



Hence we have [5]

$$\alpha_1 = 0.87 \frac{1}{M+1} \frac{r_{\text{cath}}^{0.25} (T/11600)^{0.125}}{C_{\text{sph}}^{-0.25} U_{\text{acc}}^{0.125}}, \quad (9)$$

$$r_{f.s} = 1.33(M+1) \frac{r_{\text{cath}}^{0.75} C_{\text{sph}}^{-0.25} (T/11600)^{0.375}}{U_{\text{acc}}^{0.375}}. \quad (10)$$

Results of assessment of the radius and half-angle of beam convergence in the plane of the workpiece, removed to different distances from the gun, are given in Figure 4.

As follows from Figure 4, at increase of the distance from the middle of the gun non-magnetic gap to the workpiece practically by 5 times (from 120 to 570 mm) the focal spot radius increases 3 times. However, owing to a decrease of the angle of convergence of the beam, the length of beam isthmus increases and, accordingly, the depth and geometry of the cast zone of formed penetrations changes only slightly.

A certain decrease of penetration depth at a limit small working distance is attributable to the fact that value of half-angle of beam convergence of  $10^{-2}$  rad is critical for the experimental conditions, as the isthmus length turns out to be insufficient for formation of a deeper penetration.

## CONCLUSIONS

1. While in electron beam welding of 3–4 mm thick metal geometrical dimensions of penetration are de-

termined by cross-sectional radius of low-power electron beam, in welding thick metal by a higher-power beam, respectively, the depth of the cast zone depends on the length of beam isthmus, which is determined by the angle of convergence of the beam on the workpiece.

2. Length of the isthmus of the beam, formed by a specific welding gun, changes only lightly in a rather wide range of distances to the workpiece, therefore the cast zone depth remains practically unchanged.

3. For the most widely used welding guns of ELA-60 type of 10–60 kW power the recommended optimal distance from gun edge to the workpiece is 150–200 mm, allowing for the need for a good reflection of the butt zone in secondary electrons.

1. Menhard, C., Loewer, T. (2009) The electron beam geometry – definition, measurement and significance for the welding process. *Welding and Cutting*, 8(3), 138–142.
2. Mladenov, G., Koleva, E. (2007) Evaluation and some applications of the electron beam emittance. In: *Proc. of 7th Int. Conf. on Beam Technology* (17–19 April 2007, Halle, Germany), 85–92.
3. Der-Shvarts, G.V. (1971) To calculation of spherical aberration of axisymmetric magnetic lenses. *Radiotekhnika i Elektronika*, 7, 1305–1306.
4. Nazarenko, O.K., Kajdalov, A.A., Kovbasenko, S.N. et al. (1987) *Electron beam welding*. Ed. by B.E. Paton. Kiev: Naukova Dumka.
5. Bas, E.B., Cremonnik, G., Lerch, H. (1962) Beitrag zum Problem der Erzeugung des Elektronenstrahles fuer Schmelzen. *Verdampfen, Schweißen und Rohren mit Elektronenstrahlen: Schweizer Archiv fuer angewandte Wissenschaft und Technik*, 112–121.



## 10th International Conference-Exhibition «Corrosion-2010»

June 8–10, 2010

Lvov, H.V. Karpenko Physico-Mechanical Institute of the NAS of Ukraine

### Conference topics

- ◇ fundamental aspects of corrosion and corrosion-mechanical fracture
- ◇ hydrogen and gas corrosion
- ◇ new corrosion-resistant materials
- ◇ thermal, galvanic and other coatings
- ◇ inhibitory and biocidal protection
- ◇ electrochemical protection
- ◇ methods of investigation and corrosion control
- ◇ anti-corrosion protection of oil and gas industry equipment
- ◇ anti-corrosion protection of power and chemical equipment
- ◇ corrosion and economic problems
- ◇ problems of training corrosion experts

Phone/Fax: (031) 263-15-77

E-mail: corrosion2010@ipm.lviv.ua

http://www.corrosion2010.ipm.lviv.ua



# RELIABILITY OF WELDED STRUCTURE OPERATION. ASSESSMENT AND CONTROL

B.E. PATON<sup>1</sup>, L.M. LOBANOV<sup>1</sup>, A.Ya. NEDOSEKA<sup>1</sup>, A.Yu. FEDCHUN<sup>2</sup>, A.A. YOLKIN<sup>2</sup> and B.M. OBODOVSKY<sup>2</sup>

<sup>1</sup>E.O. Paton Electric Welding Institute, NASU, Kiev, Ukraine

<sup>2</sup>Odessa Priportovy Zavod, Odessa, Ukraine

The paper presents the technology and instrumentation for NDT of the condition of welded structures with assessment of breaking load and residual life. The predicted breaking load and residual life are determined during operation at working load. Application of the system in control of equipment at Odessa Priportovy Zavod is described.

**Keywords:** *welded structures, operating reliability, technical diagnostics, acoustic emission, strength*

Some time ago we dreamt that a time will come, when it will be possible to sufficiently accurately determine the condition of a particular structure, whether it should be put out of service, or it is still capable of operation [1]. Now developments in the field of material strength, diagnostics and prediction of their serviceability, computational and measuring instrumentation have made such a progress that there appeared a possibility of practical implementation of such methods. Developed technologies allow remote assessment from one center and prediction of the condition of an operating structure, whatever its location. This is a significant achievement of science and technology. Monitoring from routine and labour-consuming process is gradually turning into convenient office control. We can already see the future, when continuous monitoring systems will operate in all the high-risk facilities of Ukraine, providing safety and reliability of their operation [2].

Modern progress of engineering led to development of large-sized welded metal constructions, operating under rather complicated conditions. Such objects, primarily, include large-sized storages of hazardous substances, ship hulls, blast furnaces, their air heaters and charging equipment, TV towers, tower-pipes of thermal power plants more than 300–500 m long, power plants proper, bridges, super-capacity walking excavators, tower cranes of shipbuilding yards, compressor units of gas pipelines, etc.

Reliable operation of the above metal structures is mainly determined by load-carrying capacity of their load-carrying parts and welded components. However, calculation of load-carrying capacity of structural elements, providing sufficient reliability, is difficult for a number of reasons.

At present difficulties in assessment of the condition of welded metal structures are overcome in most cases by taking design decisions during their development by specifying high margins for the main strength properties. This not only makes the construction more

expensive, but also lowers its technical and cost parameters.

Such an approach involves high time and labour consumption and costs, and does not always yield the desirable results, and it is very difficult to reproduce the entire range of operating conditions at testing of complex structures. Under the actual conditions, a structure can operate in modes essentially different from those accepted at testing and even more so from those used in calculations of its load-carrying capacity.

A means for solving the problem of ensuring safe operation of welded structures is development of information-measuring systems, allowing assessment of structure reliability already at the testing stage, as well as monitoring performance of structures or prototype model directly in operation.

The purpose of this paper is analysis of PWI developments in the field of technology and instrumentation for continuous monitoring of welded structures, as well as realization of these developments in industry.

Current progress of means of computer engineering, radio electronics, applied mathematics, test procedures, science of material strength and continuum mechanics allows solving the problem of continuous monitoring of performance for various types of welded structures.

Operation of information-measurement system requires regular acquisition of real-time data, primarily, on the state of structure components and various kinds of defects, which accumulate during service. In case of availability of data on the structure and appropriate processing of this information, it is possible to quickly assess its load-carrying capacity in real time.

This, in particular, can yield considerable technical and cost benefits in those fields of engineering, where because of a lack of knowledge of actual operating loads, costly full-scale structures are tested to fracture to obtain strength characteristics and develop technical documentation for their batch production.

Overall scope of work in the field of development of «intelligent» structures fitted with continuous monitoring systems with issuing recommendations to



Figure 1. General view of OPZ ammonia storage

service personnel, has increased lately [1–7]. Monitoring systems of this kind should ensure the ability of the structure to provide information on its state, its suitability or unsuitability for further operation, define conditions, at which further operation of the structure remains to be safe.

Beginning from 1978, Odessa Priportovy Zavod (OPZ) started operating four isothermal tanks designed for storage and transfer of ammonia, supplied to the plant by a special pipeline from Toliatti, and further reloaded into tanker partitions [8, 9]. General view of ammonia storage of 34,000 m<sup>3</sup> volume, 52 m in diameter and 21 m height is given in Figure 1.

Volume of ammonia transfer was equal to about 5 mln t per year, including 1 mln produced directly in the plant.

Ammonia production, storage and overloading belong to the hazardous production sphere. Therefore, in 2002, when the specified term of operation of storage and equipment of the plant was over, a meeting of scientific-technical board of the plant was conducted, in which the need to take additional measures to ensure their further safe operation was noted. Meeting of scientific-technical board took a decision to develop a 10-year plan of fitting the plant with con-



Figure 2. General view of OPZ ammonia production shop

tinuous monitoring systems of the main productions, based on advanced monitoring technologies allowing timely assessment and prevention of an emergency situation with process equipment, without interrupting its operation. In keeping with the plan, work on development of such instrumentation and its mounting on structures of the main productions using ammonia was started.

The first diagnostic system for ammonia storage monitoring, based on acoustic emission (AE), was developed by PWI together with Videoton Company, Hungary. The system was mounted on ammonia storage ST-4 and commissioned in 2003. During the next three years continuous monitoring equipment was mounted on three more storages, and in 2006 and 2007 such instrumentation began operating in ammonia production shops (Figure 2).

Figure 3 gives a block diagram of the technology providing a solution for the defined problem. Technology is based on information coming from AE transducers. There are two data-processing modules. The first module is that of preprocessing, where measurement data are brought into a format, required for analytical module operation. In the second module the data are step-by-step converted into values predicting the breaking load and residual life of the operating structure. The technology further envisages specialist training for operation of monitoring equipment, development together with the state bodies of normative documents required for operation. Measuring components of the instrumentation are certified, and required documents are issued. The entire package of work accompanying supply of diagnostic equipment, is sufficient for successful practical operation in the enterprises and plants.

Diagnostic system put into operation in OPZ storages already at the start of its functioning has found propagating microdefects in the region of welding ammonia pumping pipe holders to the case of storage cylindrical shell. Defects were found in locations, which were not subject to control earlier according to current normative documentation, and were sites, where more serious damage can form later on, accumulating with time. Thus, a qualitatively new approach to monitoring the state of structures demonstrated its effectiveness directly after commissioning of the monitoring system. Development of instrumentation and technology for monitoring the storage condition allowed for modern achievements in the field of science of the strength of materials, and in the field of computational and measuring instrumentation.

Many years of PWI activity in the field of development of AE-based information-measuring systems, as well as experience of Videoton Company in the field of instrumentation development, allowed designing, manufacturing and commissioning commercial control-diagnostic equipment for long-time continu-

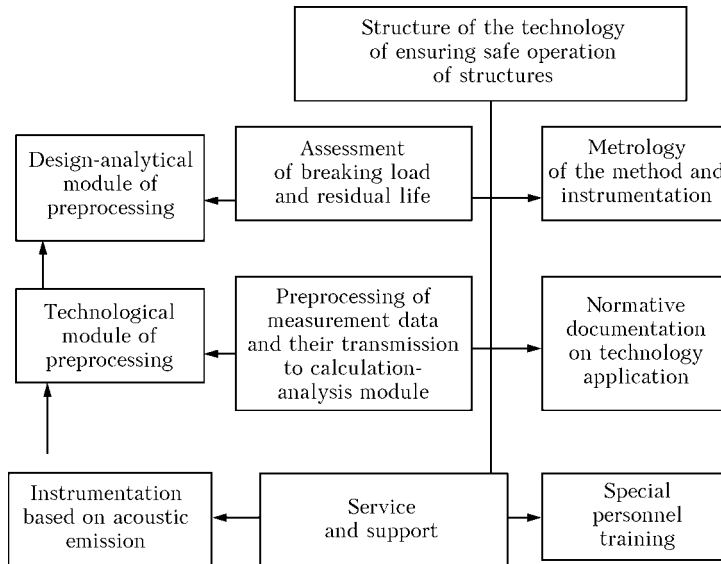


Figure 3. Schematic of technology of EMA-3 system control

ous monitoring. By now, four ammonia storages and equipment of two shops for its production have been fitted with it.

Calculation-analytical work on development of diagnostic continuous monitoring system was preceded by investigations of the stressed state of individual components of storage case structure. Walls of cylindrical storage tanks are made of sheets of low-carbon steel of A-537C1 grade (ASTM) of varying thickness, decreasing with its height. It was necessary to assess the storage case and shop equipment with detection and classification of zones with different levels of the stressed state and defects. In particular, it was established that during more than 20 passed years of storage operation the residual welding stresses in welds did not undergo any essential changes, and reached, similar to the initial state, the yield point of materials being welded ( $\sigma_y = 360$  MPa for steels accepted for case manufacture). Figure 4 shows summary residual welding stresses and stresses caused by load from tank filling with liquid ammonia in the chime weld area. As is seen from the Figure, maximum stresses are concentrated in welds, where they reach the yield point in a narrow band of 10–12 mm at tension.

Figure 5 gives a typical block-diagram of a continuous monitoring system, developed specially for

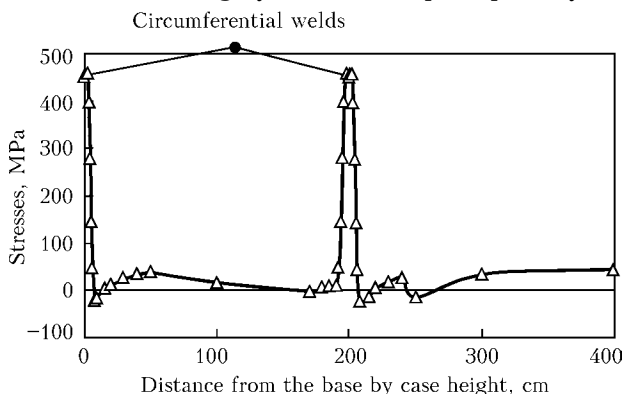


Figure 4. Total stresses in the storage case shell

monitoring ammonia storage and equipment of shops for its manufacturing, with data transmission to plant diagnostic center and for larger distance through the Internet. The diagram includes 57 information chan-

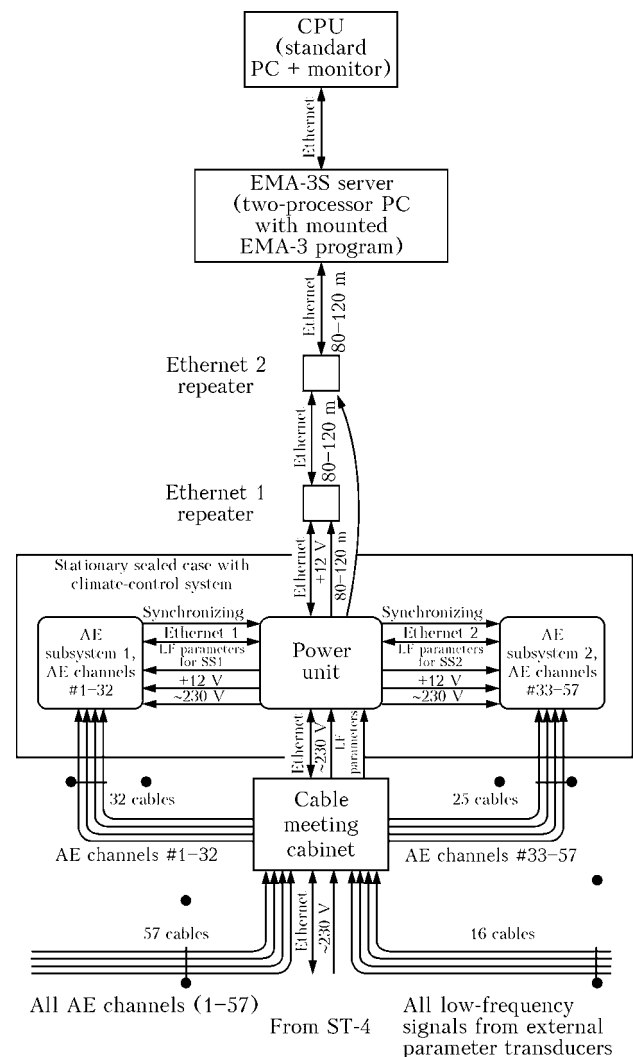


Figure 5. Typical block-diagram of the system of continuous monitoring of OPP equipment

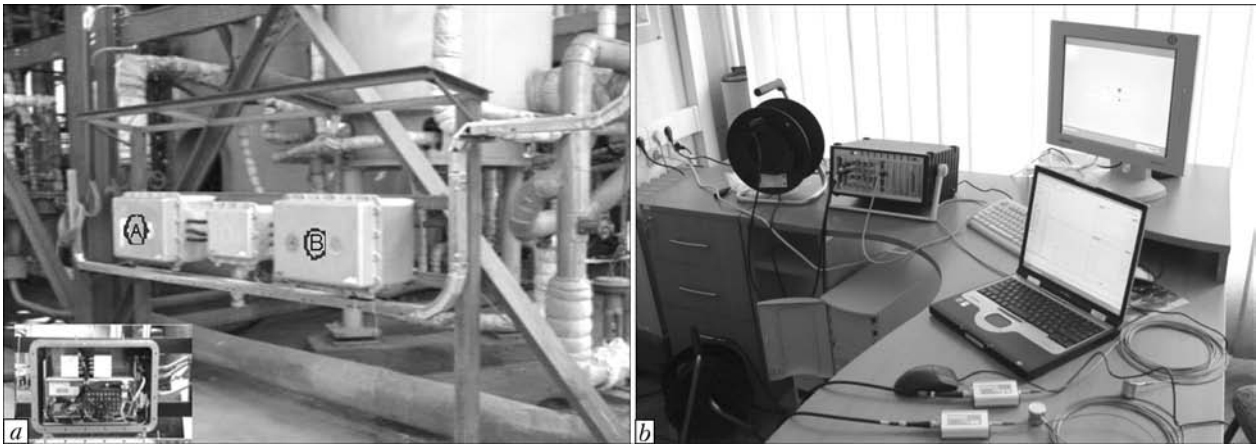


Figure 6. Stationary (a) and mobile (b) variants of diagnostic system of EMA family

nels in each storage (48 acoustic and 9 additional channels, including standby channels), continuously monitoring about  $4 \times 3500 \text{ m}^2$  of storage surface.

Data of measurements come by communication channels to two modules fitted with measuring and computer systems, where data preprocessing is performed. Considering that the modules operate continuously in open air, climate-control inside the modules is envisaged to ensure normal service conditions. Then data come to the central server via communication lines, and the server performs the main data processing with issuing of a decision on the state of the controlled objects. In particular, predicted breaking load and residual working life of structures of storage cases are calculated. Data are displayed on a computer monitor in the central diagnostic center of the plant.

Conducted preliminary investigations and calculations allowed detecting storage case areas, which should be monitored with increased care. General views of a stationary system EMA-3S of continuous monitoring, mounted in ammonia production shop, as well as mobile system of EMA family, are shown in Figure 6. Figure 7 shows the schematic of successive processing of diagnostic data, coming from the controlled objects.

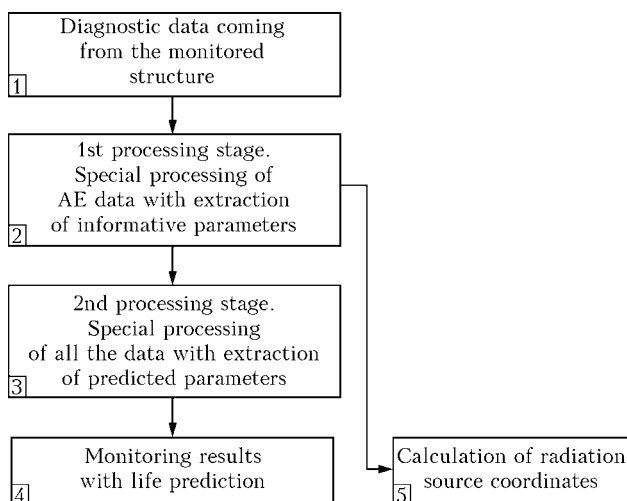


Figure 7. Stages of data processing by AE-based diagnostic instrumentation

Metrological characteristics of the instrumentation are specified by the following parameter sets: electronic modules of instrumentation; measuring transducers for set measurement of AE event coordinates; module of breaking load prediction.

The most serious technical requirements are made of module 1 (1st stage of processing), which transmits initial data to module 2 (2nd stage of processing). Module 1 is connected to measuring instruments and transducers, mounted on the object.

Accuracy of prediction of breaking load and residual life depends on reliability and accuracy of the data coming to module 3 and further on to modules 4 and 5. While modules 3–5 are quite well established in the world practice, organizing operation of module 2 is associated with considerable difficulties of data extraction with the set probability and accuracy before its subsequent transmission to module 3. Presented considerations lead to fundamentally new, very serious requirements to construction of diagnostic equipment architecture and its certification procedure. For systems of AE monitoring of EMA family, certification by four parameter sets is envisaged. Final stages of certification are stages of changing the coordinates of AE sources and determination of breaking load.

**Technology of AE monitoring of operation of OPZ storages and equipment.** EMA-3S system conducts the monitoring process in a continuous and automatic mode. Each measuring system EMA-3S uses a separate control computer, which stores files of conducted measurements. Data are stored at intervals set by the operator. Recommended data storage interval is 0.5–2 h.

The program uses measurement results for calculation of breaking load and residual life of the monitored structures, the data on which are stored in the database, and displayed in the numerical and graphic form on the computer.

Figure 8 shows the working window of EMA-3S program. The right upper part of the window displays real time graphs showing the current load and tempo of continuous AE appearance, which characterize the overall condition of the object of control and accu-

mulation of minor damage. Indicator of predicted breaking load and hazard warning is located in the upper left quarter of EMA-3S program test window. At normal condition of metal, the indicator is green, and there is no prediction of breaking load. If a higher acoustic activity is detected during measurement, the indicator changes colour according to the warning level (change of band colour is accompanied by a short sound signal): 1<sup>st</sup> warning — yellow colour; 2<sup>nd</sup> warning — orange colour; 3<sup>rd</sup> warning — red colour, divided into two levels — hazardous and emergency (Table). At prediction of breaking load by the system, the indicator displays the predicted value (shown by lower and upper values in the error range of not more than  $\pm 15\%$  at 0.95 probability) and coordinates of the hazardous location. The lower right quarter of EMA-3S program test window shows the schematic of the tested object, for instance, for ammonia storages in the form of a scan of side surface carrying AE transducers. Locations of appearance of acoustic emission activity are noted by flagged rectangles. Rectangle colour indicates the amplitude level of the last AE event in keeping with EMA-3S program settings, and flag colour indicates the level of the state criticality in keeping with the above colour scale for the 1<sup>st</sup>–3<sup>rd</sup> warnings.

The lower left part of EMA-3S window displays data on AE level in the graphical form by active measurement channel (blue colour) and acting load in conditional units (mv) ( $1\text{ mv} = 5.6 \cdot 10^{-3}\text{ kg/cm}^2$  (red)). Shape of curves shown in the graph at normal condition of the structure should be horizontal or regularly inclined.

Calculation of breaking load and residual life of ammonia storage is performed automatically. Results of AE monitoring are displayed on the control computer. Data obtained during monitoring are accessible via the Internet for its periodic analysis by specialists and its use at formation and improvement of standards for prediction of breaking load and residual life. In

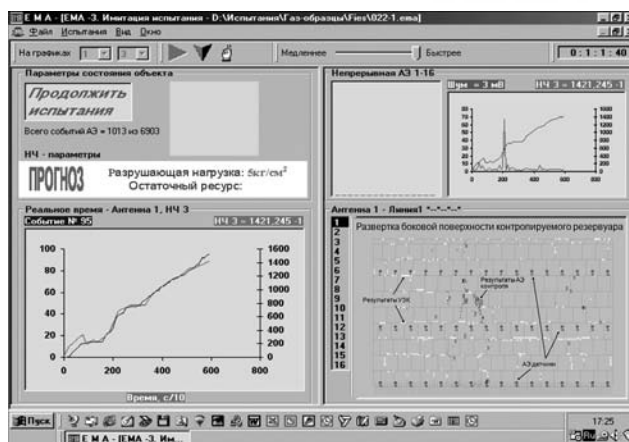


Figure 8. Variant of working window of EMA-3S system

case of development of a situation complex for structure state analysis, additional work on its evaluation is performed. For instance, more precise evaluation of ammonia storage condition is performed after interruption of loading-unloading process and other operations, creating acoustic noises and electric interference in the tank case.

If required, ammonia storage is kept idle for some time and a decision on its condition is taken by readings of indicators in EMA-3S program. Tentative criteria of tank case performance assessment are given in the respective normative tables for the first 10 min of tank monitoring during testing.

In case of development of a critical situation by the table, items 3, 4, the necessary measures for unloading of ammonia storage should be taken.

EMA-3S automated system of continuous AE monitoring has the following built-in means for ensuring continuous operation:

- UPS;
- instrumentation for following the operation of AE measurement subsystems;
- special devices for forced recharging of AE subsystems;

Personnel actions at different indication on EMA-2S system display

#	Indicator readings in the left upper corner of the display	Personnel actions
1	Green band	Normal mode. Operation can go on
2	Yellow band	Attention. At appearance of predicted breaking level of filling and its exceeding the working level by more than two times. Operation can go on
3	Brown band	Assess the predicted breaking level of filling by indicator readings. At predicted level exceeding the working level by more than 30 %, interrupt operation. Conduct additional analysis of received data in keeping with the instructions
4	Red discontinuously pulsating band	Interrupt operation. Conduct additional checking of the strength of storage case in keeping with the instructions
5	Red continuous band or continuously pulsating band	Emergency situation. Interrupt operation. Urgent relieving of load

\* Change of band colour is accompanied by short sound signal.

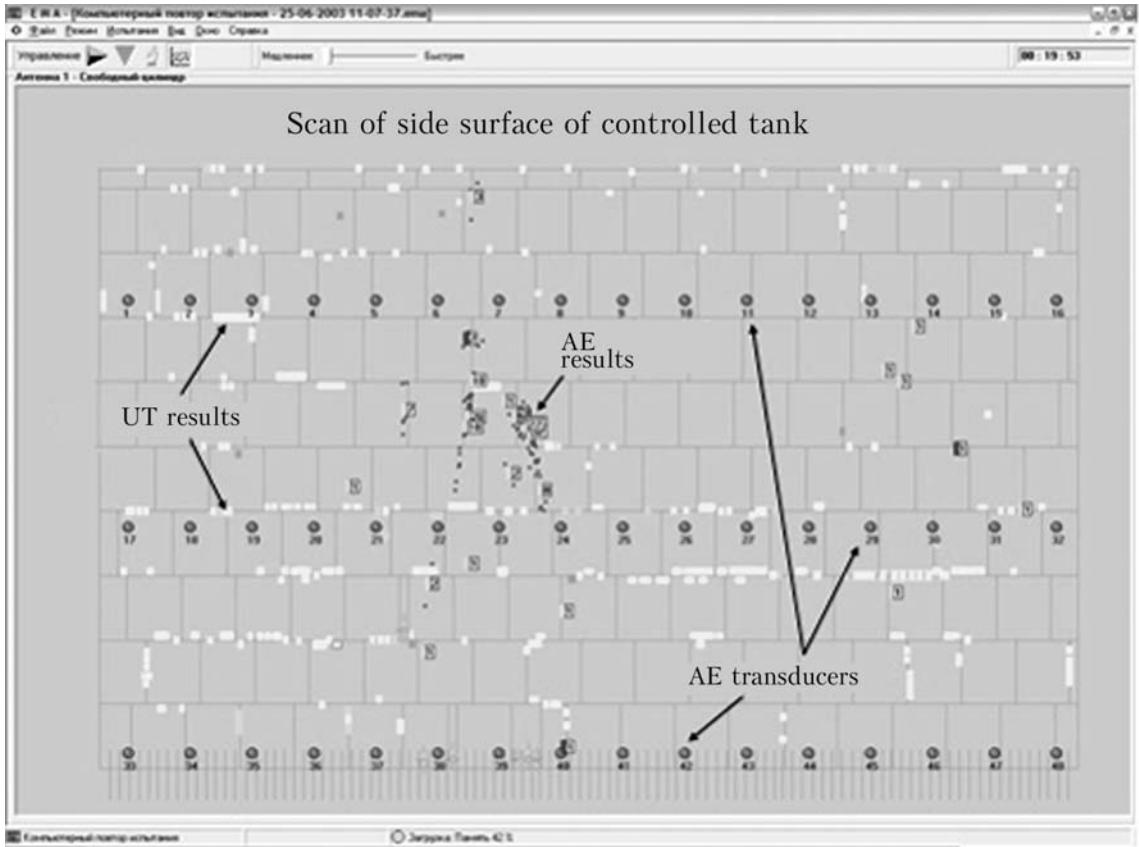


Figure 9. Scan of side surface of storage of 3500 m<sup>2</sup> area on the monitor screen (points show sites of fatigue damage accumulation)

- upper-level soft robots for ensuring uninterrupted operation of EMA-3S and STIntegrator programs, performing their forced restarting in case of failures or malfunctions.

Operation of all the above means as a complex ensures uninterrupted operation of the system in the normal mode and in the majority of contingencies.

The term of regular technical inspection of monitored structures and equipment can be assigned by the actual condition, based on readings of EMA-3S system of continuous AE monitoring.

The system is designed for uninterrupted operation in the continuous monitoring mode for 16 years.

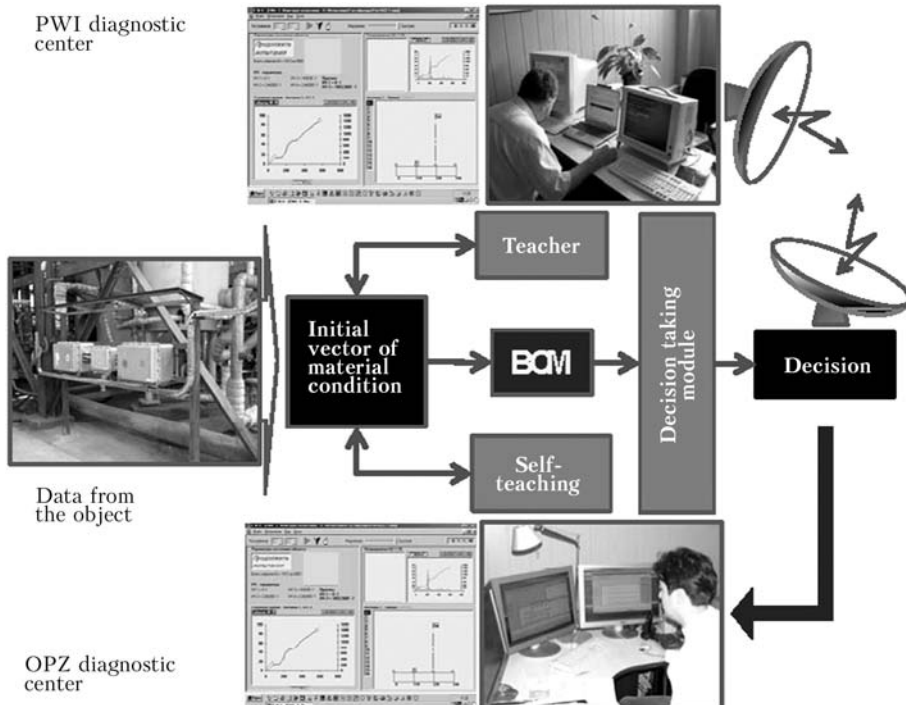


Figure 10. Remote control of operation of monitored structures

Figure 9 gives the scan of the side surface of ammonia storage of the total area of 3500 m<sup>2</sup>, extracted from the working window of EMA-3S system program. As was noted above, four such storages are controlled by 48 × 4 AE transducers. Also strain and filling level gages are mounted, which in their totality make up the material state vector. Analysis of the material state vector at each moment of tank operation allows taking a decision on the breaking load and residual life of the storage. In Figure 9 the black round dots in the middle part of the expanded side surface of the tank are seen more clearly. They mark the sites of AE clusters, where service damage is accumulated. These areas coincided with the sites of fastening the brackets of pressure pipeline making oscillatory motions as a result of non-uniform operation of the pump pumping up the ammonia.

The possibility of remote control of the process of monitored structure operation becomes highly important. The control center can be located at any distance from the controlled object, including considerable distances. Such a possibility has great importance and sense. If required (for instance, in mastering new control technologies), consultative assistance can be quickly provided by highly qualified experts to the staff of plant diagnostic centres, located at another often quite remote site. Figure 10 shows the schematic of the technology operating in the mode of remote control of the monitored structure operation, organized jointly by OPZ and PWI. Specialists of the analytical center in Kiev can observe the same readings of control monitors, as the staff of control units of the plant. This enables discussion of control results and taking joint weighted decisions on them.

**State of storage cases by the data of the continuous monitoring system.** Ammonia storages, as was noted above, were manufactured and put into operation in 1978. Time of specified operation for such structures is usually taken to be equal to 20–25 years. During this period absence of any considerable influence of inner destructive processes running in structure materials at normal operation modes is assumed.

With time, however, negative processes of damage accumulation in materials begin to be manifested in the form of individual microdamage spikes. On the one hand, defects present in the materials, which did not manifest themselves earlier during acceptance testing due to high initial properties of materials, begin to become active. On the other hand, structural transformations on the micro- and macrolevels result in initiation and development of new defects, which gradually form cluster sites. Continuous control system showed permanent in time and not hazardous at this moment of operation spikes of acoustic activity in materials of storage cases, which is indicative of continuous running of changes, associated with operating life process. The above circumstances require that operation of storage cases in the post-specified period was accompanied by stricter control of material condition, which is exactly what is provided by the continuous monitoring diagnostic system.

1. Paton, B.E., Kudryavtsev, I.V., Nedoseka, A.Ya. et al. (1974) Some ways of construction of automatic information-measuring systems for diagnostics of welded structure reliability. *Avtomatich. Svarka*, **9**, 1–5.
2. (2007) 15 years ago (based on the paper of Academician B.E. Paton and Prof. A.Ya. Nedoseka on Concept of Technical Diagnostics of Pipeline Transport, published in journal «Tekhnich. Diagnostika i Nerazrush. Kontrol», **3**, 1992). *Tekhnich. Diagnostika i Nerazrush. Kontrol*, **4**, 6–10.
3. Paton, B.E., Lobanov, L.M., Nedoseka, A.Ya. (2003) Technical diagnostics: yesterday, today and tomorrow. *Ibid.*, **4**, 6–10.
4. Paton, B.E., Nedoseka, A.J. (1999) Diagnostic of designs and safety of an environment. In: *Proc. of Int. Conf. on Human Factor and Environment* (July 19–20 1999, Lisbon, Portugal). IIW.
5. Harris, D.O., Dunegan, H.L. (1972) Verification of structural integrity of pressure vessels by acoustic emission and periodic proof testing. In: *ASTM STP 515: Testing for prediction of material performance in structures and components* (Philadelphia, PA: ASTM), 158–170.
6. Nedoseka, A.Ya. (2001) *Principles of design and diagnostics of welded structures*. Ed. by B.E. Paton. Kiev: Indprom.
7. Kharebov, V.G., Borodin, Yu.P., Shaporev, V.A. (2006) System of complex diagnostic monitoring of hazardous industrial objects. *V Mire Nerazrush. Kontrolya*, **4**, 13–17.
8. Obodovsky, B., Fedchun, A., Nedoseka, A. (2006) Application of permanent acoustic emission monitoring of four ammonia storage tanks. *Ammonia Technical Manual*, 23–24.
9. (1998) *PB-03-182–98: Safety rules for on-land storages of liquid ammonia*. Moscow: Gosgortekhnadzor.



# NARROW-GAP WELDING OF UP TO 110 mm THICK HIGH-STRENGTH TITANIUM ALLOYS

S.V. AKHONIN, V.Yu. BELOUS, V.S. ROMANYUK, V.V. STESIN, S.I. VELIKY,  
A.V. SEMENENKO and A.K. POLISHCHUK  
E.O. Paton Electric Welding Institute, NASU, Kiev, Ukraine

A method was developed for narrow-gap welding of thick titanium alloys (20–110 mm), having the following advantages: decrease in requirements to edge preparation, reduction of costs for preparatory operations, lowering of angular distortions and residual welding stresses in welded joints, and saving of welding wire and electric power, while ensuring a high quality of the welded joints. Guaranteed fusion of side walls of the groove with the weld is achieved due to application of the controlling transverse alternating magnetic field.

**Keywords:** TIG welding, titanium alloys, filler wire, large thickness, narrow gap, controlling magnetic field, edge fusion, structure, mechanical properties

Substantial growth in scopes of application of titanium alloys in different industries has been observed lately. Titanium alloys have found wide acceptance in chemical engineering, in addition to traditional application in aerospace engineering and ship building. The trend is to a more extensive utilisation of high-strength titanium alloys, such as VT6, VT20 and VT23 ( $\sigma_t = 835\text{--}1400$  MPa). Many 20–110 mm thick welded joints were produced by multi-layer argon-arc U- or V-groove welding. An important drawback of this welding method is a large volume of deposited metal, the cost of the titanium wire used being much in excess of the cost of the titanium rolled stock. The narrow-gap TIG welding technology is most efficient in a number of cases to join 20–110 mm thick structures. To successfully realise this technology, it is necessary to provide the following conditions: reliable shielding of the welding zone and tungsten electrode from oxidation with air, quality formation of the weld metal

and guaranteed fusion of the vertical walls of the narrow groove, viewing of the welding zone to monitor the process, and monitoring of position of tungsten electrode in the central plane of the groove during welding.

Narrow-gap welding of titanium is recommended to perform by two schemes: with the protective nozzle lowered into the gap [1], and with the protective nozzle located over the surface of the parts welded [2]. When using the second welding scheme, only the tungsten electrode is placed into the gap. Welding can be performed in the narrow gap with a width of 8–12 mm, which makes it possible to decrease consumption of an expensive filler metal 1.5–2 times, compared with welding by the first scheme, as well as to reduce welding strains. However, the use of the second scheme involves a problem of shielding of the welding zone and deposited metal from absorption of oxygen and nitrogen from air. The investigations conducted by the E.O. Paton Electric Welding Institute showed a high potential of the second scheme of narrow-gap welding of titanium. The AD238 unit of a cantilever type was made for welding titanium plates up to 100 mm thick and up to 2000 mm long [2].

The main problem in narrow-gap welding is to ensure a reliable and uniform fusion of vertical walls of the narrow groove with the deposited bead, as well as between the beads. In narrow-gap TIG welding without deflection of the welding arc, a substantial portion of its heat is consumed for re-penetration of the previous pass. This may cause lacks of penetration in the vertical walls of the groove. The lacks of penetration are especially frequent in a zone of intersection of the vertical walls of the groove with the surface of the previous pass, which is related to an intensive heat removal in this zone of the welded joint.

Transverse motion of the welding arc, which can be carried out mechanically (by weaving or rotating the tungsten electrode) [3] or by applying an external magnetic field, is used, as a rule, to achieve the guaranteed fusion of the side walls. This results in deflec-

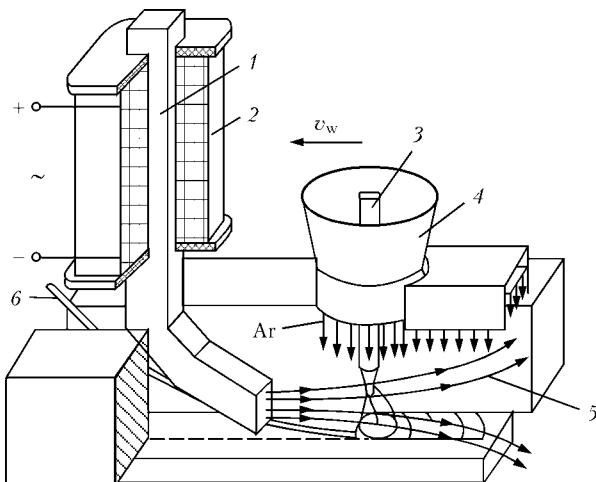


**Figure 1.** Schematic of the narrow-gap welding process using the controlling magnetic field: 1 – magnet limb; 2 – magnetic coil; 3 – tungsten electrode; 4 – protective nozzle; 5 – force lines of controlling magnetic field; 6 – filler wire

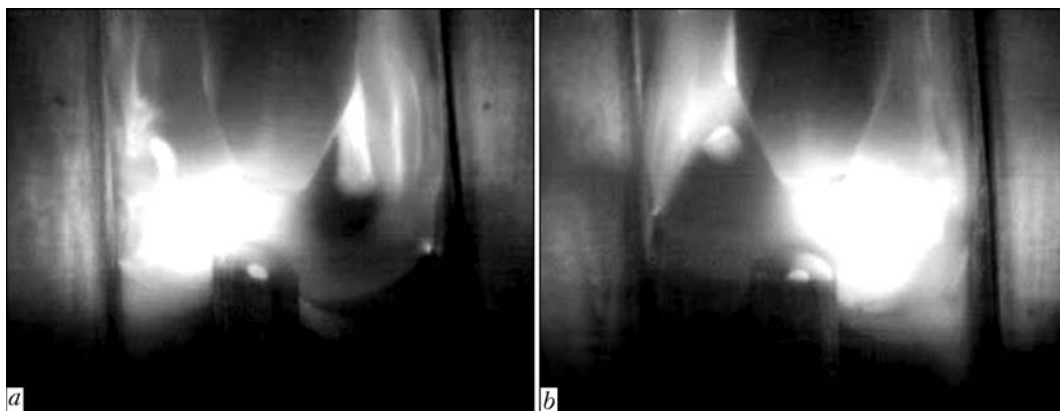


**Figure 2.** Video pictures of the process of narrow-gap TIG welding using the external controlling magnetic field with deflection of the arc to the left (*a*) and right (*b*) walls of the groove

tion of the welding arc [2] and displacement of its anode spot. As titanium and titanium-base alloys are non-magnetic materials, the most efficient method for ensuring the reliable and uniform fusion of the side walls of the groove is to apply electromagnetic control of deflection of the welding arc.

The magnetic coil power source BUMP-2 (Limited Liability Company «Rostock-SPARKS»), generating trapezoidal pulses with an amplitude of up to 6 A, was used to control the welding arc. In welding, the magnet limb performs the function of a magnetic core and is placed into the narrow gap (Figure 1). The current flowing through the magnetic coil induces the magnetic field within the arc zone, the force lines of the field within the arc zone being oriented mainly along the welding direction. This magnetic field is transverse with regard to the arc. Alternating deflections of the welding arc to the side walls of the groove and respective displacement of the anode spot of the arc to the side walls are provided by a change of polarity of the current flowing through the magnetic coil. Maximal induction of the controlling magnetic field within the arc zone may amount to 8 mT, the longitudinal component of induction of the controlling magnetic field being not higher than 20 %. The frequency of reversing of the magnetic field by using the BUMP-2 system developed for formation of the controlling magnetic field is adjustable

from 1 to 80 Hz, the magnetic induction being adjustable from 0 to 8 mT.

Investigations of peculiarities of formation of welds on titanium alloys in narrow-gap welding using the controlling magnetic field showed that penetration of the side walls grew with increase in a transverse component of induction of the magnetic field and decrease in frequency of its reversing. The maximal depth of penetration of the surface of a previous layer was fixed at the weld centre at a frequency of reversing of the controlling magnetic field equal to more than 20 Hz. The welds made at optimal parameters are free from lacks of penetration and lacks of fusion.

The electric arc in narrow-gap welding burns under restrained conditions, the narrow gap comprising a filler wire guide and magnetic core, in addition to tungsten electrode. This hampers an operator to directly monitor the welding process. The small size video camera VK-27 equipped with a right-angle attachment was developed to visually observe the welding process and monitor the state of tungsten electrode and position of filler wire in the groove. The camera is intended for TV observation of the process of TIG welding of structures made from titanium and titanium alloys at a current of up to 500 A. The video camera comprises a light filter, objective, optical detector array and microprocessor controller based on

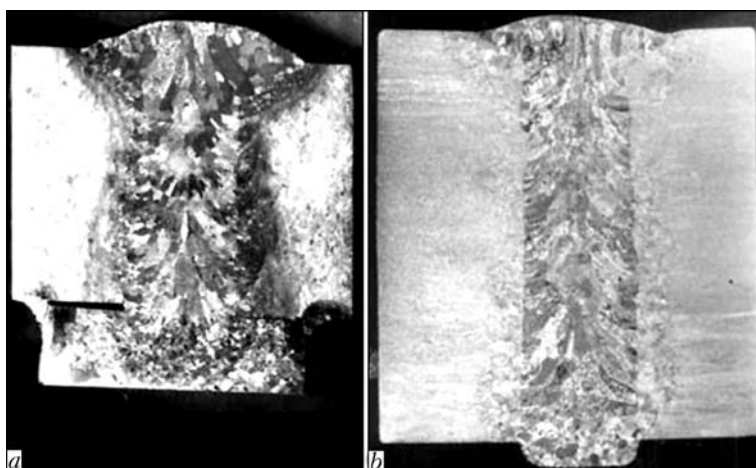


**Figure 3.** Macrosections of welded joints produced by narrow-gap TIG welding using the controlling magnetic field on a permanent (*a*) and forming (*b*) backing

**Table 1.** Content of gases in welded joints on alloy VT23, wt.%

Gas	[O]	[N]	[H]
Base metal	0.07	0.024	0.002
Filler wire SP15	0.06	0.016	0.0023
Weld metal	0.06	0.020	0.0022

the digital signal processor. The camera generates an output video signal of the PAL format. TV viewing of the narrow-gap welding process may help to solve another problem, i.e. in-process control of position of tungsten electrode in the central plane of the groove (see Figure 2).

Two schemes of fit-up of parts for narrow-gap welding were developed, and corresponding process parameters were selected on the basis of the investigation results. The first scheme provides for the use of a backing, which is welded to the reverse side of the parts to be joined. An important drawback of this scheme for titanium alloys is that the backing should be removed, as a rule, this leaving defects on the surfaces of the parts. The second scheme of fit-up and welding using a forming water-cooled backing [4] was suggested to eliminate this drawback. In this case, the backing serves as a crystalliser for the first-pass bead, protects the reverse side of a part from oxidation with air, and functions as a current conductor. Macrosections of the welded joints produced by using the above scheme are shown in Figure 3.

As indicated by the results of determination of the content of gases in the weld metal (Table 1), it is not in excess of that in the base metal, and depends upon their content in filler wire. This proved the high quality of gas shielding in welding.

The investigations conducted evidence that strength of the welds made on titanium alloy VT6 by narrow-gap TIG welding using filler wire SPT2 in the as-welded condition is at a level of 95 % of that of the base metal (Table 2), this meeting requirements to the welds of category 1.

Examinations of structure of the welds made on two-phase titanium alloy VT23 using high-alloy filler wire SP15 revealed a coarse-acicular structure with

**Table 2.** Mechanical properties of base and weld metals

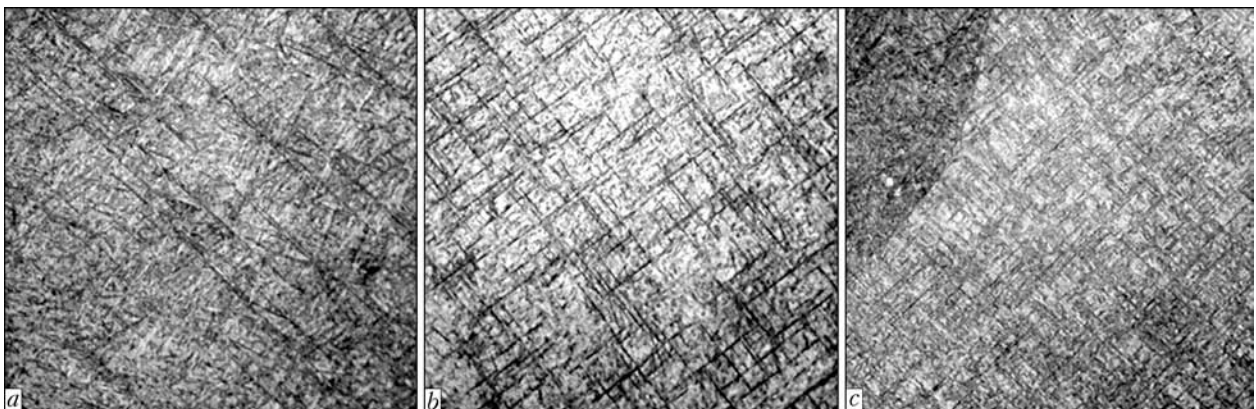
Investigation object	$\sigma_t$ , MPa	$\sigma_{0.2}$ , MPa	$\delta$ , %	$\psi$ , %	KCV, J/cm <sup>2</sup>
Base metal — alloy VT23	1030	980	13	30.0	35
Weld metal	1010	978	4	3.9	21
Welded joint	960	—	—	—	—

long martensite needles present both in the central and peripheral parts of the weld at the absence of induction without oscillations of the welding arc. The martensitic structure is coarser in the peripheral part of metal of the welds made with a magnetic induction of 6 mT. However, the martensite needles in this case are shorter than in the welds made without oscillations of the welding arc.

Metal of the welds made with a magnetic induction of more than 6 mT has a homogeneous structure, no coarse martensite needles being revealed in the central and peripheral parts of the welds. Increase in the reversing frequency to above 20 Hz has almost no effect on length of the martensite needles.

Analysis of microstructure of the narrow-gap TIG welds on titanium alloy VT23 with filler wire SP15 showed that the average length of the martensite needles at the absence of the magnetic field was 0.10–0.05 mm. In welding with a field reversing frequency of 10 Hz and magnetic induction of 6 and 12 mT, the average length of the martensite needles decreased to 0.06–0.08 and 0.04–0.05 mm, respectively. At a magnetic induction of 8 mT and frequency of reversing of the magnetic field increased from 2.5 to 20 Hz, the average length of the martensite needles decreased from 0.10–0.15 to 0.03–0.04 mm. Further increase in the frequency of reversing of the magnetic field had almost no impact on length of the martensite needles in the weld metal.

It can be concluded on the basis of the investigations conducted that magnetic control of the welding arc in welding allows decreasing the average length of the martensite needles almost 4 times and obtaining a more homogeneous and fine-acicular structure of the weld metal (Figure 4). It is the opinion of the authors


**Figure 4.** Microstructures ( $\times 400$ ) of metal of the welds made without (a) and with the controlling magnetic field at an induction of 6 (b) and 8 (c) mT

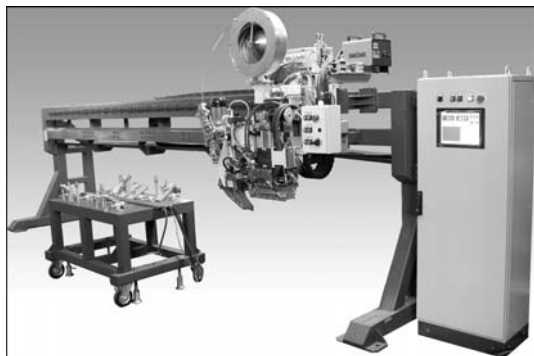


**Figure 5.** Gantry-type unit for narrow-gap welding of 20–110 mm thick titanium and titanium-base alloys

that improvement of the secondary structure of the weld metal on two-phase titanium alloys is related to formation of transverse oscillations of the weld pool. Transverse oscillations of the melt in a tailing portion of the weld pool are fixed on a video of the narrow-gap welding process, and show up as a change in ripples on the weld surface: distance between the ripples decreases with increase in frequency of reversing of the controlling magnetic field. Transverse oscillations of the weld pool result in a periodic incipient melting of metal at the solidification front, as well as in formation of a finely dispersed structure of the welds on two-phase titanium alloys, wherein the average size of the martensite needles decreases from 160 to 40  $\mu\text{m}$ .

Solution of the above problems allowed development of a welding unit to produce joints on up to 110 mm thick high-strength titanium alloys by narrow-gap welding using magnetic control of the welding arc (Figure 5). The unit performs welding by the second scheme. The welding torch with a cylindrical protective nozzle was developed to solve the problem of shielding of the welding zone. The nozzle is located over the surface of the parts joined (Figure 6), its internal surface having a generating line with a shape close to the Vitoshinsky curve [5]. The use of this welding torch made it possible to guarantee a reliable shielding of the welding zone in production of welded joints on up to 110 mm thick titanium and titanium-base alloys.

The welding unit consists of the following main components: fixed gantry to position the welding head over the welding zone; carriage with a mechanism for movement of the welding head along the weld; welding torch with a protective spout; mechanism for vertical movement of the welding head with a system for automatic adjustment of the arc voltage; mechanism for transverse movement of the welding head; filler wire feed mechanism; system for magnetic control of the welding arc, system for TV observation of the welding process; table for welded specimens; power supply VDU-511 with arc exciter VSD-02; control cabinet with a touch display, and local control panel.

The unit control system is intended to implement the process of TIG welding of titanium alloys and provide functioning of the equipment in the following modes: «Setting up» – to check operation of all mechanisms of the unit and perform setting displace-

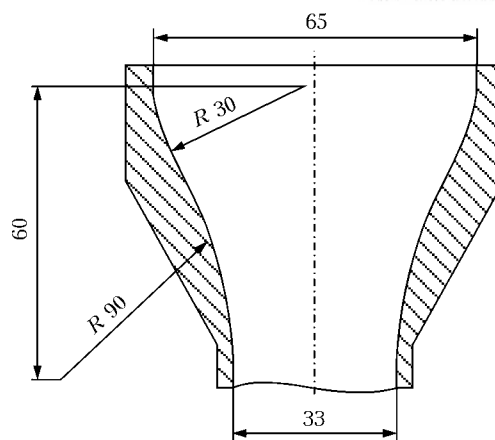


**Figure 6.** Schematic of protective nozzle for narrow-gap welding of titanium and titanium-base alloys

ments prior to welding, and «Automatic» – for automatic control of the welding process following the preset program. Both visual observation of the welding process and fixation of its parameters, such as arc voltage and current, welding speed, wire feed speed, frequency and induction of the magnetic field, are performed by means of this control system.

The welding unit performs multi-pass welding in the automatic mode, providing welded joints on 20–110 mm thick and 4000 mm long commercial titanium and titanium-base alloys by narrow-gap straight-line welding, thickness of the deposited layer per pass being 5–7 mm.

The developed welding technology and unit provide a high quality of the welded joints.

## CONCLUSIONS

1. Based on the investigations conducted, the technology was developed for narrow-gap welding of high-strength titanium alloys using the external controlling magnetic field. The technology provides a high quality of the welded joints and their mechanical properties at a level of not less that 90 % of those of the base metal.
2. Narrow-gap welding of two-phase titanium alloys using the controlling magnetic field provides the weld metal with a finely dispersed structure, the average size of martensite needles being decreased 4–5 times (from 160 to 40  $\mu\text{m}$ ), compared with the weld metal produced without the controlling magnetic field.
3. The gantry-type unit was developed for multi-pass narrow-gap straight-line welding of 20–110 mm thick and up to 4000 mm long titanium and titanium-base alloys in the automatic mode, providing a high quality of the resulting welded joints.

1. Mikhajlov, V.I., Sakharov, I.Yu. (2006) Welding of structures of thick titanium alloys (problems of technology). In: *Proc. of Int. Conf. on Ti-2006 in CIS* (21–24 May 2006, Suzdal, Russia). Kiev: Naukova Dumka, 109–111.
2. Paton, B.E., Zamkov, V.N., Prilutsky, V.P. (1996) Narrow-groove welding proves its worth on thick titanium. *Welding J.*, 4, 37–41.
3. Grinin, V.S., Shtrikman, M.M. (1982) High-productivity automatic narrow-gap welding. *Svarochn. Proizvodstvo*, 7, 21–23.
4. Belous, V.Yu. (2009) TIG welding of thick titanium plates by using forming backing. *The Paton Welding J.*, 10, 32–34.
5. Ardentov, V.V., Fedorenko, G.A. (1973) Influence of design of the flow part of torches on characteristics of gas shielding. *Svarochn. Proizvodstvo*, 10, 24–26.

# CONSUMABLE ELECTRODE PULSED ARGON-ARC WELDING OF SHEET ALUMINIUM ALLOYS

V.S. MASHIN, M.P. PASHULYA, V.A. SHONIN and I.N. KLOCHKOV  
 E.O. Paton Electric Welding Institute, NASU, Kiev, Ukraine

Technological features of consumable electrode pulsed argon-arc butt welding of 1.0–2.8 mm thick sheet aluminium alloys AMts, AMg2, AMg6, 1915T1 and AD33T1 were studied. The effect of welding modes on geometrical parameters of welds, their macrostructure and mechanical properties of welded joints is shown. Recommendations on welding technology are given.

**Keywords:** consumable electrode welding, sheet aluminium alloys, pulsed arc, welding modes, welded joints, weld geometry, mechanical properties

Two arc welding processes — by consumable and non-consumable electrodes in inert gases — are the most widely used in fabrication of sheet structures from aluminium alloys of low- and medium strength. They allow making joints with comparatively high levels of strength and ductility of welds, and provide the required service properties of welded joints [1].

Consumable electrode welding, unlike tungsten electrode welding, provides a more highly-concentrated application of thermal energy of the arc to the metal being welded, deep penetration of aluminium alloys, high welding speeds, narrow HAZ and lower product deformations. Such a process is irreplaceable in making sheet joints, particularly, tee-joints, in

which the process of nonconsumable electrode welding does not ensure a sound formation of the weld and complete penetration of the tee-section walls, because of instability of filler wire melting and arc erring over two sheets [2].

Disadvantages of the process of consumable electrode welding are «coarse-ripple» formation of weld surface, small radius and larger angle of weld transition to base metal surface, as well as considerable losses of volatile alloying elements from the electrode metal [3]. Pores often form in the welds and fusion zone, which result from a relatively high content of hydrogen in the base and filler metal, electrode metal overheating [4] and slight violation of the technological process of welding. Therefore, in keeping with GOST 14806–80, developed at the start of 1970s and still in force now, the process of consumable electrode

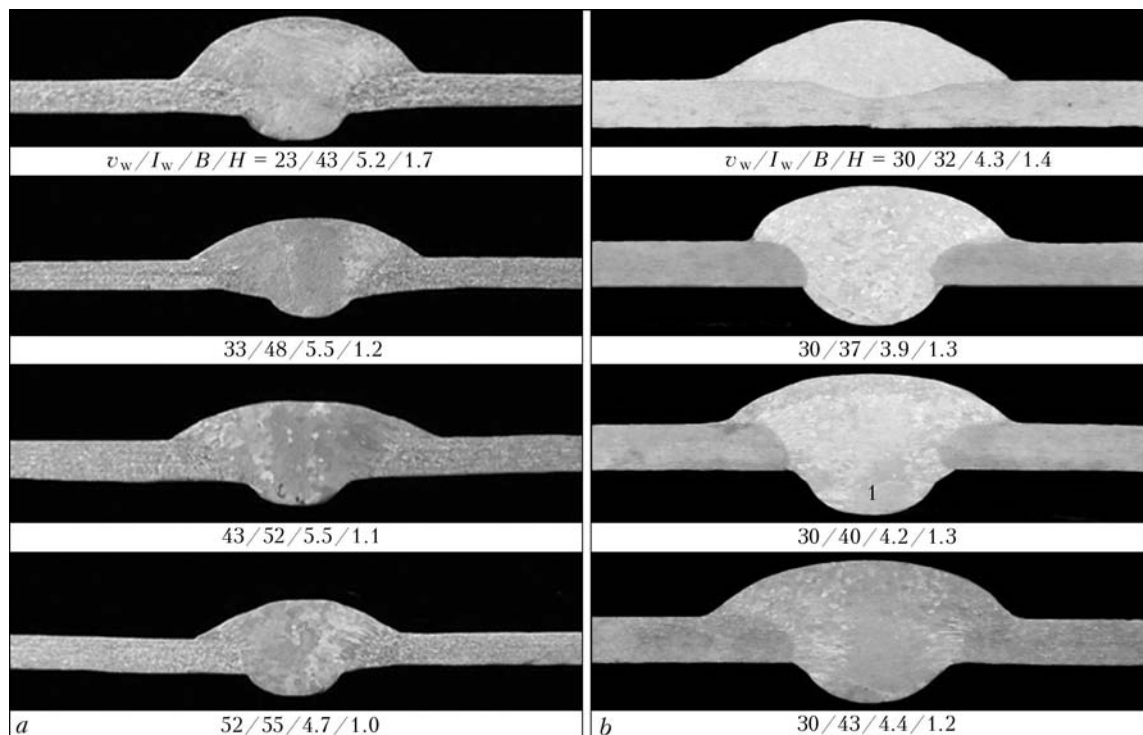


**Figure 1.** Influence of welding mode on geometry of joints of AMts (a) and AMg2 (b) alloy 1 mm thick. Here and further on the number in the area of weld metal corresponds to the number of test weld with heat input according to Figure 3

welding of aluminium alloys can be applied only for not less than 3 mm thick metal for butt and tee joints and not less than 4 mm metal for fillet and overlap joints.

Consumable electrode pulsed-arc welding, compared to DC welding, allows stabilization of the process of electrode metal drop transfer, improvement of weld formation, reduction of the loss (evaporation) of readily boiling alloying elements from the electrode wire and improvement of mechanical properties of welded joints [5, 6].

Welding machines, including pulsed power sources with synergic control of the process of transfer of electrode metal drops to maintain the synchronous process of «one pulse—one drop» [7] and push-pull type feed mechanisms for welding wires of 0.8–1.6 mm diameter, have been recently manufactured in Europe, USA and Japan. The most efficient of such units are systems of the type of TransPulseSynergic (TPS), which are designed for automated and robotic lines

for manufacturing products for various purposes. Application of this equipment for nonconsumable electrode pulsed-arc welding allows widening the ranges of welded metal thicknesses towards their lowering.

The purpose of these investigations is production of sound joints from sheet aluminium alloys of different aluminium systems up to 3 mm thick when using consumable electrode pulsed argon-arc (MIG) process.

**Experimental procedure.** Procedure optimization was based on the known principles of the need to reduce thermal impact of the fusion welding process on heat-hardenable aluminium alloys by application of high energy density heat sources. This is achieved, for instance, in laser welding [8], or in hybrid laser-arc consumable electrode welding [9] when helium or helium-argon mixtures ( $\text{He} \geq 70\%$ ) are used as shielding gas [10, 11]. Therefore, at pulsed MIG welding of sheet aluminium alloys relatively high welding currents and increased welding speeds were used as efficient means of welding heat input lowering. In order

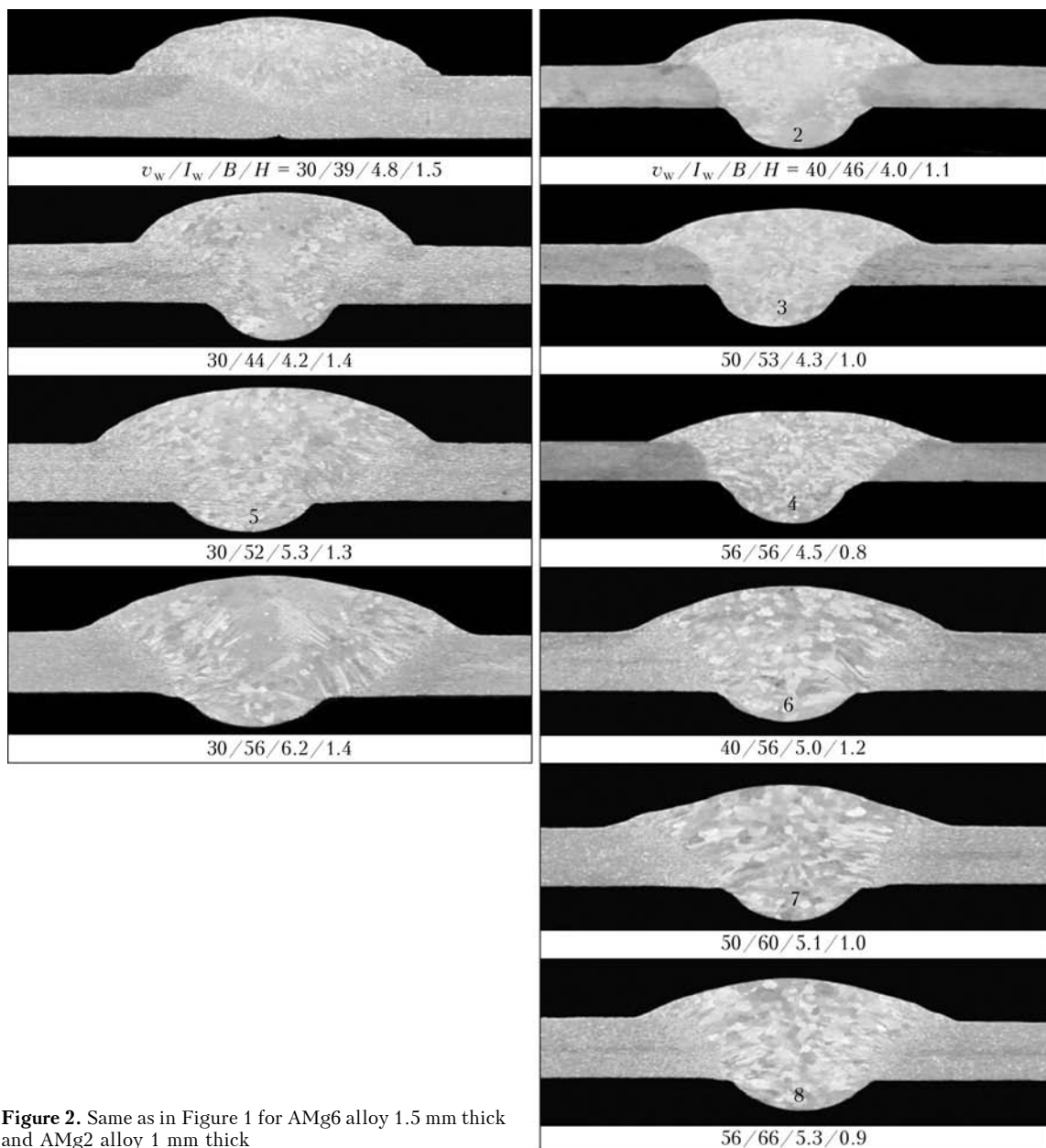


**Figure 2.** Same as in Figure 1 for AMg6 alloy 1.5 mm thick and AMg2 alloy 1 mm thick



Average values of mechanical properties of welded joints (numerator) made by pulsed MIG welding and base metal (denominator) (in all the tested samples metal rolling direction coincides with weld axis)

Alloy grade	$\delta$ , mm	$\sigma_t$ , MPa	$\sigma_{0.2}$ , MPa	$\sigma_{0.01}$ , MPa	$\delta_5$ , %	$\sigma_t^{w.j}/\sigma_t^{BM}$	$\sigma_{0.2}^{w.j}/\sigma_{0.2}^{BM}$	Fracture zone
AMg2	1.0	180	82	79	12.3	0.94	1.0	HAZ, BM
AMg2*	1.0	$\frac{177}{192}$	$\frac{80}{82}$	$\frac{78}{80}$	$\frac{12.4}{22}$	0.92	0.98	Same
AMg6	1.5	352	182	146	15	0.96	0.93	FZ and HAZ
AMg6*	1.5	$\frac{312}{365}$	$\frac{171}{196}$	$\frac{139}{148}$	$\frac{12}{20}$	0.85	0.87	Weld
AMg6	1.8	348	166	111	17	0.97	0.86	FZ and HAZ
AMg6*	1.8	$\frac{319}{357}$	$\frac{158}{192}$	$\frac{97}{151}$	$\frac{14}{20}$	0.89	0.82	Weld
AD33T1	2.8	218	126	81	8.8	0.69	0.44	HAZ
AD33*	2.8	$\frac{216}{314}$	$\frac{124}{277}$	$\frac{79}{151}$	$\frac{8.7}{14.9}$	0.68	0.45	Same
1915T1	2.8	346	216	185	9.2	0.82	0.72	BM
1915T1*	2.8	$\frac{297}{426}$	$\frac{173}{297}$	$\frac{155}{205}$	$\frac{5.7}{19}$	0.70	0.58	Weld

\*Weld convexities are removed.

to produce sound joints the following principle was applied: the higher the welding current (higher arc voltage and welding speed, respectively), the smaller the weld width and their reinforcement height (at unchanged depth of metal penetration) and, as a consequence, lower residual deformations of the joints.

Aluminium alloys AMts 1 mm thick, AMg2 1 mm thick, AMg6 1.5 and 1.8 mm thick, AD33T1 and 1915T1 2.8 mm thick and SvAMg6 welding wire (GOST 7871-75) of 1.2 mm diameter were used in investigations. Highest grade argon was used as shielding gas. Automatic pulsed MIG welding of butt joints was performed in Fronius TPS-450 welding system. Before welding the metal surface was scraped. Angle of welding torch inclination was 10-15°, distance from torch nozzle to metal being welded was 8-12 mm, argon flow rate being 20 l/min.

Welding of butt joints was performed on removable backing from stainless steel with grooves of 2 mm width and 0.8 mm depth for 1-2 mm alloys, and grooves of 3.8 mm width and 1 mm depth for 2.8 mm alloys. Geometrical parameters of welds – width  $B$  and height  $H$  of face reinforcement – were determined on transverse macrosections. Values of heat input of pulsed MIG process were calculated by the following formula:  $q_{h,i} = K_{ef} I_w U_a / v_w$ , kJ/cm, where  $K_{ef}$  is the effective arc efficiency (0.72 for argon). Mechanical properties of base metal and welded joints were determined on standard samples to GOST 6996-66.

Figures 1 and 2 give the microstructures of joints of AMts, AMg2 and AMg6 alloys, depending on welding mode. It is determined that the optimum weld width and their smooth transition to base metal are observed at  $I_w \geq 55$  A and  $v_w \geq 50$  m/h ( $q_{h,i} \leq 0.5$  kJ/cm), at  $v_w$  of 30 m/h optimum formation of reinforcement is observed at  $I_w \leq 40$  A. It should be noted that such a speed ( $v_w \leq 30$  m/h) is the most acceptable at semi-automatic process, when the welder still can reliably maintain the welding torch extension and its uniform displacement.

Calculations showed that at maintaining of the same depth of penetration of 1-3 mm thick metal, increase of welding speed by 3 times (for instance from 20 to 60 m/h) requires increasing the welding current by just 1.7 times and increasing the arc voltage only by 1.15 times, leading to 1.6 times lowering of the welding process heat input (Figure 3). This is, most probably, accounted for by the fact that aluminium alloy penetration depth  $h$  is proportionately dependent on arc pressure  $P$ , which, in its turn, depends on the square of welding current and is determined by the following equation [12]:  $h = f(P) \approx B_0 + B_1 I_w + B_2 I_w^2$ , where  $B_0, B_1, B_2$  are the coefficients of regression equation dependent on shielding gas composition, diameter and grade of electrode wire, etc.

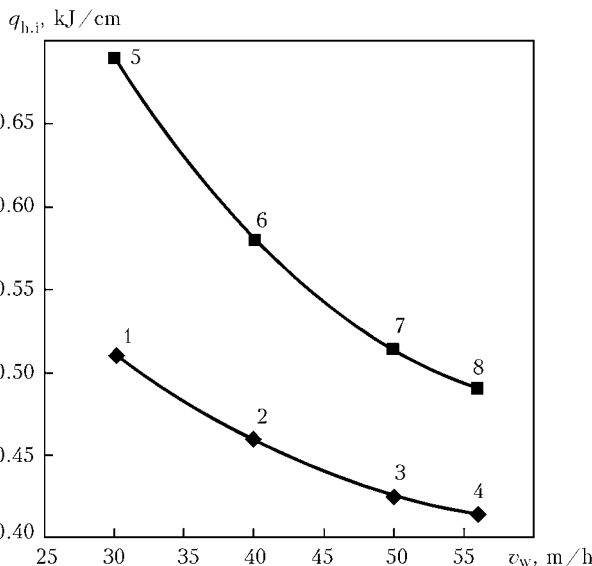


Figure 3. Influence of welding speed on average value of heat input of pulsed MIG welding of AMg2 alloy 1 mm thick (points 1-4) and AMg6 alloy 1.5 mm thick (5-8)

Analysis of the data, given in Figures 1–3, leads to the conclusion that automatic pulsed MIG welding of aluminium alloys 1–2 mm thick should be performed at  $I_w \geq 55$  A and  $v_w \geq 50$  m/h ( $q_{h,i} \leq 0.5$  kJ/cm). This is true for welding technologies without application of systems of following the welding torch displacement over the butt joint edges. In the case the above-mentioned following systems are used, welding speed can be increased considerably.

Figure 4 shows the dimensions of weld reinforcement and macrostructure of joints of 1915T1 alloy, depending on welding modes. It is established that welds of joints made in optimum welding modes ( $v_w = 40$ – $50$  m/h) have no pores of more than 0.1 mm diameter.

Investigations showed that the geometrical dimensions of welds made by pulsed MIG welding do not exceed the respective values, which are specified by state standards (GOST 14806–80) and industry standards on welded aluminium joints in manual and automatic tungsten-electrode welding.

Results of investigations of mechanical properties of welded joint samples are given in the Table and are indicative of the fact that for non-heat-hardenable alloys of Al–Mg–Mn type the conditional tensile strength of joints (with two-sided weld reinforcement) decreases compared to base metal by not more than 6 %, and proof stress – by not more than 14 %. The greatest lowering of  $\sigma_t$  and  $\sigma_{0.2}$ , compared to base metal, is observed for joints of heat-hardenable alloys: for AD33T1 alloy – by 32 and 55 %, and for 1915T1 alloy – by 16 and 28 %, respectively. A feature of fracture of welded joints with weld reinforcements consists in that all of them fail beyond the weld metal. With removed reinforcement, joints of AMg2, AMg6 and 1915T1 alloys fails through the weld metal, and lowering of mechanical properties compared to base metal is respectively equal to: for joints of AMg6 alloy  $\sigma_t$  – up to 15 %,  $\sigma_{0.2}$  – up to 16 %, for joints of 1915T1 alloy  $\sigma_t$  – up to 16 %, and  $\sigma_{0.2}$  – up to 28 %. For joints of AD33 alloy presence or absence of weld reinforcement practically does not affect the values of conditional tensile strength or proof strength, as the joints fail across the HAZ metal.

## CONCLUSIONS

1. Modern pulsed power sources with synergic control of pulsed MIG process allow widening the ranges of welded metal thicknesses towards their lower values. Optimization of welding modes, providing stabilization of uniform formation of the weld root, improves the quality of joints of sheet aluminium alloys.

2. Pulsed MIG welding in argon can be used to produce joints of aluminium alloys 1.0–2.8 mm thick with a sufficiently good quality of weld formation and their high tightness. Geometrical dimensions of the deposited metal do not exceed the respective values of parameters of welds made by manual or automatic tungsten electrode welding.

3. In order to lower the heat input of pulsed MIG process and to produce sound joints from sheet aluminium alloys, it is necessary to apply relatively high welding currents and increased welding speeds.

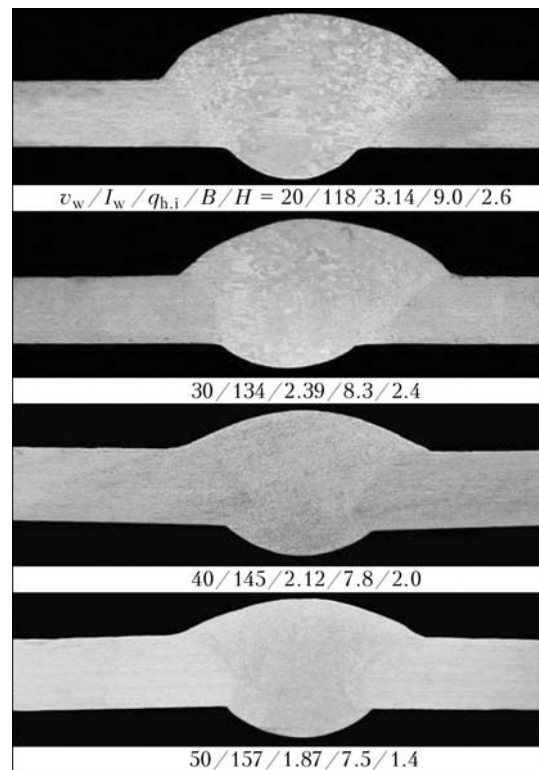


Figure 4. Influence of welding speed, welding current and welding heat input on geometry of welded joints of 1915T1 alloy

4. Results of investigation of the process of pulsed MIG welding of sheet alloys can be used to modify the current state and industry standards for welded joints of aluminium alloys and will promote further wide application of the technology of high-speed consumable electrode welding of sheet products from high-strength aluminium alloys.

- Ishchenko, A.Ya., Labur, T.M., Bernadsky, V.N. et al. (2006) *Aluminium and its alloys in current structures*. Kiev: Ekotekhnologiya.
- Mashin, V.S., Poklyatsky, A.G., Fedorchuk, V.E. (2005) Mechanical properties of aluminium alloy joints in consumable and nonconsumable electrode arc welding. *The Paton Welding J.*, **9**, 39–45.
- Levchenko, O.G., Mashin, V.S. (2003) Sanitary-hygienic characteristic of the process of consumable electrode inert-gas welding of AMg6 aluminium alloy. *Ibid.*, **1**, 46–48.
- Ishchenko, A.Ya., Mashin, V.S., Dovbishchenko, I.V. et al. (1994) Mean temperature of electrode drop metal in inert-gas welding of aluminium alloys. *Avtomatich. Svarka*, **1**, 48–49.
- Mashin, V.S., Pavshuk, V.M., Dovbichchenko, I.V. et al. (1991) Influence of conditions of pulsed arc welding of aluminium AD0 on shape and porosity of welds. *Ibid.*, **4**, 57–60.
- Zhernosekov, A.M., Andreev, V.V. (2007) Pulsed metal-arc welding (Review). *The Paton Welding J.*, **10**, 40–43.
- Voropaj, N.M., Ilyushenko, V.M., Lankin, Yu.N. (1999) Peculiarities of pulsed arc welding with synergic control of welding parameters. *Avtomatich. Svarka*, **6**, 26–31.
- Drits, A.M., Ovchinnikov, V.V. (2009) Peculiarities of laser welding of aluminium-lithium alloys 1420 and 1460. *Tsvetn. Metally*, **9**, 59–63.
- Shelyagin, V.D., Khaskin, V.Yu., Mashin, V.S. et al. (2009) Features of laser-MIG welding of high-strength aluminium alloys. *The Paton Welding J.*, **12**, 21–27.
- Dovbishchenko, I.V., Ishchenko, A.Ya., Mashin, V.S. (1997) Application of helium in consumable electrode welding of aluminium alloys. *Avtomatich. Svarka*, **2**, 14–19.
- Ishchenko, A.Ya., Mashin, V.S., Budnik, V.P. (1995) About porosity of welds in consumable electrode inert-gas welding of aluminium alloys. *Ibid.*, **1**, 16–18.
- Ishchenko, A.Ya., Mashin, V.S., Dovbishchenko, I.V. et al. (1994) Mean temperature of pool metal in inert-gas arc welding of aluminium alloys. *Ibid.*, **11**, 15–19.



# APPLICATION OF METHOD OF DRY UNDERWATER WELDING IN REPAIR OF UNDERWATER PASSAGES OF GAS AND OIL PIPELINES IN RUSSIA

V.Ya. KONONENKO

SE «Ekotekhnologiya» of STC «E.O. Paton Electric Welding Institute», Kiev, Ukraine

Application of dry underwater welding in repair of underwater passages of main gas and oil pipelines across rivers is considered. A new specialized mobile diving complex, designed for repair main gas pipelines of 1020 and 1220 mm diameter at the depth from 2 up to 30 m using the dry underwater welding, passed the full-scale tests, is described in detail.

**Keywords:** *dry underwater welding, main gas pipelines, repair of underwater passages, mobile diving complex*

Nowadays the method of hyperbaric underwater welding which started its development since the 1960s is the most challenging in solution of tasks connected with construction and repair of underwater oil and gas pipelines and other hydraulic engineering constructions at different depths. The development of this method was proceeded by application of materials with higher mechanical properties, increase of depth of works performance and requirements to performers which should provide joints with predicted quality level. In this welding method the contact with water of reaction zone and metal being welded is absent and more convenient conditions for the work of divers-welding operators are provided in comparison with wet welding methods, that allows producing welded joints of equal strength independent of environmental conditions and depth of works fulfillment. This has particular importance for Russian Federation, where by the end of 2008 a number of underwater passages of main pipelines (MP) across water barriers of total length 5800 km was 1855 units (or 2687 lines). Due to different reasons the influence of environment and hard-to-reach underwater passages of MP are complex objects for conductance of underwater technical operations using underwater welding.

Aim of the work is to present information about technology of dry welding of underwater passages of oil and gas pipelines and equipment used for its realization in Russian Federation during last 30 years.

The main volume of works in dry chambers is performed in repair of underwater pipelines. The chambers are designed and manufactured individually according to the order [1–3]. Such a chamber of weight from 8 to 20 t, as a rule, is included into ship diving complex. A number of mobile simplified modifications of chambers has also been designed for quick delivery to the site of failure in the containers. Except the chamber itself, the complex includes hydraulic hoists

and aligning devices necessary for displacement of pipes in vertical and horizontal planes at their fixation and sealing in the chamber ends. The chambers are completed with a set of sealing elements providing sealing pipes of different diameters. The additional set includes equipment for cleaning, cutting and fitting-up of pipes, a sealed power source allowing welding using the technology of manual arc welding (MAW), TIG and MIG/MAG welding and heat treatment of welded joints, sealed containers for storage of tools and accessories, equipment for heat treatment and control of welded joints.

The camera equipment includes also systems of smoke removal, fire extinguishing, control of composition of gas environment and hydraulic system for fixation and movement at small distances of a pipe being repaired in case of its aligning during its assembly. In the upper part of the chamber a hatch is located to which a diving-bell is connected. From the bell the divers-welders can travel directly to the chamber. In the period of assembly on the pipe, when the chamber is sunk, the welders perform work in diving suits. After the site works are finished they work without diving suits, but put on a face mask, when necessary, which is connected to the system of gas supply of diving-bell.

Underwater welding works are performed by experts who passed many-month training under the supervision of specially trained engineers and technologists, who constantly monitor the physical state of divers-welders, composition and humidity of gas mixture, and also control all electric parameters of the arc process.

In the practice of repair of underwater passages at the territory of the former USSR the dry welding practically was not almost used excluding repair of oil pipeline Aleksandrovskoe–Anzhero-Sudzhensk in the place of its crossing through the Ob river [4, 5]. In this case both defects of the 1020 mm diameter steel 18G2AF pipe of 16 mm wall thickness were in the upper part of site butt welds. In February–March 1979, at the depth of 6 m the first defect — a crack,

the visible part of which was 250 mm — was repaired in caisson. As a caisson a vessel for water of  $1.8 \times 1.5 \times 2.2$  m, found in the nearest region, was used, that allowed performance of welding jobs on the pipe in the «sector» from 9 to 3 h. The water was forced out by compressed air, and welding aerosol from the burning zone was removed by local exhaustion. The entry and exit of divers-welders and also supply of all necessary things were performed through a lower part of the caisson. The defective area of  $400 \times 650$  mm size was removed using gas-oxygen cutting, and a patch with a backing were placed into the formed hole. A root weld was performed using a wet mechanized welding and the groove was filled using covered electrodes in the dry environment. The diving equipment allowed diver-welders to perform only two diversings for 45–50 min during one working day. The total time spent for manufacturing of chamber, its assembly and performance of welding works was 65 days.

The second defect was repaired in February-March, 1980. The soil washing out was carried out in summer-autumn period, and cleaning of pipe from hydraulic insulation and installing the same caisson used during repair of the first defect was performed during 10 working days. As in the first case the crack was located in the «sector» from 13 till 14.30 h, its visible part was 200 mm. The technology of welding works performance was the same as during repair of previous butt. During welding works the welders applied the machine ShAP-62, that allowed working under water without coming out to the surface during 3–4 h. In repair of this defect welding works were carried out for 10 h (including pre-heating of pipe and welds cleaning).

Nowadays in Russian Federation a number of works was performed in MP using dry welding [6]. For this purpose a specialized underwater caisson of Zakharov (SUCZ) of the modification I was used, representing an open diving-bell installed by a side surface on MP. The SUCZ of different types and sizes provides repair of MP of diameter from 325 to 1420 mm.

SUCZ, the schematic diagram of which is shown in the Figure 1, is composed of a metallic casing 18, connected to four guides 9 and fastening bracket 16, to hinged devices 3. The side surfaces of the casing 18 have segment cut 6, the radius of which corresponds to the radius of MP being repaired 4. The air-tightness of installation SUCZ on the outer surface of MP is provided by a packing 7, made of a microporous rubber, positioned in the circumferential gap between a casing segment cut 6 and surface of MP. At the surface of the casing 18 two ventilation holes 10 and 14 (respectively, main and auxiliary) are located where taps to control discharge of shielding gas and welding fume are mounted. To the main vent hole 10 the ventilation bell is linked through the hose providing removal of welding fume from the caisson. The casing 18 is fixed

on two rods-weights 2 at the required height using hinged devices 3. The stability of structure is provided by ballast boxes 19 with ballast loads 1 positioned in them. The SUCZ is fixed on the defective area of pipeline being repaired by means of clamping semi-rings 11 and turnbuckles 12, 13, and its position on the MP surface is fixed by four bolts-rests 5, arranged on guides 9 which provide the fixation of required position of SUCZ relative to MP axis. Assembly loops 15 are welded-on to fastening brackets 16 for mounting of casing 18 of SUCZ on a load-carrying frame in its lifting and lowering under the water.

SUCZ made it possible to perform a number of repair works using a MAW in shielding gases on MP, the list of which is given in the Table.

For all the works, described in the Table, the technological process was approximately the same and included the following operations:

- washing out and cleaning of surface of pipeline from hydraulic insulation;
- installing of caisson and water forcing out by supply of argon or carbon dioxide;
- cleaning of pipe surface for the width of not less than 150 mm from the boundaries of supposed removal of defective area using mechanical method;
- fixation of crack ends by drilling and removal of defect metal by grinding with formation of two edges;
- preheating up to 100–150 °C and welding;
- non-destructive testing of welded joint;
- dismantling of chamber, installing of coupling, restoration of damaged hydraulic insulation and hydraulic deposition of soil on repaired area of pipeline.

During repair of a through defect of circumferential butt welded joint of underwater passage of gas pipeline Khatassy–Pavlovsk across the Lena river a coupling PGM was not installed.

The preparation of defects of circumferential butt welded joints of pipes for MAW was performed in the following sequence:

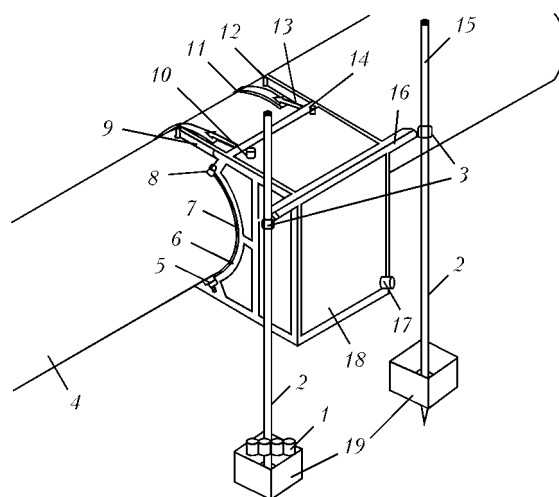


Figure 1. Scheme of SUCZ [7] (1–19 see in the text)



Repair of defects of MP, made by «Spetspodvodremont Ltd» using method of a dry underwater welding

MP and its characteristics (depth of defects location)	Customer, year of performance	Defect	Method of repair
Petrovsk–Novopskov, 1020 mm diameter at the Don river (5 m)	«Volgogradtransgaz Ltd», 2006	Through defect in the form of a crack in cross weld of 180 mm length	MAW with further installing of coupling MPSS (length $L = 1400$ mm, pressure $P = 217$ MPa)
«Pipe-bend for Zarechie», 350 mm diameter at the Lena river (10 m)	«Sakhatransneftegaz Ltd», 2006	The same of 360 mm length	MAW with further installing of coupling PGM (length $L = 990$ mm, $P = 171$ MPa)
Gas pipe-bend Hatassy–Pavlovsk, 530 mm diameter at the Lena river (10 m)	The same, 2007	The same of 280 mm length	MAW
Yamburg–Elets 2, 1220 mm diameter at the Ob river (8 m)	«Tyumentransgaz Ltd», 2007	Cracks (stress-corrosion) on the body of a pipe in longitudinal direction: the first crack of the 1660 mm length and 8 mm depth; the second crack is 580 mm length and 10 mm depth	MAW with further installing of coupling MPSS (length $L = 5200$ mm, pressure $P = 1060$ MPa)

- the pipe surface was cleaned in mechanical way for the width of not less than 150 mm from the boundaries of supposed removal;

- to prevent crack propagation its edges were fixed by 5 mm diameter drill at the distance of 15–30 mm from crack boundaries in the direction of its possible propagation;

- the layered removal of defective metal by abrasive discs was performed to produce necessary shape of edges for welding, here the removal should have U-shape with parallel boundaries and rounded angles; its length should overlap a defect for not less than by 30–50 mm on each side (+30–50 mm at run of abrasive disc to each side from the boundaries of defect). In case if the through removal was not required, the defective area was removed by grinding until residual thickness of metal of 3.0–3.5 mm. If a through removal was required, the welding of a root layer was performed by areas of a length of not more than 75 mm at a curvilinear position of a crack along the circumferential area of welded joint. At its straight-linear position the simultaneous removal and welding of weld root layer is admitted. Welding of filling layers of a weld was performed by a step-back method along the whole length of defective area, and a finishing weld layer was made along the whole length of defective area to suit requirements.

The works on preparation for repair, welding and quality control of welded joint after repair were performed by divers-welders in diving outfit in caisson in CO<sub>2</sub> atmosphere.

To weld a root layer, the electrodes of the type E50A of 2.0–3.25 mm diameter of LB-52U grade, and for welding of filling and finishing layers the electrodes of the type E60 of 3.2–4.0 mm diameter of OK 74.70 grade were used.

The quality control of welding was performed in operation-by-operation way visually and by check out

of continuity of deposited metal using ultrasonic method in the volume of 100 %. The admissible sizes of defects of welds should not exceed values given in RD 558–97.

SUCZ of modification II is the following step in the development of technology of repair of gas pipelines using dry underwater welding in Russian Federation. It represents a specialized underwater complex (SUC) consisted of a caisson and installation frame (Figure 2) and designed for welding pipelines of 1020 and 1220 mm diameter with 14–20 mm wall thickness at the depth from 2 to 30 m. The full-scale tests were held in the period of 27–31 October, 2009. Using SUC one can cut out and replace damaged areas of pipelines, reweld through and non-through defects, to butt weld the pipelines under water and perform other welding works on underwater MP. The total weight of complex is 25.5 t.

A casing of caisson of this modification is made sectional for reducing dimensions during transportation (Figure 3). Caisson is composed of five main parts (see Figure 2): casing 5 (upper and lower part); sealing flap 9; supporting beam 6; outrigger 8; pneumatic sealing 7.

The caisson of 5.9 t weight of sizes 2.74 × 4.14 × 3.06 m and 16.2 m<sup>3</sup> volume allows performing works of two divers-welders simultaneously using standard welding consumables and technologies. In the ends of caisson changeable sealing flaps 9 are located which are opened inside during installing. Sealing of flaps is provided by a porous rubber gasket and around the pipeline – by floating rubber packings 7. In the upper part of caisson the II-shape projection is foreseen where fastening of loading pulley blocks, reducers of expiration and inputs of TV cables, lighting and hoses of inlet-outlet of gas mixture are located. In the upper part of the caisson, support beams 6, aligning the

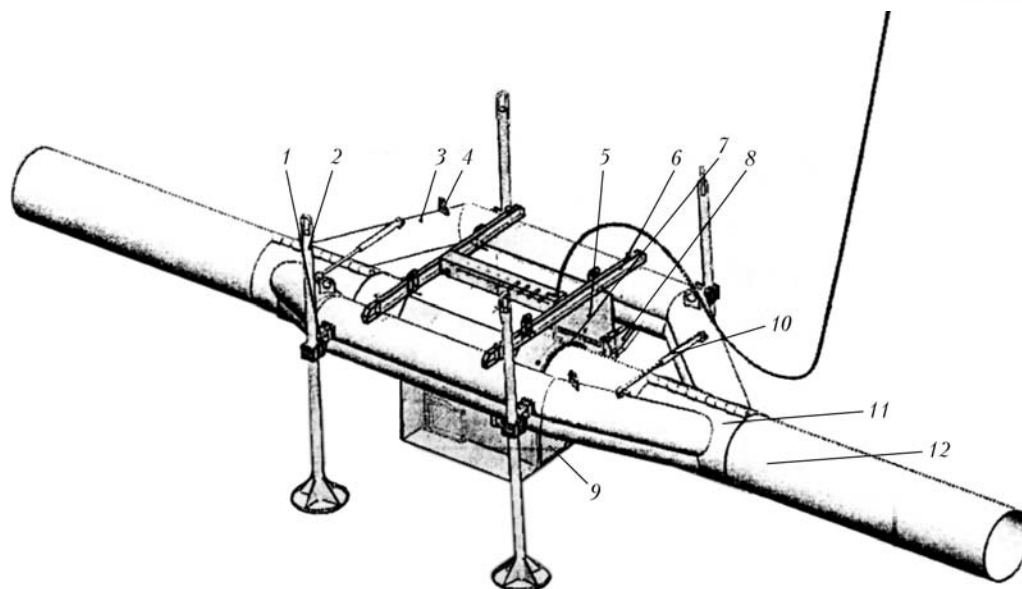


Figure 2. Scheme of SUC (1–12 see in the text)

caisson relative to a pipe, along which it slides along the frame, are located and on the forward and backward wall of the caisson the rests 8, maintaining the caisson from the coming to the surface and aligning it are located. The caisson is filled with carbon dioxide or argon to prevent explosion in case of ingress of gas from a pipeline being repaired inside the working zone. The air expired by divers-operators through special system, is removed to the surface without penetration inside the caisson. In the corners four video cameras with lighting are located to control the state of divers and sequence of performance of operations by them. The set of equipment includes two pulley blocks of 2 t loading capacity each used for assembly of pipe insert. The voltage for lighting and operation of equipment is supplied by electric cable of 70 m length with a connecting coupler. The electrodes are transported to the working area in a specialized sealed container.

Installation frame 3 (see Figures 2 and 4) is designed for rigid fixation in the initial position of emergency area of a pipeline 12, during cut out of a pipe section, and also to prevent caisson from floating during its complete blowing. It is composed of two halves of 9.8 m length and 8.8 t weight each, pipe grips 11 with polyurethane gaskets, hydraulic stretchers 10, supports 2, hinges 1 and loading staples 4. The hinges of frame are axles of pipe grips 11 positioned on the edges of installation frame. The as-assembled frame width is 6.1 m, height – 3.1 m. To clamp the pipe on installation frame, two hydraulic stretchers 10 are mounted, providing the closing-opening of pipe grips of a force up to 300 kN, operating from pump station with a pneumatic drive. Fixation of the installation frame on pipeline from a longitudinal movement is realized on both sides by bolts through the grip flaps, which are tightened a dynamometric wrench. The clamping force is transferred to the pipeline through the polyurethane inserts of pipe grips 11, mounted in

edge parts of the installation frame 3. The inner cavity of the installation frame is divided into six ballast bays of 12.8 m<sup>3</sup> total volume, which can be filled with water or blown, in this case the vertical load to the pipeline is changed.

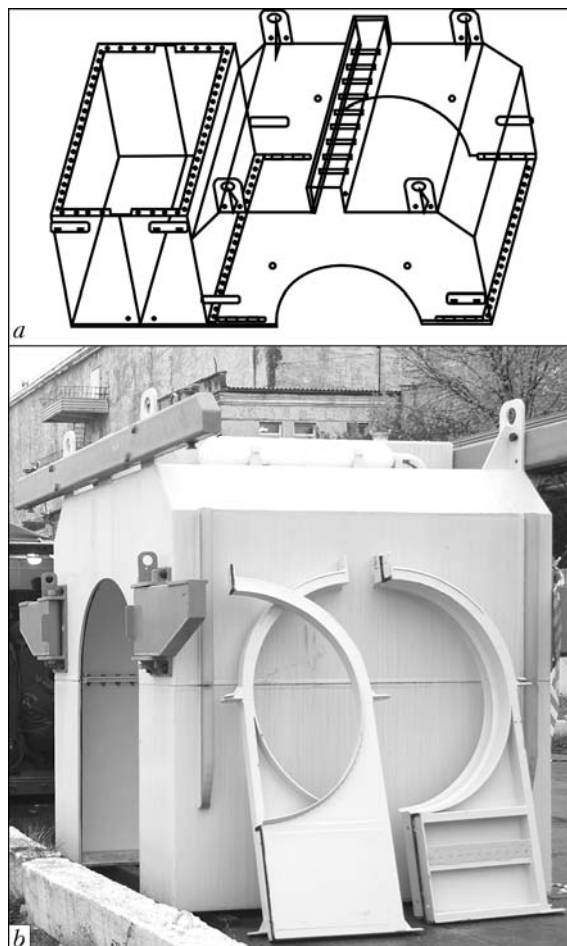


Figure 3. Scheme of transportable arrangement of caisson (a) and its appearance (b)



Figure 4. Appearance of installation frame

Installation frame 3 is rested on soil by four adjustable vertical supports 2, which release the weight load of the complex to the pipeline. They have hydraulic inserts with a manul pumping, developing the force of 200 kN each, the piston stroke is 360 mm. The supports are connected to the frame by hinges 1, having two degrees of freedom. This allows all the complex to move in a horizontal plane thus helping to align pipeline during mounting of a pipe section.

To purify the caisson gas medium from fumes, the ventilation is provided. The welding fumes from the caisson inner cavity enter the fume filter with changeable filtering element and gas analyzer by a separate hose. The purified gas is returned to the caisson inner cavity by hose through a low-pressure compressor and dryer with a selicogel filter. The gas leakage in system is compensated from transported cylinders with CO<sub>2</sub> and argon, located on the surface.

Welding and other kinds of operations are also realized inside the caisson by divers-welders, having diving suits. Air for breathing is supplied by a hose-cable through a lower part of the caisson. The air breathed out by divers is removed from masks through hose connected to an outlet reducer connection pipe into an expiration reducers located in opposite corners

inside the upper part of the caisson casing and beyond it. Operation of pneumatic tools inside the caisson is realized by connection of hoses through connection pipes to receivers valves located inside its upper part.

The cutting out of defective area of the caisson is made by mechanical mill cutter, having a pneumatic drive. Cutting out of defect by oxygen cutting is possible. Pneumatic tool used for fitting up the welded-in pipe section and cleaning of welds is supplied by compressor which removes the inert gas from the caisson through a dryer and filter. The aligning and fixation of pipe insert is realized using two standard aligning devices. The complex includes two inverter arc power sources with falling and rigid external volt-ampere characteristics.

All the constituent elements of the complex can be transported in parts using different kinds of transport including automobile with a body of 12 m length. The installation can be assembled on the shore in any convenient place and then towed afloat to the site of works performance at minimal depth of fairway of 2 m. The asymmetry of installation frame allows using complex in shallow water, for its installing the foundation pit of minimal size is required. These peculiarities are very important in performance of works in non-navigable and small rivers.

The described examples of application of technology of dry welding in the chamber are most probably will be widely used in assembly and repair under water of critical hydraulic engineering constructions and also at low level of transparency of water.

1. Bellamy, G. (1977) Hyperbaric welding comes of age on frigg gas line. *Pipe Line Industry*, 1, 41–43.
2. Coriatt, G. (1979) Hyperbaric welding in the repair of offshore pipelines and structures. In: *Proc. of 2nd Int. Conf. on Pipe Weld* (London, 1979), 343–355.
3. Kononenko, V.Ya. (2008) Hyperbaric dry underwater welding (Review). *The Paton Welding J.*, 4, 36–40.
4. Galyuk, V.Kh., Zabela, K.A., Kononenko, V.Ya. et al. (1981) Repair of oil pipeline by underwater welding. *Transport i Khranenie Nefti i Nefteproduktov*, 12, 22–24.
5. Kononenko, V.Ya. (2004) *Technologies of underwater welding and cutting*. Kiev: Ekotekhnologiya.
6. Kononenko, V.Ya., Pashkin, V.V., Bespalov, V.I. (2008) Technologies and equipment for underwater-technical operations in welding repair of defects of pipes and welded joints in underwater passages of gas pipelines. In: *Proc. of Branch Meeting on State-of-the-Art and Trends of Development of OJSC «Gazprom» Welding Production* (10–12 Nov. 2008, Razvilka, Moscow Reg., Russia).
7. Zakharov, A.N. *Caisson for repair of underwater pipelines*. Pat. 2342492 RF. Int. Cl. U 0.2 D 23/00. Publ. 27.12.2008.



# HYDROGEN DISTRIBUTION IN FLASH-BUTT WELDED JOINTS ON STEEL 10G2FB

S.I. KUCHUK-YATSENKO, G.K. KHARCHENKO, O.D. SMIYAN, Yu.V. FALCHENKO,  
V.F. ZAGADARCHUK and E.I. BUTKOVA

E.O. Paton Electric Welding Institute, NASU, Kiev, Ukraine

Peculiarities of hydrogen distribution in flash-butt welding of steel 10G2FB were studied. It was found that the nature of hydrogen distribution in contact zone is defined by the upsetting value.

**Keywords:** flash-butt welding, low-alloy steel, upsetting value, friction welding, hydrogen, abnormal mass transfer, deformation

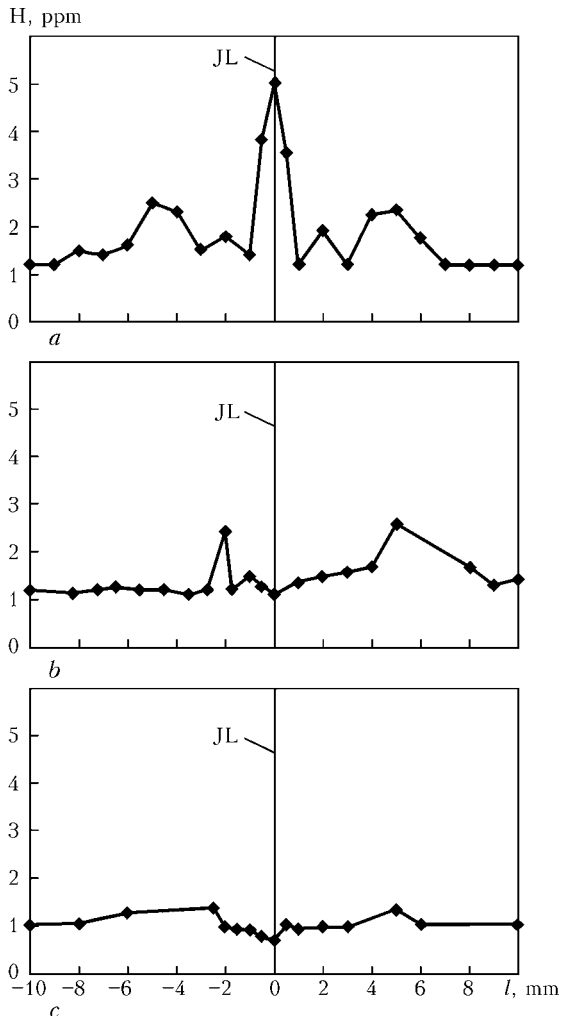
Distribution of gas-forming interstitial impurities (hydrogen, oxygen and carbon) in joints made by different pressure welding methods was shown earlier in studies [1–4]. Evaluation of the hydrogen content in joints on steel 10G2FB [1] and nickel alloy EI-698VD [2], made by friction welding (FW), was carried out by employing the local mass spectrum analysis techniques and equipment using the laser beam. It was shown that a 2 time reduction of hydrogen is observed in a 4 mm wide area in the joining zone in conventional FW of steel 10G2FB [1]. General reduction of the hydrogen content takes place in an area around 8 mm wide, which corresponds to the width of the plastic deformation zone. It was found that inertia FW provides approximately a 6 time reduction of the hydrogen content across the joining line (JL), in comparison with that in the base metal. The temperature of metal and rate of its plastic deformation have an influence on the character of distribution and local content of hydrogen in the joining zone.

In addition, as determined in studies [1, 2], not only the content of hydrogen, but also the content of carbon in a joint reduces during FW. The same picture is observed in carbon distribution in flash-butt welding (FBW) of steel 10G2FB [4]. However, there are no publications considering peculiarities of hydrogen distribution in zones of the FBW joints on low-alloy steel, in particular 10G2FB. A gas environment containing fumes of metal and alloying elements of steels forms in a spark gap in FBW, in contrast to FW. Hydrogen in the atomic form can be present in the gas environment of the spark gap, reacting with its other components. In FW, there is almost no gaseous environment of a similar content in the contact zone. Comparative investigations of hydrogen distribution in the joints on the same steels, made by different pressure welding methods under optimal conditions, allow obtaining information on the dominating factors affecting the hydrogen distribution in the joints produced by pressure welding.

The aim of this paper consisted in studying the distribution of hydrogen in the FBW joints. Investigations were carried out on samples of pipe steel 10G2FB with the  $\delta = 8$  mm thickness. The samples were cut out from the 200 mm wide plate and welded under the conditions recommended for this grade of steel [5]. The hydrogen content in the base metal was 1.2 ppm on the average. The rate of deformation of the HAZ metal of the joints was varied during the welding process by changing the upsetting value in a range of  $(0.1-2.0)\delta$ .

The character of hydrogen distribution in a joint on plates welded was investigated by the method of local mass spectrum analysis using the laser beam according to the procedure described in studies [1, 2]. It should be explained what the «joining line» term means for the authors of the present study. For them it is a reference point in assessment of the hydrogen content on both sides of this line. The so-called light band 0.4–1.2 mm wide, the content of carbon in which is up to 50 % of its content in the base metal [4], can be visually observed within the joining zone on microsections of the FBW steel joints. The ferritic band with JL situated in its middle [6] is revealed at the central part of the microsections after corresponding heat treatments and etching.

The Figure shows the hydrogen distribution at different upsetting values. The hydrogen content in JL exceeds that in the base metal 4–5 times at a small upsetting value comparable with the spark gap of 0.1 $\delta$ . As the upsetting value and, accordingly, the deformation degree in all the areas of the heated HAZ metal are increased, the hydrogen content along JL decreases down to the level of that in the base metal. At the same time, increase in the hydrogen concentration is observed at a distance of 3–6 mm to both sides of the welding line. The near-contact volumes having the increased hydrogen content go to the flash with increase in the upsetting value to more than 0.8 $\delta$ . The metal region along JL becomes depleted in hydrogen. For example, in the welded joint made at an upsetting of 1.2 $\delta$ , the most noticeable reduction of the hydrogen content is observed on both sides of JL



Hydrogen distribution in the zone of FBW joints on steel 10G2FB at upsetting of 0.18 (a), 0.38 (b) and 1.28 (c)

in a region with a total width of around 8 mm. The hydrogen content across JL reduces approximately 2 times in comparison with that in the base metal. The peak values at a level of the hydrogen content in the base metal are observed at a distance of up to 6 mm from JL. Non-uniformity of the distribution of hydrogen on both sides of JL is observed in FBW. Experimental results indicate that hydrogen escapes most intensively from the area situated on the side of action of compressive force. It should be noted by comparing the distribution of hydrogen in the HAZ metal, shown in the diagram, with that FW of the same steel that they are identical in many respects. Reduction of the hydrogen content across JL, as well as increase in it on its both sides is observed in both cases.

It can be supposed that transfer of hydrogen from the joint occurs by the following mechanism. Hydrogen transfers most intensively from the center to flash in the process of deformation of the melt. This process is accompanied by a simultaneous displacement of hydrogen in a direction normal to the contact plane, i.e. into the near-contact metal volumes. The character of the distribution of hydrogen in a volume interaction area can be explained by appearance of the effect of abnormal mass transfer [7] and formation of the compression and tension zones in FBW, which are situated in sequence one after another and in parallel to JL. The main compression region is situated across the JL. Therefore, hydrogen transfers from the compression zone to the tension one adjoining this material. The obtained experimental data are in full agreement with the Gorsky effect [8] on transfer of interstitial impurities into the tension zones in plastic deformation of metal. Along with the regularities of hydrogen distribution common for FW and FBW, there are also differences that are non-specific for FBW. In steel joints welded under the optimal conditions of FBW the hydrogen content reduces 1.5–1.7 times, and in FW it reduces 4–5 times, compared with the base metal.

Therefore, in the FBW joints on steel 10G2FB the hydrogen content in the joining zone depends on the upsetting value. As it increases, the hydrogen content in the joint decreases, but to a lesser degree than in FW.

1. Smiyan, O.D., Kuchuk-Yatsenko, S.I., Kharchenko, G.K. et al. (2007) Distribution of interstitial impurities within the joining zone in friction welding. *The Paton Welding J.*, **9**, 2–5.
2. Smiyan, O.D., Zyakhov, I.V., Kharchenko, G.K. et al. (2008) Distribution of hydrogen, oxygen and carbon in joining zone of heat-resistant nickel alloy during friction welding. *Visnyk ChDTU. Technical Sciences Series*, **34**, 138–143.
3. Butkova, E.I., Smiyan, O.D., Kaleko, D.M. et al. (1988) Distribution of hydrogen and oxygen in weld metal during capacitor-discharge percussion stud welding of AMg6 alloy. *Avtomatich. Svarka*, **2**, 17–22.
4. Kharchenko, G.K., Smiyan, O.D., Kuchuk-Yatsenko, S.I. et al. (2008) Decarbonization of steel in flash-butt welding. *Visnyk ChDTU. Technical Sciences Series*, **37**, 120–131.
5. Kuchuk-Yatsenko, S.I. (1992) *Flash-butt welding*. Kiev: Naukova Dumka.
6. Kuchuk-Yatsenko, S.I., Kharchenko, G.K., Grigorenko, G.M. et al. (2002) Heterogeneity of pipe steel joints made by flash butt welding. *The Paton Welding J.*, **2**, 2–5.
7. Gertsriken, D.S., Mazanko, V.F., Falchenko, V.M. (1991) *Pulsed treatment of metals and mass transfer at low temperatures*. Kiev: Naukova Dumka.
8. (1996) *Physics of solid: Encyclopaedia*. Vol. 1. Ed. by V.G. Bariakhtar. Kiev: Naukova Dumka.



## NEWS

## NEW LINE OF PROFESSIONAL WELDING MACHINES «FORSAZH»

New line of professional welding machines «Forsazh» embodied all recent achievements in the field of inverter technologies. The sixteen years' experience in design and manufacture of welding equipment at the Ryazan Instrument-Making Plant, RF, and perma-

Welding machines «Forsazh» are manufactured under the conditions of high-technology up-to-date production of a large Russian enterprise, which is a guarantee of stable operation of the equipment during the entire life cycle.



nent dialog with customers allowed developing the efficient machines with a wide range of functions, optimal properties of the welding arc and usability.

Light-weight and compact welding machines «Forsazh» of a new line provide mobility in carrying out works in any hard-to-reach place. Among them are Forsazh-301PRO (MMA), Forsazh-302 (MIG/MAG, MMA), Forsazh-315 (TIG, MMA), and Forsazh-200 (MMA, inverter).

The highest level of quality and reliability of the equipment was provided owing to original circuit solutions implemented on the modern cell base of leading foreign companies, rigid system of factory tests and obligatory pilot experimental operational tests of the new machines on production facilities.

The «Forsazh» trade mark has a high level of customers' confidence, which is maintained by a well-developed network of regional dealers, qualified technical support from the enterprise, 17 service centers on the territory of Russia and the Republic of Belarus.

*Main advantages of «Forsazh» welding machines:*

- easy arc ignition;
- electronic regulation of the welding arc current;
- automatic control of fan operation;
- capability of working in a long-term mode;
- welding in all spatial positions;
- long service life;
- low energy-consumption.



## «SELMA» ELECTRIC TRANSPORT

Company «Selma», one of the biggest manufacturers of welding equipment in Ukraine, proposes a new type of products – environmentally clean type of transport: passenger and freight electrocycles.



The electrocycle is a three-wheel electric vehicle equipped with a handle bar, one front guide wheel and two rear guide wheels.

The driver's seat and a seat for two passengers are installed on a general frame of the electrocycle. A body for transportation of freight can be installed instead of the rear seats for passengers when necessary.

An electric motor is mounted on a drive beam of the rear wheels. Traction batteries serve as a power source for the electric motor. The electrocycle is controlled using a speed selector.

### *Main advantages of electrocycles:*

- environmentally clean type of transport (non-polluting);
- low energy consumption;
- costs for charging the batteries for a haul length of up to 60 km is 1 UAH;
- small dimensions and low weight;
- high mobility;
- noise-free;
- possibility of moving indoors due to small dimensions;
- charging of traction batteries is carried out from the common 200 V mains;
- simple design and control.

### *Specifications:*

- the travel speed (smoothly adjustable) is up to 20 km/h forward and up to 5 km/h backward;
- haul without recharging is up to 60 km;
- getting over a slope is up to 10 %;
- capacity of a driving motor is 1500 W;
- parameters of the traction batteries are 12 V: 50 A·h;
- load-carrying capacity is up to 300 kg;
- and recharging time is 10 h.

## FOR SPECIALISTS

On June 16–17, 2010 Ukrainian-German Seminar on the subject «Plasma and Electron Beam Technologies for Protective Coatings» will be held in Kiev at the E.O. Paton Electric Welding Institute.

Seminar subject complies with such a priority field as «New materials and production technologies», developed by the Federal Ministry of Education and Science of Germany within the framework of scientific-technical cooperation with Ukraine. The project was planned as a pilot project and is intended to support internationalization of SMEs. It should promote practical implementation of internationalization strategy.

The Seminar envisages exchange of information on the above subject between specialists of both enterprises and scientific institutions. The main circle of seminar participants will include scientists and specialists of manufacturers and users of functional products with optimized tribological properties, as well as specialists working in such production sectors, as automotive industry, mechanical engineering, etc. Poster presentations and possibility for cooperation negotiations will also be provided during the seminar.

**Contacts:** Tel./Fax: +38(044) 289 22 02. E-mail: Yu.kon@paton.kiev.ua  
Prof. Konstantin A. Yushchenko,  
Deputy Director of the E.O. Paton Electric Welding Institute of the NASU



## OJSC «MEZHGOSMETIZ-MTSENSK» — ON A WAY OF MASTERING PRODUCTION OF ALL WELDING CONSUMABLES RELEVANT IN THE MARKET

OJSC «Mezhgosmetiz-Mtsensk» is a Russian manufacturer of high-quality welding consumables, which has been functioning for 10 years and holding the leading positions in the Russian market.

*The stable company profit through high production quality* motto is a secret of success. A priority in the area of quality makes the basis of our work. Considerable operational experience, unique manufacturing technologies, quality control and careful investigation of customers' demands make our products an optimal choice for carrying out welding operations of any complexity. Our welding consumables are applied in machine building, ship building, power engineering, chemical industry, as well as in bridge construction, car building, manufacture of pipes and metal structures.

Italian line «Subarc» for manufacture of large-diameter wires, including the 5.0 mm diameter, was bought in January 2008 to meet requirements of our customers in greater scope. This allowed us to deliver this type of wire to the biggest pipe plants of Russia. The «Subarc» line permitted widening of a grade range of the produced wires: Sv-08G2S-O, Sv-08G1S-O, Sv-08A-O, Sv-08GA-O, Sv-10GAA-O, Sv-08GM-O, Sv-08GNM-O, Sv-08G1NMA, Sv-08GSMT-O, Sv-08GSMT-O, Sv-10NMA-O, Sv-08KhM-O, which, in turn, made it possible to satisfy requirements of the customers working in different branches of the national economy. Those customers who had already have an experience of working with our wire, sighed with relief: the money invested in rearrangement of their enterprises started paying back. Also, we should note and thanks our partners in metallurgy, who actively responded to our request and manufactured a raw material of the required quality.

Today «Mezhgosmetiz-Mtsensk» can offer to its customers a high-quality copper-clad wire from 2.0 to 5.0 mm in diameter in different packing variants, namely:

- *packing in reels K-415* of up to 28 kg in weight with layer-by-layer row layout. Reel K-415 provides stable operation of feeding mechanisms, stable arcing, and improved efficiency of welding equipment;

- *heavy-load bundle B-500* of 300–700 kg in weight: layer-by-layer winding of wire with cross-like layout in width of a bundle; reliable securing of wire at four points; and special fixture for lifting and mounting on an uncoiling device provides wasteless recycling;

- *packing in heavy-load bundles* of up to 700 kg in weight with cross-like row layout, with the in-house manufactured uncoiling device developed for uncoiling of these bundles;

- *packing «Ariadna» B-500* of up to 250 kg in weight and *B-600* of up to 300 kg in weight — a new

type of packing of welding wire developed on the basis of the European experience in wire delivery.

The wire is coiled by a special method, which provides straightening of the wire while it comes out of a packing. Straight welding wire can be readily fed to the welding device feeder. The packing is compact and made from environmentally clean raw materials.

As shown by the practice, this type of packing is most promising. «Ariadna» takes the small space in a working area, provides easy unwinding of the wire, allows increasing efficiency of welding equipment due to a continuous welding process, reduction of the quantity of defects in welds owing to protection of the welding wire from dust and other contaminants, and decrease in wear of the feeder components;

- *rectangular section bundles* of 80–100 kg in weight. In September 2009, «Mezhgosmetiz-Mtsensk» started manufacturing this packing of 2.0–5.0 mm diameter copper-clad welding wire. This packing of the Sv-08G2S, Sv-08GSMT, Sv-08GA, Sv-08GM, Sv-08KhM, Sv-10NMA, Sv-08GNM, Sv-08KhGSMFA and Sv-08KhGSMA wire grades is applied with the welding technologies intended for reduction of wire wastes caused by tangling, providing of continuous welding process, and decrease of additional costs for winding of the wire.

The wire provides stable continuous arcing and quality welds. Besides, such a technological operation as re-winding of the wire on process coils is eliminated, when the copper-clad welding wire in the form of rectangular section bundles is used.

### Rectangular section bundle MP-100

Outer diameter, mm .....	736
Inner diameter, mm .....	588
Width, mm .....	100
Weight, kg .....	50–100
Wire diameter, mm .....	2.0, 3.0, 4.0, 5.0

Row arrangement of the wire in each layer is carried out on cardboard core. Each bundle is hermetically sealed into a shrinkable film.

We participate in specialized exhibitions, test and certify our products, extend our product line, and constantly expand the range of products to meet requirements of the market. Permanent and continuous control of quality of welding consumables, constant implementation of innovations and our aspiration to correspond to requirements of a volatile market, individual approach to interaction with clients, stability and reputation of one of the best manufacturers of welding consumables in Russia — we do all this for You!

**Our quality — Your choice!**

Kostyuchenko V.P.

Director General OJSC «Mezhgosmetiz-Mtsensk»

## 10th INTERNATIONAL SPECIALIZED EXHIBITION «WELDING AND CUTTING»

10<sup>th</sup> International Exhibition «Welding and Cutting» took place at the «BelExpo» Exhibition Complex in Minsk on March 23–26. It was organized by CJSC «MinskExpo» with the information support rendered by the «Avtomaticheskay Svarka», «Svarshchik v Belorussii», «Alians Svarshchikov», «Mir Metalla» and other journals. International Exhibition «Corrosion Protection. Coatings» was held in parallel at the same pavilion.

The historically established wide inter-branch application of welding and related processes is characteristic of the economy of the Republic of Belarus (RB) at the current stage. Today its enterprises are in a great need for replacement of out-of-date equipment by more recent analogues. The need for mastering automated welding complexes, modern energy-saving technological welding equipment and quality welding consumables has aggravated under conditions of the world financial crisis, growth of competition and requirements to the quality of products. In this relation, the «Welding and Cutting» Exhibition provided potential customers with high opportunities not only for acquaintance with innovations in the area of welding, but also for finding the ways of more effective and rational improvement of welding productions.

55 companies from 4 countries of the near and far abroad — Russia, Ukraine, Belarus and France — gathered at the Exhibition. The subject area of the Exhibition traditionally included the following sections: welding consumables; equipment for welding, cutting, surfacing, brazing, soldering and heat treatment; equipment for orbital welding and treatment of pipes; electron beam, laser and plasma welding and cutting; automation of welding processes and production fixtures; modern technologies for welding, cutting, surfacing, brazing, soldering and heat treatment;

and occupational and environmental safety in welding production.

Welding equipment and machines for arc and plasma welding processes and for plasma and gas-oxygen cutting were presented by manufacturing enterprises (companies) (S.A.S. Polysoude, France; Ryzan State Instrument Plant, Russia; «Elektroteplopribor» plant, Bel-ELSO, Ltd., Belarus; OJSC «Zont», Ukraine), as well as by multiple trade organizations from Belarus, such as «Belevrotekh», «Belgazpromdiagnostika», «BelSvaMo», «VneshITS», «Kemfin», «Oliver», etc.

Characteristic feature of the jubilee Exhibition in Minsk is that the leading players from the CIS and «far-foreign» countries in the market of welding equipment and consumables were represented by their Belarusian partners:

- «BelSvaMo» — the largest Belarus supplier of professional equipment, consumables and instruments of such companies as Lincoln Electric (USA), Dalex (Germany), Tecna (Italy), Multimet (Poland), Eckert (German-Poland);
- «Oliver» — the first Belarusian manufacturer of copper-clad welding wire Sv-08G2S and supplier of industrial inverters, semiautomatic devices and machines for butt welding, which are assembled under licenses;
- «Kemfin» — distributor of Finnish companies Kemppi, Kemecweld and Heatmasters in the RB;
- «Rywal Svarka» — distributor and wholesale supplier of welding equipment and consumables in RB, offered by Polish Company Rywal-RHC, as well as Lorch (Germany), Thermal Dynamics (USA), etc.;
- «Belgazpromdiagnostika» and CJSC «Obiednyennaya Svarochnaya Kompaniya», offering welding equipment, consumables, welders' protective equip-





ment of such internationally recognized companies as Fronius (Austria), Boehler-Thyssen Welding Group, UPT and Weldotherm (Germany);

- «Alvi-Torg» – distributor of equipment and materials of leading manufacturers from Russia, France, Italy, Spain, Germany and Ukraine, as well as of in-house cutters and torches for gas-plasma treatment;

- «Promsvarka» – distributor of the ESAB Company (Sweden);

- «Belevrotekh» – quick-growing company specializing in delivery of welding equipment, consumables and components from manufacturers in the CIS and far-foreign countries;

- «VneshITS» – supplier of equipment of the ITS Company and companies SELMA and ESVA.

«Abikor Binzel Techniques Ltd.», a supplier of welding torches, electric holders and plasma torches from Abikor Binzel (Germany), was positioned for the first time at the Exhibition in Minsk.

Manufacturers of welding consumables from the CIS countries were represented at the Exhibition by «Mezhgosmetiz» Commercial House (Russia), Gomel Starting Engines Plant, Svetlogorsk Welding Electrodes Factory (Belarus), Artyomovsk Machine Building Plant «Vistek», OJSC «Plazmatek» (Ukraine), as well as distributors of Zelenograd Electrode Plant («Amios-stroj» Ltd.) and Losinoostrovsk Electrode Plant («Briz» Company).

Auxiliary equipment for arc welding and surfacing, guards and welding masks, professional clothing for welders, systems of local exhaust devices, filters, units for exhaust and cleaning of air in shops were also demonstrated at the Exhibition.

One-day International Workshop «Welding and Related Technologies» was held under plenary conditions in the framework of the Exhibition on March 24. It was opened by A.F. Iliushchenko, Director General of SSPA PM, corresponding member of the NAS of Belarus. Then 15 papers were presented by scientists and specialists of the Belarussian Institute of Welding and Protective Coatings, Belarussian-Russian University (Mogilyov), Belarussian National Technical University (Minsk), Joint Institute for Power and Nuclear Research in Sosny, Alliance of Welders (Saint-Petersburg) and other organizations. Subjects of the presentations covered the information on the state-of-the-art in production of electrodes for arc welding in the RB, new multi-operator welding equipment, modern machines for thermal cutting and robots, etc.

Good organization of work of the Exhibition and its high attendance should be noted. Undoubtedly, it will stimulate development of business relations between manufacturers and customers of welding engineering products.

*Prof. V.N. Lipodaev, PWI*

# SUBSCRIPTION FOR «THE PATON WELDING JOURNAL»

If You are interested in making subscription directly via Editorial Board, fill, please, the coupon and send application by fax or e-mail.

The cost of annual subscription via Editorial Board is \$324.

Telephones and faxes of Editorial Board of «The Paton Welding Journal»:

Tel.: (38044) 287 6302, 271 2403, 529 2623

Fax: (38044) 528 3484, 528 0486, 529 2623.

«The Paton Welding Journal» can be also subscribed worldwide from catalogues of subscription agency EBSCO.

<b>SUBSCRIPTION COUPON</b>	
Address for journal delivery	
Term of subscription since	200      till      200
Name, initials	_____
Affiliation	_____
Position	_____
Tel., Fax, E-mail	_____



## ADVERTISEMENT IN «THE PATON WELDING JOURNAL» (DISTRIBUTED ALL OVER THE WORLD)

### «АВТОМАТИЧЕСКАЯ СВАРКА»

#### RUSSIAN VERSION OF «THE PATON WELDING JOURNAL» (DISTRIBUTED IN UKRAINE, RUSSIA AND OTHER CIS COUNTRIES)

**External cover, fully-colored:**

- First page of cover (190×190 mm) – \$700
- Second page of cover (200×290 mm) – \$550
- Third page of cover (200×290 mm) – \$500
- Fourth page of cover (200×290 mm) – \$600

**Internal cover, fully-colored:**

- First page of cover (200×290 mm) – \$400
- Second page of cover (200×290 mm) – \$400
- Third page of cover (200×290 mm) – \$400
- Fourth page of cover (200×290 mm) – \$400

**Internal insert:**

- Fully-colored (200×290 mm) – \$340
- Fully-colored (double page A3) (400×290 mm) – \$570
- Fully-colored (200×145 mm) – \$170

- Article in the form of advertising is 50 % of the cost of advertising area
- When the sum of advertising contracts exceeds \$1000, a flexible system of discounts is envisaged

**Technical requirement for the advertising materials:**

- Size of journal after cutting is 200×290 mm
- In advertising layouts, the texts, logotypes and other elements should be located 5 mm from the module edge to prevent the loss of a part of information

**All files in format IBM PC:**

- Corell Draw, version up to 10.0
- Adobe Photoshop, version up to 7.0
- Quark, version up to 5.0
- Representations in format TIFF, color model CMYK, resolution 300 dpi
- Files should be added with a printed copy (makeups in WORD for are not accepted)